
Sequence-defined oligo(amidoamines) for the multivalent presentation of natural and non-natural binding motifs and their protein interactions

Inaugural dissertation

for the attainment of the title of doctor
in the Faculty of Mathematics and Natural Sciences
at the Heinrich-Heine-University Düsseldorf

presented by

Peter Pasch

Düsseldorf, November 2021



Submitted:

Peter Pasch

Born on January 11, 1992 in Mönchengladbach

1st reviewer:

Prof. Dr. Laura Hartmann

2nd reviewer:

Prof. Dr. Thomas J. J. Müller

Datum der mündlichen Prüfung: 08.04.2022

The research presented in this Inaugural dissertation was carried out from December 2016 to September 2020 in the Institute for Macromolecular Chemistry at the Heinrich Heine University of Düsseldorf under the direction of Prof. Dr. Laura Hartmann.

Declaration of authorship

I, Mr. Peter Pasch, swear that the presented dissertation is written by myself and without making use of impermissible aids. Further all sources used are acknowledged in the bibliography as reference.

Pasch 19.11.2021

Signature

Date

Table of contents

Abstract	II
List of Publications and Drafts	VI
1. Introduction.....	1
1.1 Solid phase polymer synthesis of oligo(amidoamines).....	2
1.2 Multivalency	7
2. Ligands for multivalent presentation	8
2.1 Carbohydrates as natural binding motifs and carbohydrate based amphiphiles	8
2.2 Guanidiniocarbonylpyrrole	10
3. Aggregation-induced Emission.....	11
4. Motivation.....	13
5. Results.....	15
5.1 PEGylated sequence-controlled macromolecules using supramolecular binding to target the Taspase1/Importin α interaction	15
5.2 Take your Positions and Shine: Effects of Positioning Aggregation-Induced Emission Luminophores within Sequence-Defined Macromolecules	49
5.3 Sequence-defined glycomacromolecules using AIE for direct read-out of lectin binding	82
5.4 Amphiphilic glyco(oligoamidoamines) with AIE luminophores to visualize cluster formation in self-assembled systems.....	108
6. Summary & Conclusion	122
7. References.....	131
8. Appendix	137
8.1 List of abbreviations	137
9. Acknowledgments.....	140

Abstract

In this dissertation a library of monodisperse sequence-defined macromolecules, so called precision macromolecules, was synthesised using solid-phase polymer synthesis (SPPoS) to selectively combine supramolecular binding motifs, carbohydrate ligands and AIE luminophores and achieve modulation of protein-protein interactions (Figure 1). Four different groups of precision macromolecules can be differentiated based on their use as ligand or inhibitor in protein binding as well as their ability to allow for readout of binding or clustering events through their conjugated AIE luminophores.

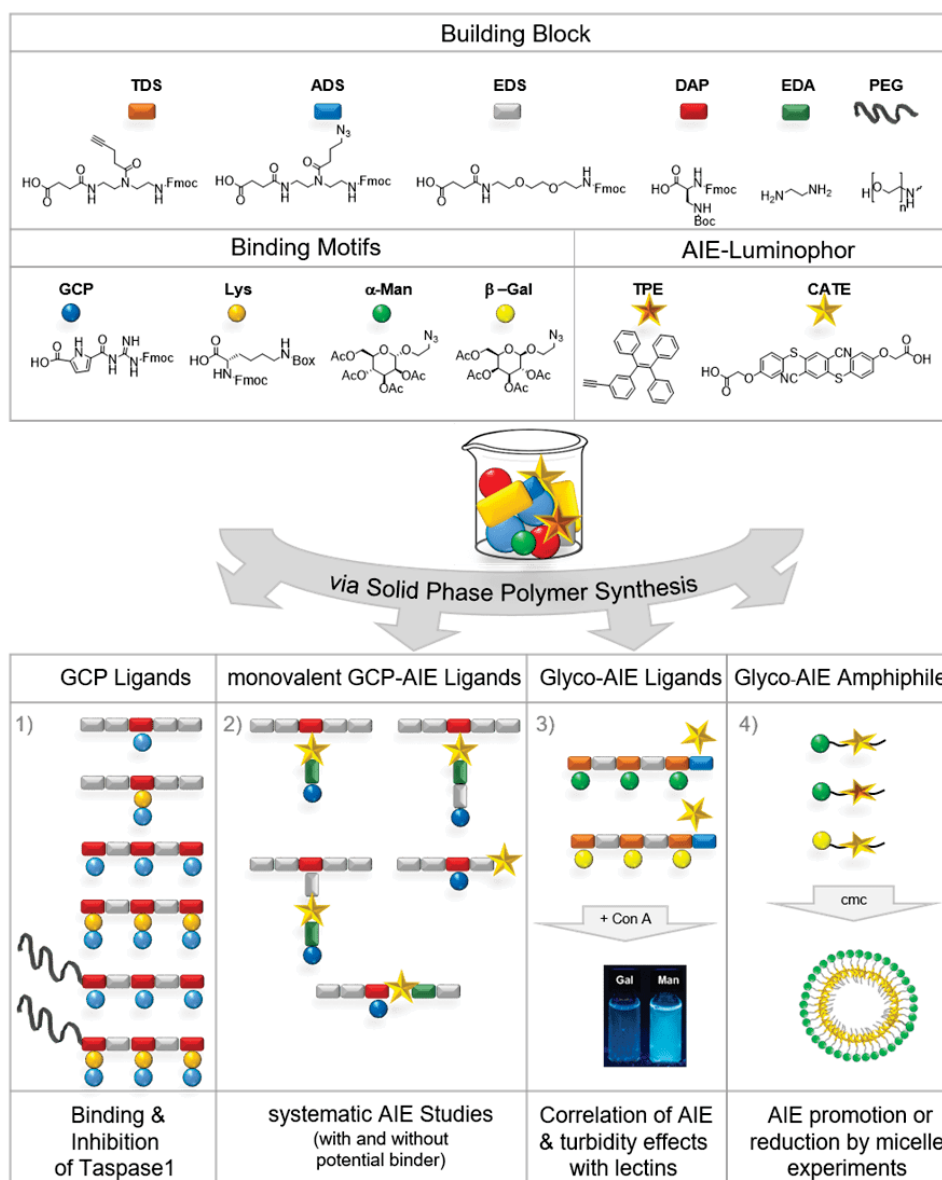


Figure 1: Building blocks, binding motifs and AIE luminophores used for the SPPoS, as well as the obtained groups of precision macromolecules: 1) GCP Ligands, 2) monovalent GCP-AIE Ligands, 3) Glyco-AIE Ligands and Glyco-AIE Amphiphiles. Lastly, the applications of each group are mentioned.

In the first part of the dissertation, a novel inhibition mechanism of the oncologically relevant protease Taspase1 was targeted. For this purpose, different homomultivalent as well as heteromultivalent

guanidiniocarbonylpyrrole (GCP) -containing ligands were synthesised. The non-natural arginine mimetic GCP offers the possibility to bind to oxyanions that are located on a protein surface. In addition, the design of the trivalent ligands was extended to include the general concept of steric shielding with PEGylated ligands to achieve more efficient inhibition. In the binding assay using SPR experiments with immobilised Taspase1, binding in the mM range could only be detected for the trivalent homo- and heteromultivalent macromolecules. Moreover, the binding strength of the ligands to Taspase1 increased for heteromultivalent structures due to the incorporated lysine motifs. In the subsequent in vitro pull-down assays, the inhibitory effect of the ligands was investigated. Only PEGylated ligands disrupted the interactions of Taspase1 with its partner protein Importin α in a concentration-dependent manner, resulting in a novel inhibitory mechanism for the Taspase1 protease.

The first part of the project also showed how difficult it is to detect binding events, which is why the second part of this work aimed at a systematic study using AIE luminophores to read out ligand-protein binding events. For a luminophore construct to be used as an AIE-based sensor, it should be flexible without the presence of the target molecule or dissolve completely and thus not give an AIE response. Only with binding to the target molecule or after aggregation its movement is restricted, leading to AIE and thus readout of the binding event. Therefore, the AIE luminophore must be precisely combined with the binding motif, which raises a central question in the development of such multifunctional macromolecular ligands. Where to put the AIE and where to put the binding motif in the structure? Therefore, in the second part, five monovalent GCP ligands with AIE luminophore were synthesised. The special feature of the five structures is that they are all based on a combination of sequence-defined oligo(amidoamine) scaffolds, one conjugated GCP and one AIE luminophore, but the position of the luminophore varying from the immediate vicinity of the binding motif to the middle of the side or main chain to the end group. All macromolecules were systematically evaluated for their fluorescence properties, both in solution and in solid state, and for their AIE behavior when binding to various natural and synthetic polyanions. Surprisingly, only one of the macromolecules showed clear AIE behavior. None of the derivatives where the AIE was placed in the main chain or where the GCP motif was directly bound to the main chain showed AIE behaviour with any binder in solution. However, differentiation in terms of AIE and GCP function was also observed for the derivatives with AIE in the side chain. It appears that direct linkage of AIE and GCP motifs via the ethylenediamine linker does not provide AIE behaviour, whereas the introduction of an additional EDS building block leads to AIE properties. This study showed that the position of the AIE within the ligand structure indeed influences the function of the ligand for detection. Furthermore, a first correlation between structure

and properties of AIE- ligand was revealed, which will facilitate the development of similar new AIE-based biosensors from a synthetic point of view in the future.

In the third part of this dissertation, an AIE luminophore was again conjugated to ligands, whereby the binding motif was exchanged to carbohydrates. Either α -Mannose or β -Galactose as binding motifs were conjugated to the two trivalent ligands, resulting in a clear difference between them for possible binding partners. The obtained AIE glycomimetics could subsequently be used to study carbohydrate-protein interactions, e.g. with the α - Mannose-specific lectins ConA, GNA, PSA, LCA. Starting from a weak initial fluorescence of the two structures in aqueous medium, changes in emission as well as turbidity could be obtained by titrating the different lectins. For the tetrameric lectins Con A, GNA and the dimeric lectin PSA, an increase in emission as well as turbidity was obtained with the Mannose TPE derivative, resulting in an AIE probe. Only for the dimer LCA no increase in turbidity and emission could be achieved. Furthermore, this study showed that a cluster effect of the ligand with the lectins is required to obtain a pronounced aggregation-induced emission signal, as a correlation of emission and turbidity was clearly demonstrated.

In the previous chapter, glycooligomers equipped with AIE luminophores showed AIE effects with different lectins, but also that cluster effects take on a key function. Since, cluster effects are essential in many biological phenomena, such as the clustering of receptors in a membrane after binding to a multivalent ligand, a novel study on clustering of amphiphiles with AIE luminophores will be achieved in the fourth part of this dissertation. For this purpose, three derivatives with AIE luminophores and carbohydrates as binding motifs were selected to be assembled into amphiphilic sequence-defined surfactants by solid-phase synthesis. The aims are to synthesise hydrophobic AIE micelles that show a pronounced AIE effect in aqueous medium and to reduce this fluorescence by adding a second non-fluorescent surfactant without AIE. First, the clustering of the surfactants to micelles could be shown by detecting the critical micelle concentration (CMC) for all three derivatives. In the second step, the addition of SDS (sodium dodecyl sulfate) to the micelle system altered the clustering so that fewer interactions of the AIE moieties occurred within the resulting mixed micelles, reducing fluorescence intensity. Since the AIE surfactants already carry carbohydrates as binding motifs, future binding studies with lectins should be carried out in a similar way as in project 3, whereby it would be exciting to increase the emission intensity through interactions and clustering of the AIE parts with the lectins. If successful, this approach could also be used in the long term for the detection of clusters in membranes.

Overall this thesis demonstrates how tailor-made precision macromolecules can give access to novel ligands and inhibitors of protein-protein interactions and allow for detailed structure-property relation studies giving new insights relevant also beyond the class of precision macromolecules.

List of Publications and Drafts

Publications included in this work:

PEGylated sequence-controlled macromolecules using supramolecular binding to target the Taspase1/Importin α interaction

P. Pasch, A. Höing, S. Ueclue, M. Killa, J. Voskuhl, S. K. Knauer, L. Hartmann, *Chem. Commun.* **2021**, 57, 3091-3094.

Own contribution:

Collaborative design of structures and conceptualisation of the project was done in collaboration with the cooperation partners. Synthesis and purification of all building blocks (except GCP building blocks) and the oligomers. Characterization of the oligomers (LC-MS, NMR, UHR, MALDI-ToF-MS). Collaborative evaluation of the binding studies. Collaborative writing of the manuscript.

Take your Positions and Shine: Effects of Positioning Aggregation-Induced Emission Luminophores within Sequence-Defined Macromolecules

P. Pasch, M. Killa, H. L. Junghans, M. Schmidt, St. Schmidt, J. Voskuhl, L. Hartmann, *Chem. Eur. J.* **2021**, 27, 10186–10192.

Own Contribution:

Collaborative conceptualisation and design of the project. Synthesis and purification of all building blocks (except GCP building blocks). Supervision of oligomer synthesis performed by Hauke Lukas Junghans within his bachelor thesis. Oligomer characterization (LC-MS, NMR, UHR). Evaluation of fluorescence studies. Collaborative manuscript writing.

Publications in preparation:

Sequence-defined glycomacromolecules using AIE for direct read-out of lectin binding

P. Pasch, J. Voskuhl, L. Hartmann

Own Contribution:

Collaborative project design. Synthesis and purification of building blocks and oligomers. Measurement and evaluation of all LC-MS experiments. Evaluation of all NMR and UHR experiments.

Performance and evaluation of fluorescence and turbidity measurements. Collaborative writing of the manuscript.

Amphiphilic glyco(oligoamidoamines) with AIE luminophores to visualize cluster formation in self-assembled systems

A. Banger, P. Pasch, M. Otten, M. Karg, L. Hartmann

Own Contribution:

Collaborative design and development of the project. Synthesis, purification and characterization of all oligomers. Fluorescence measurements and evaluation (aggregation-induced emission behavior, CMC detection). Experiments regarding the fluorescence reduction by mixed micelle systems with SDS. Collaborative writing of the manuscript.

Publications not included in this work:

Highly Fluorescent Merocyanine and Cyanine PMMA Copolymers

P. Pasch, J. Papadopoulos, A. Goralczyk, M. L. Hofer, M. Tabatabai, T. J. J. Müller, L. Hartmann

Macromol. Rapid Commun. **2018**, 1800277.

1. Introduction

The development and research of synthetic multivalent ligands has been gaining interest for years, as their development can contribute to a better understanding of biological processes as well as to their targeted control.^[1] In nature, multivalent interactions are an essential part of many processes, e.g. fertilisation, inflammatory response or even adhesion of pathogens to cells, which makes their importance for science increasingly recognised.^[2-4] A major focus in the development of new multivalent ligands is the presentation of tailored recognition motifs for natural binding epitopes, thereby achieving high affinity and ideally selectivity of the ligand for the receptor. The binding strength of multivalent ligands is based on non-covalent molecular interactions, which develop sufficient binding strength through the interplay of multiple weak ligand-receptor interactions.^[5,6] In this context, for example, the group of carbohydrates should be mentioned, which have been shown to achieve strong multivalent effects with carbohydrate-recognising protein receptors called lectins.^[7,8] The importance of carbohydrates and multivalence can also be demonstrated by the glycocalyx, which, like a sugar coating, envelops all cells in living organisms and thus enables fertilisation or the attachment of pathogens, as mentioned above.^[9,10] In addition to natural binding motifs, however, new non-natural binding motifs have been developed in recent decades that can achieve multivalent effects with receptors. Their advantage over natural motifs is often a strong affinity for certain amino acids located on protein surfaces, which allows access to more efficient synthetic multivalent ligands.^[11-13] A well-known non-natural motif is guanidiniocarbonylpyrrole (GCP) with its ability to bind oxyanions, so that it could be presented multivalent e.g. for DNA detection and inhibition of human tryptase.^[14-17]

Besides the different binding motifs, their presentation along a scaffold is crucial for their mode of action. Multivalent ligands have to reach different binding epitopes and can therefore range from small molecules, copolymers, polymers to precise macromolecules. Within the research group of Prof. Dr. Laura Hartmann, so-called precision oligo (amidoamines) were developed and explored by means of solid phase synthesis and custom-made building blocks. This platform offers the possibility to synthesise a sequence-defined and monodisperse scaffold with a well-defined number of binding motifs, so that systematic binding studies with respect to valence can be performed.^[18-21] In addition, aggregation-induced emission luminophores can also be conjugated to the precision macromolecules in this way, which should simplify the readout of binding events.

The following chapters give a brief overview of the most important basics of solid-phase polymer synthesis, multivalence, the different binding motifs and aggregation-induced emission luminophores.

1.1 Solid phase polymer synthesis of oligo(amidoamines)

Solid phase polymer synthesis (SPPoS) for the synthesis of oligo(amidoamines) is based on the solid phase synthesis (SPS) approach developed by Merrifield, which made it possible for the first time to efficiently synthesise monodisperse, sequence-controlled peptides.^[22] For this purpose, Merrifield uses an insoluble carrier material, a resin, to which the peptide to be formed is covalently bound throughout the synthesis.^[23] In this way, peptide synthesis could be both accelerated and simplified. The ability to wash the resin means that unreacted excess reactants, degradation products of the activating reagents and unwanted by-products can be removed after coupling without further chromatographic purification steps. In addition, reactants could now be used in excess, allowing higher yields, purities and shorter reaction times of the peptides.

Based on Merrifield's peptide synthesis, tailor-made building blocks are now linked together using solid-phase polymer synthesis (SPPoS) instead of amino acids, giving access to sequence-defined, monodisperse non-natural macromolecules. Chemically, the linkage of the building blocks on the resin is a condensation reaction of a carboxylic acid with an amino group linked by an amide bond. The coupling reaction starts at the C-terminus towards the N-terminus and in the first synthesis step, the carboxyl group of the customised building blocks is covalently bonded to the resin linker.^[24,25] In all coupling reactions, however, it is essential to prevent the building blocks from polymerising into an oligomer or polymer. For this purpose, the building blocks used carry a protective group that temporarily prevents further undesired coupling reactions and can then be completely removed. Two common protecting group systems for this purpose are the fluorenylmethoxycarbonyl (Fmoc) protecting group, which is labile under basic conditions, and the butyloxycarbonyl (Boc) protecting group, which is labile under acidic conditions.^[23,26]

In recent years, many different custom-made building blocks have been developed that are now suitable for the synthesis of multifunctional oligo(amidoamines).

The functions of the custom-made building blocks can essentially be divided into two subgroups: spacer and functional building blocks (see Figure 2). The spacer building blocks are centrally based on a linear diamino structure and the functional building blocks on a linear triamino structure. Starting from the central di-/triamine, they can eventually be converted into building blocks bearing a free carboxy and an Fmoc-protected amine via multi-step synthesis steps. One of the earliest developed building blocks is the spacer building block EDS ((ethylenedioxy) to (ethylamine) succinamide), which contains a flexible and amphiphilic diethylene glycol unit. In addition to the properties of the previously mentioned spacer component EDS, it can also be used to achieve a certain distance between the binding motifs and to obtain a desired overall contour length of the oligo(amidoamine).^[18,20,27,28] Other spacer building blocks from the library of L. Hartmann are ODS, the hydrophobic counterpart of EDS,

and SDS, which is significantly shorter than EDS with an ethylenediamine unit.^[29] The functional class of the building blocks ranges from TDS (alkynes), DDS (alkenes), MDS (carboxylic acids) to the BADS building block (benzyl azide), ADS (azide) and many others (see Figure 2).^[18, 20, 29, 30-32]

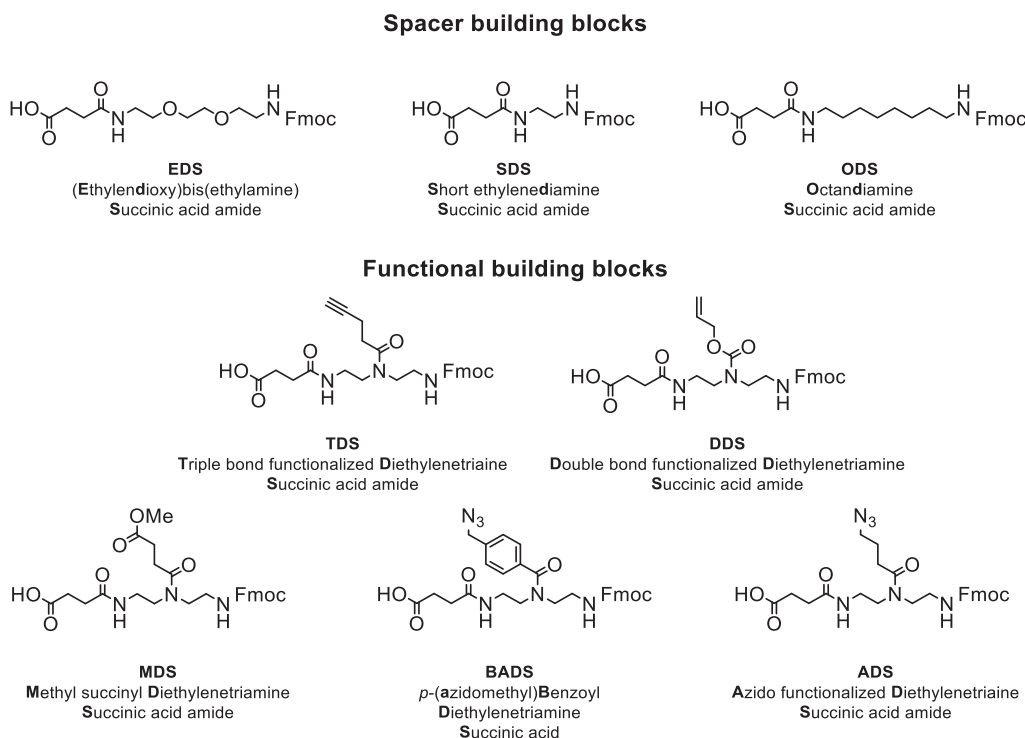


Figure 2: Examples of functional and spacer devices established by Hartmann et al, EDS, SDS, ODS, TDS, DDS, MDS, BADS, ADS.^[18, 20, 29, 30-32]

The TDS can be used for ligand incorporation after incorporation into an oligomeric scaffold for functionalisation via a CuAAC click reaction. For example, TDS can be used to conjugate azide-functionalised ligands such as 2-azidoethyl- α -D-mannopyranoside or 2-azidoethyl- β -D-galactopyranoside to the oligo(amidoamine).^[29] Alternatively, BADS and ADS can be used to conjugate alkyne-functionalised ligands.

Next, the synthesis of an oligo(amidoamine) consisting of an EDS and TDS building block is shown according to the SPPoS as an example (see Figure 3). The choice of support material is also essential for a successful SPPoS. The resin for the synthesis must be stable and inert to the solvents, coupling reagents, catalysts and building blocks used. They also require sufficient pore size and swelling capacity, as the coupling of amino acids is achieved by a high diffusion potential.^[33,34] The resin used in this example is TentaGel S RAM[®] resin with a rink amide linker that is Fmoc-protected at the N-

terminus. To remove the Fmoc protecting group, the resin is first swollen in DCM as well as DMF in the first step. Both solvents are particularly well suited for SPPoS as they cannot cause side reactions.

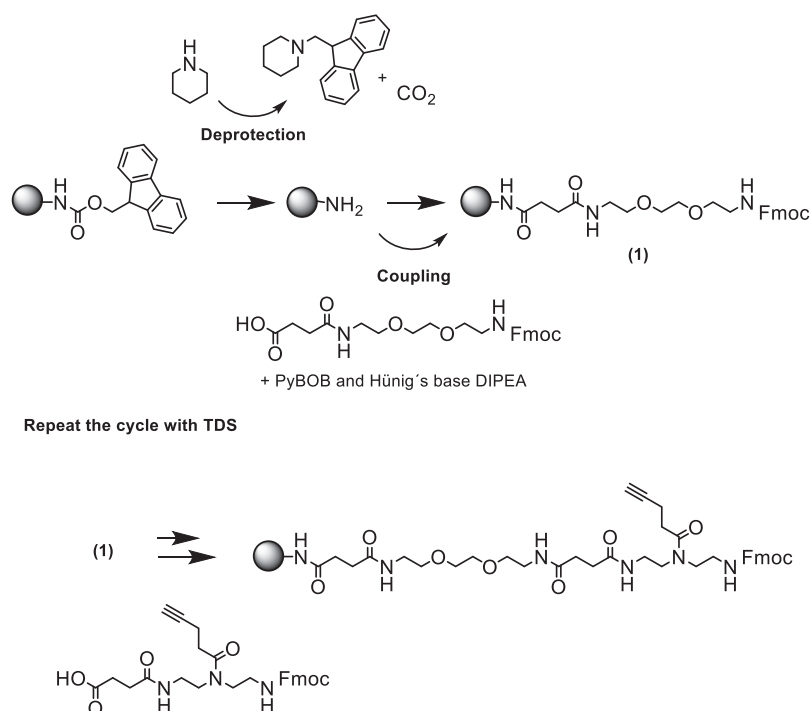


Figure 3: Exemplary synthesis steps of a SPPoS of an oligo(amidoamine) consisting of an EDS and a TDS building block.

In the next step, the resin is deprotected with a piperidine solution.^[33] The piperidine deprotonates the fluorene at the non-aromatic ring carbon, resulting in Hückel aromatisation. The elimination mechanism E1CB is triggered and causes the release of carbon dioxide and 9-methylene fluorene, which is trapped by excess piperidine (in a Michael-like electrophilic addition reaction). After intensive washing with DMF, the first component EDS can be coupled in DMF. The building block and its carboxy group are first activated to form an amide bond. In the chosen PyBOP-mediated coupling, the carboxy group is first activated by deprotonation with DIPEA (diisopropylethylamine), and the resulting carboxylate then reacts with the positively charged phosphorus of PyBOP, splitting off hydroxybenzotriazolate (see Figure 4). The resulting active carboxylic acid phosphoric anhydride can

react with the free amine of the resin to form an amide, with deactivated tripyrrolidinophosphine oxide being cleaved off.^[35]

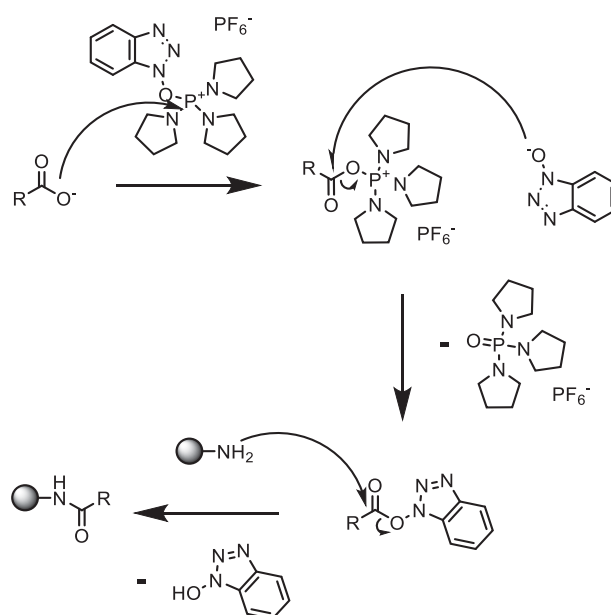


Figure 4: Coupling mechanism of PyBOB for the SPPoS.

After completion of the coupling reaction, the excess of starting materials, all coupling reagents and their degradation products are removed by intensive washing. The backbone of the oligo(amidoamine) can be obtained by another cycle of Fmoc cleavage and TDS coupling.

After completion of the oligomer structure, functionalisation of the TDS, here using 2-azidoethyl- α -D-mannopyranoside as an example, is possible by a CuAAC click reaction (see Figure 5). The CuAAC click reaction (Copper (I) -catalyzed azide-alkyne cycloaddition) used in this work is an advanced copper-catalyzed (2 + 3) cycloaddition of an azide and an alkyne.^[36] The postulated mechanism of the copper (I)-mediated azide-alkyne cycloaddition to a 1,4-functionalised 1,2,3-triazole is explained below.

Essential as a catalyst for the reaction is the oxidation-sensitive copper (I), which is obtained in the reaction mixture by adding sodium ascorbate as a reducing agent to copper (II).^[37] The reaction begins with the twofold coordination of the catalyst copper (I) to the alkyne, whereby the alkyne is deprotonated. The first ring formation from the coordinated alkyne with the azide occurs via the doubly coordinated copper. Subsequently, the ring system is reduced in size, first releasing a copper metal by forming a five-membered ring system, and finally the second copper (I) is replaced by a proton.^[59,60] With the CuAAC click reaction, motifs can be stereoselectively conjugated to the oligomeric structure via a 1,4-functionalised 1,2,3-triazole.

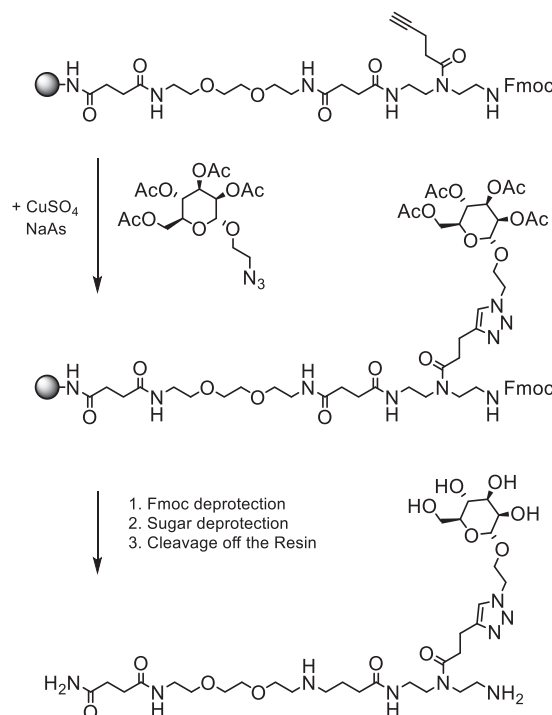


Figure 5: First, the conjugation of the 2-azidoethyl- α -D-mannopyranoside unit via CuAAC click reaction to the oligomer consisting of EDS and TDS is shown and secondly, the final deprotection plus the cleavage off the carrier resin.

In the final step, the finished oligomer can be cleaved from the resin. In the selected Tentagel S-RAM resin, the cleavage solution consists of 95 % TFA (trifluoroacetic acid) and 5 % triisopropylsilane, a hydride donor scavenger. At the linker, the trifluoroacetic acid cleaves the site of the first built-up amide bond, which is activated by the substituents 2,4-dimethoxyphenyl and 4-methoxyphenol, into an oligo(amidoamine) with a terminal carboxamide. After cleavage, the hydride donor scavenger hydrates the cationic linker residues, preventing further reaction with the oligo(amidoamine). The oligo(amidoamine) can then be isolated from the impurities of the cleavage process by transferring the entire cleavage solution to diethyl ether. If the desired purity is not achieved by freeze-drying, the product can be further purified by preparative HPLC (high performance liquid chromatography). The idea of SPPoS, therefore, is to obtain non-natural functional polyvalent macromolecules that have targeted physicochemical properties and architectures so that they can have new applications in biomedicine, e.g. cancer therapy as well as biochemistry.^[38,39] Crucial for functionality for diverse applications is that the polyvalent ligands interact specifically with the desired receptor. Receptors can be considered to be either a molecule or a surface such as a protease, protein or cell. The different binding mechanisms of the multivalent ligand with the receptor are described by the principles of multivalency.

1.2 Multivalency

Multivalent interactions can be used universally for targeted binding enhancement between different ligands and receptors. The binding partners form multiple weak ligand-receptor interactions, which lead to an increase in avidity in an additive manner.^[40] In contrast to multivalent interactions, single monovalent binding is often too weak and only through the interaction of multivalent binding events can this stronger binding be achieved.^[41] However, the multivalent binding process remains reversible, which is crucial for processes that require a limited contact time. Cell-cell communication can be cited as an example of a reversible process enabled by multivalency. Overall, multivalent interactions are essential in biological systems such as recognition, adhesion and signalling processes.^[42]

The multivalent binding mechanisms can be broadly classified into four different multivalent binding modes:^[42-47] These four multivalent binding mechanisms are chelation, statistical rebinding, clustering and steric shielding. The four different modes are exemplified in Figure 6 for a trivalent ligand and a tetravalent receptor.

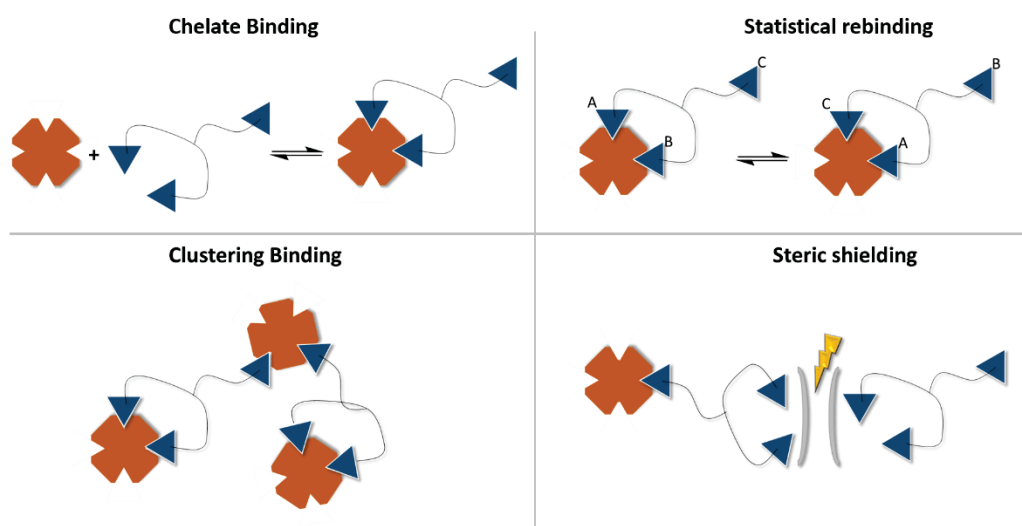


Figure 6: Illustrated are the four multivalent binding mechanisms chelate binding, statistical rebinding, clustering and steric shielding.

The establishment of binding of a multivalent ligand to a multivalent receptor initially occurred through translational, entropic losses.^[48] The subsequent binding events proceed without further energy losses for ligands with rigid scaffolds and with the same energy losses per further binding event for flexible scaffolds.^[49] If the ligand and receptor are already in contact, the four different modes can occur.

The first binding mode is the chelating effect, which describes the multiple binding of a multivalent ligand to a multivalent receptor. To the first binding event from the ligand to the receptor, another binding motif of the ligand can bind to another receptor site.^[50,51] This binding process is entropically favoured by the release of the maximum number of free-moving components.^[40]

The second mode for multivalent ligands is random rebinding. It is based on reversible binding of motifs at the binding site, where a free binding motif of the ligand displaces the previously bound binding motif. Similarly, dissociation of a bound binding motif of the ligand can be followed by rapid reassociation by an adjacent binding motif of the ligand. The overall binding strength of the multivalent ligand to the receptor is increased by the chelating effect and random back-binding.^[52,53]

Clustering is the combination to aggregation of multivalent ligands with receptors. Depending on the concentration of ligand and receptor, one ligand can bind multiple receptors as a cross-linker, forming agglomerates.^[42]

Fourthly, steric shielding is important. Here, an unbound part of a bound multivalent ligand can protect the formed ligand-receptor complex from further competing ligands.^[40,54,55] The unbound part of the ligand can be both free binding motifs and the backbone of the ligand that is not involved in the binding, thus achieving the shielding.

2. Ligands for multivalent presentation

2.1 Carbohydrates as natural binding motifs and carbohydrate based amphiphiles

One of the most important building blocks in a living organism are carbohydrates. The research field of glycobiology encompasses the study of carbohydrates in biological processes, e.g. their binding to proteins or lipids.^[2] Since Dwek first demonstrated the importance of carbohydrates in living organisms for information storage and release, signal transduction and pathogen recognition in 1988, scientific interest has increased rapidly. Today, carbohydrates are considered essential components of cell adhesion, cell communication, signal transduction and pathogen recognition in bacterial or viral infection.^[55-62] However, knowledge of carbohydrates in biological processes has been slow to be gained because carbohydrates have a high structural complexity. For example, two monosaccharides can be linked together at different sites, as each hydroxyl group can potentially serve as a glycosidic bond. In addition, saccharides also have conformational differences for some binding positions, resulting in sixteen different disaccharide structural variants for just two monosaccharides. This diversity of possibilities can generate specific information, as different monosaccharides can be linked in a variety of different arrangements. In addition, saccharides can also interact with receptor proteins, and it is even possible to achieve a high selectivity and affinity of the interactions.

This approach led to the development of carbohydrate-presenting macromolecules for science that mimic the structural properties of their natural counterparts, with a simplification of the structural complexity of these carbohydrate ligands. The reduction in complexity of these carbohydrate ligands is the removal of all unnecessary carbohydrate units that presumably do not show binding to a

receptor, and in their place build an artificial scaffold to which the carbohydrates are bound. This approach has made the so-called glycomimetics more accessible and can subsequently reveal diverse architectures.

Over the years, a large number of different glycomimetics have been introduced with different architectures to investigate the influence of carbohydrate presentation as well as the physicochemical properties of the scaffold. Glycomimetics range from low molecular weight compounds to high molecular weight, multivalent macromolecules and polymers.^[63,64] Glycomimetics can be linear^[65], as dendrimers^[66,67] as well as star-shaped^[68] or even glycopolymers^[69] (see Figure 7). The carbohydrate-presenting macromolecules are particularly exciting, as they can serve as model substances for initial results up to pharmaceutically active compound.^[70-71]

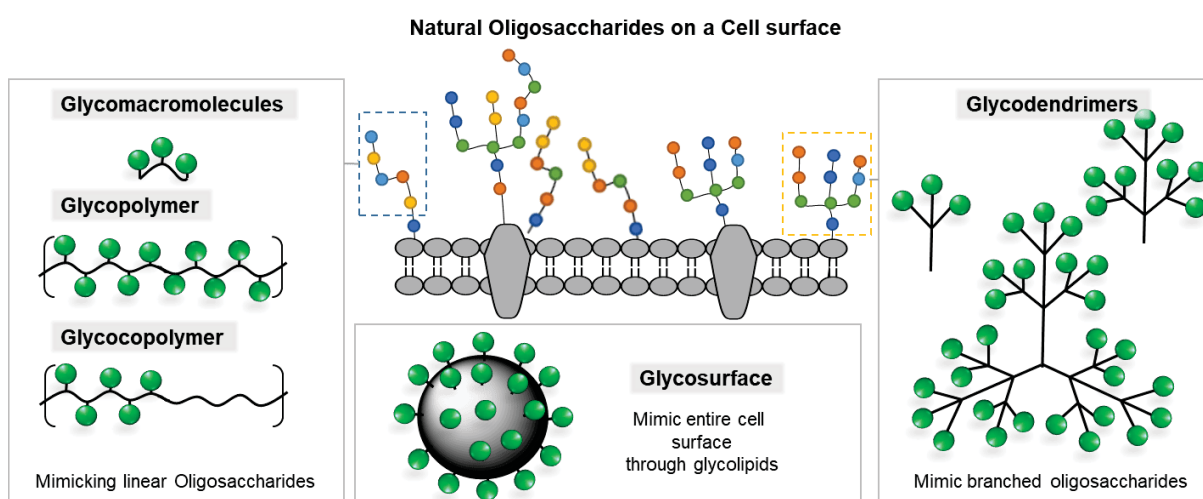


Figure 7: Schematic structure of the natural oligosaccharides on the cell surface and the various mimicking artificial macromolecules, dendrimers as well as a replica of the cell surface by glycolipids assembled into a micelle itself.^[72]

In the research field of glycomimetics, Hartmann and co-workers have synthesised some solid-phase glycooligo(amidoamines) in recent years to explore their binding behaviour with various lectins. The first examples of glycooligo(amidoamines) were linear in structure and, after their synthesis, were tested for their binding behaviour to the tetrameric lectin Concanavalin A.^[20,27,29,30] This lectin is isolated from jack bean and binds selectively to Mannose and Glucose at different intensities and explicitly not to Galactose. The surface plasmon resonance assay (SPR) against Con A showed a higher affinity at higher degrees of functionalisation of carbohydrates.^[29] Subsequently, the architectures gradually became more complex. For example, Baier et al. were able to synthesise branched glycomacromolecules, whereby the branches differed in their valence and degree of branching. By means of SPR assays, it could be shown that not only a higher valence of the investigated molecules

causes an increase in affinity, but also the degree of branching, whereby a higher degree of branching also leads to an increase in affinity.^[73] Furthermore, larger architectures such as sequence-controlled glycopolymers were synthesised by Gerke et al. For this, he used di-cysteine-functionalised glycooligo-(amidoamines), which were reacted with di-alkene-functionalised oligomers by means of a polythiolene reaction.^[72] In the binding studies with Con A, it turned out that above a certain ligand valence, a further increase in receptor clustering cannot be achieved by increasing the carbohydrates valency. In addition to the single ligands, glycolipids that subsequently self-assemble into supramolecular micelles are also exciting mimetics, as they can mimic a simplified cell with an exposed carbohydrate envelope.^[74] Hartmann and co-workers were also able to achieve new research findings in this research area of glycolipids. Banger et al. were able to synthesise sequence-defined amphiphilic glycoligomers that assemble into micelles, demonstrating their potential as inhibitors of bacterial adhesion, which may lead to biomedical applications in the medium term.^[75] Other work also showed that a key ingredient for bioactive micelles can be saccharide compounds, which enable specific interactions with e.g. proteins and cells. For example, trisulfated monosaccharide in a peptide amphiphile was able to mimic a natural polysaccharide- heparin sulfate, demonstrating biological functions in bone regeneration.^[76]

2.2 Guanidiniocarbonylpyrrole

Besides to natural binding motifs, non-natural binding motifs also have enormous importance. For chemists as well as biologists, it is important to obtain ligands that specifically recognise, target or inhibit proteins, as they can thus contribute to the understanding and control of biological processes. An important goal of research is to achieve high affinity and selectivity to the respective binding epitopes, such as functional amino acids. Examples of non-natural binding motifs are crown ether derivatives or the tweezer for binding to lysines.^[77-79] In addition, cucurbituriles for binding to aromatic amino acids such as phenylalanine, tyrosine have been used in the literature.^[80]

Another non-natural supramolecular binding motif is guanidiniocarbonylpyrrole (GCP), which was established by Schmuck et alii.^[81] The GCP motif is an arginine mimetic that binds oxyanions via a hydrogen bridge-supported ion pairing.^[82,83] However, the combination of the guanidinio functionality with the carbonylpyrrole building block results in decisive advantages due to the physicochemical properties of the artificial binding motif in comparison to the natural amino acid. On the one hand, the motif is able to bind oxoanions electrostatically, supported by a network of three hydrogen bonds, and thereby achieves a significantly stronger affinity than natural amino acids (principle of action of the GCP motif is shown in Figure 8).^[82-85]

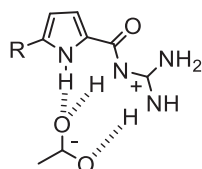


Figure 8: Binding mode of the guanidinocarbonyl pyrrole ligand with a carboxylate^[82,85]

Furthermore, the electron-withdrawing effect of carbonylpyrrole lowers the basicity of the linked guanidino group from a pKs of about 12 to about 6.6, which allows the binding motif to be present under physiological conditions to a considerable extent unprotonated.^[85] Due to the two advantages a large number of GCP-functionalised ligands have been synthesised on this basis in recent years.^[83-85] Among other things, Schmuck et al. were able to achieve a non-competitive inhibition of the protease β -tryptase with a four-armed peptide ligand containing a GCP motif at the end of each arm, thereby blocking the active side of the protease.^[17] Furthermore, the protein 14-3-3 could be targeted with a two-armed peptide ligand with two GCP motifs and a fluorescent dye, leading to specifically detected through fluorescence increase.^[83]

3. Aggregation-induced Emission

In 1954, Förster and Kasper discovered that the fluorescence of pyrene weakens with increasing concentration in solution.^[86] This concentration weakening effect was explained by the formation of sandwiched excimers of aromatic molecules in the excited state, which cause concentration quenching.^[87] In this state, the "solute" molecules are in the immediate vicinity, exposing the aromatic rings of the neighbouring fluorophores to strong π - π stacking interactions, which promotes formation of aggregates with ordered or random structures. In the excited state, the aggregates then often decay via a non-radiative transition known as aggregation-caused quenching (ACQ).^[88-90] As a result, researchers were forced to study all experiments in very dilute solutions, but this presented some difficulties. For example, it was difficult to achieve sufficient sensitivity in fluorescence sensing experiments in dilute solutions.^[91-93]

It was not until 2001 that Tang and co-workers discovered a valuable tool for fluorescence engineering as well as sensing.^[94-97] The phenomenon of aggregation-induced emission (AIE) was discovered, in which an enhancement of emission could be achieved by the formation of aggregates.^[98,99] It allowed the use of dye solutions of arbitrary concentration for bioassays as well as sensing. Since the AIE luminophor is non-emissive in solution, but becomes strongly emissive through the formation of aggregates with strong p-p stacking interactions or the restriction of their intramolecular rotation by binding. In the latter, restricting their intramolecular rotation and vibration (RIR and RIV) favours radiative transitions from the excited state of the luminophore.^[100]

Over the last decade, researchers have developed a large number of new AIE luminophores and found applications especially in the field of optoelectronics and sensor technology.^[101] One of the most widely used AIE luminophores is tetraphenylethene (TPE), which has found applications as chemical sensors or bioprobes.^[102,103] The structure of the TPE luminophore is shown in Figure 9.

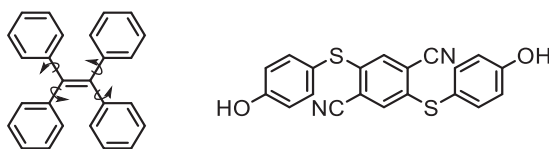


Figure 9: Shown are the two AIE luminophores TPE (left) and ATE (right). For TPE the rotation is illustrated, which takes place in a dissolved state without fluorescence appearance and on the right side for ATE the rigid fluorescent state is shown.

The ethenyl center of the luminophore can be seen as stator and the four phenyl substituents as rotors. In solution, intramolecular rotation of the phenyl rings occurs via the C-C single bonds to the center. Due to the rotations and the vibrations that also take place in solution, the previously absorbed energy is released by the luminophore into the environment without radiation. In the case of aggregation, the luminophore's ability to rotate is severely restricted, so that non-radiative transitions are inhibited. The resulting emission as transition from the excited to the ground state can be observed for AIE luminophores.

Besides the well-known TPE, a number of new AIE luminophores have been synthesized recently. Another recently developed group of AIE luminophores are the aromatic thioethers (ATE), which were developed within the working group around J. Voskuhl.^[104,105] Here, it has been possible to incorporate various substitution patterns and the introduction of different functional groups, and thus to directly influence the photophysical properties of the derivatives. The range of emission for the differently substituted derivatives ranged from 437 to 588 nm. Current applications include aromatic thioether luminophores for the detection of spermine or Concanavalin A and *Escherichia coli* bacteria.^[106-107]

4. Motivation

Many important functions in nature are based on sequence-defined macromolecules such as information storage and translation in DNA and RNA.^[108-110] Another important class of sequence-defined biomacromolecules are proteins fulfilling numerous functions e.g. as enzymes, antibodies or toxins. Their function is determined by the composition and structure, which is encribed in their primary sequence – the sequence of amino acids along the protein chain.^[111] Therefore it has been rationalized that by creating non-natural macromolecules with a monomer sequence similar to the biomacromolecules, new properties and functions should become accessible also for such synthetic materials. Indeed, it is now well understood that sequence-defined synthetic macromolecules enable functions such as data storage. Furthermore, they can be designed and applied to selectively interact with biomacromolecules such as proteins.^[38,111-116] It is particularly relevant to explore synthetic ligands as modulators of protein-protein interactions either promoting or blocking such interactions. Thereby they offer opportunities as probes to gain new insights into protein-protein interactions but also for potential treatment e.g. in cancer therapy.

The goal of this thesis is to explore previously introduced oligo(amidoamine) scaffolds for the multivalent presentation of natural and non-natural ligands, namely carbohydrate ligands and GCP motif, to derive modulators of protein interactions. Specifically, in the first part, an inhibition of the oncologically relevant protease Taspase1 is aimed at by developing PEGylated and non-PEGylated macromolecular ligands. As binding motifs, GCP will be conjugated either homomultivalent or heteromultivalent with additional lysines on the macromolecules. The aim is to bind to the Taspase1 surface and inhibit its interactions with its partner protein.

Since reading out protein-ligand interactions often proves difficult, AIE luminophores should be introduced for the first time into sequence-defined oligo(amidoamines) and tested for their capabilities as detection probe. This should be tested for both GCP and carbohydrate binding motifs to identify potential applications of AIE-oligomer conjugates. Therefore, a series of monovalent GCP oligo(amidoamines) with an AIE luminophore should be synthesised, with the AIE luminophore inserted at different positions within the compound. The aim of this part is to identify the optimal position of the AIE luminophore within a macromolecule and to investigate their detection potentials. In addition, for the AIE oligomer conjugates with carbohydrate binding motifs, their detection properties for different lectins should be investigated, with particular attention to the extent to which clustering affects the AIE effect.

Finally, the concept of AIE oligomer conjugates with carbohydrate-binding motifs will be extended to include the concept of amphiphiles. The principle of amphiphiles enables a divergent multivalent presentation of sequence-defined oligo(amidoamines) through the process of self-aggregation, which also corresponds to a form of cluster formation. The properties of the AIE surfactants will be analysed by means of fluorescence spectroscopy, focusing on the targeted formation and reduction of clusters.

5. Results

5.1 PEGylated sequence-controlled macromolecules using supramolecular binding to target the Taspase1/Importin α interaction

Peter Pasch[†], Alexander Höing[†], Serap Ueclue, Matthias Killa, Jens Voskuhl, Shirley K. Knauer, Laura Hartmann

Publication

[†] These authors contributed equally.

Own Contribution:

Collaborative conceptualisation and design of the project. Synthesis and purification of all building blocks (except GCP building blocks). Supervision of oligomer synthesis performed by Hauke Lukas Junghans within his bachelor thesis. Oligomer characterization (LC-MS, NMR, UHR). Evaluation of fluorescence studies. Collaborative manuscript writing.



Cite this: DOI: 10.1039/d0cc07139k

Received 28th October 2020.
Accepted 11th February 2021

DOI: 10.1039/d0cc07139k

rsc.li/chemcomm

PEGylated sequence-controlled macromolecules using supramolecular binding to target the Taspase1/Importin α interaction†

Peter Pasch,^{‡a} Alexander Höing,^{§b} Serap Ueclue,^a Matthias Killa,^c
Jens Voskuhl,^{§c} Shirley K. Knauer^{§*b} and Laura Hartmann^{§*a}

A novel strategy to inhibit the oncologically relevant protease Taspase1 is explored by developing PEGylated macromolecular ligands presenting the supramolecular binding motif guanidiniocarbonylpyrrole (GCP). Taspase1 requires interaction of its nuclear localization signal (NLS) with import receptor Importin α . We show the synthesis and effective interference of PEGylated multivalent macromolecular ligands with Taspase1–Importin α -complex formation.

Proteins are an important class of biomacromolecules and their interactions play key roles in almost every process of a living organism. Understanding and manipulating protein interactions offers the opportunity to treat or fight diseases.¹ Many protein–protein interactions rely on so-called multivalent binding events where multiple sites of the proteins have to interact simultaneously in order to create a strong binding.^{2,3} Accordingly, synthetic molecules to interfere with protein binding often are multivalent constructs as well, consisting of a synthetic scaffold presenting multiple binding units. The design of multivalent molecules is as diverse as the protein targets they address – one important class of scaffolds being polymers due to their synthetic ease and variability.^{3,4}

Today, polymer chemistry offers a new tool: the synthesis of sequence-controlled macromolecules. Different synthetic strategies have been introduced for the synthesis of sequence-controlled polymers and give access to multifunctional macromolecules with high levels of structural and thereby potentially also functional

control.⁵ We have developed the so-called solid phase polymer synthesis, where we employ standard peptide chemistry and tailor-made non-natural building blocks to generate sequence-defined macromolecules presenting different binding units such as carbohydrates, peptides or catechols. We have successfully demonstrated that through control over the monomer sequence and thereby parameters such as the number and position of binding units, architecture and conformation of the macromolecule, new and improved modulators of protein interactions are accessible.⁶

In this work, we extend on our previous concept with a non-natural supramolecular binding motif, the guanidiniocarbonylpyrrole (GCP) motif,⁷ an arginine mimetic that binds oxoanions via a hydrogen-bond-assisted ion pairing⁸ and shows significantly stronger affinity than natural amino acids.⁹ Our goal is to create macromolecular inhibitors of Taspase1 protease (Fig. 1). From proliferation to differentiation right up to apoptosis, almost every cellular process is regulated by or involves proteases.^{10,11} One of the 28 threonine proteases encoded in the human genome is the tumor-relevant Threonine aspartase 1 (Taspase1).^{10,12} It is usually expressed during embryonic development, but it is re-expressed in many tumor cell lines, and a knockout decreases proliferation and promotes apoptosis in correlation to their potential drug target in tumor therapy. Surprisingly, earlier studies revealed that Taspase1 is not affected by general former Taspase1 expression levels^{13,14} making Taspase1 a protease inhibitor.^{12,14,15} Previous studies focused on the enzymatic activity of Taspase1.^{13,15–17} In this study, we aim at a different inhibition mechanism for Taspase1 by targeting functionally relevant interactions with the import receptor Importin α .^{18,19} While Taspase1 effectively cleaves other pro-enzymes as a heterodimer consisting of the subunits α (25 kDa) and β (20 kDa), Taspase1 itself is also expressed as an inactive α/β -monomer (45 kDa) and undergoes autoproteolytic activation.^{12,20,21} Autoproteolysis is supposed to take place inside the nucleus where Taspase1 is transported by interaction of its bipartite nuclear localization signal (NLS) located in the Taspase1 α -subunit (Fig. 1B) with Importin α .^{18,19,21} In the nucleus, the Taspase1 monomer undergoes

^a Department for Organic Chemistry and Macromolecular Chemistry, Heinrich Heine University Düsseldorf, Universitätsstraße 1, Düsseldorf 40225, Germany. E-mail: laura.hartmann@hhu.de

^b Department for Molecular Biology II, Center of Medical Biotechnology (ZMB) University Duisburg-Essen, Universitätsstrasse 5, Essen, 45117, Germany. E-mail: shirley.knauer@uni-due.de

^c Faculty of chemistry (Organic Chemistry), University of Duisburg-Essen, Universitätsstrasse 7, 45141 Essen, Germany

† Electronic supplementary information (ESI) available. See DOI: 10.1039/d0cc07139k

‡ These authors contributed equally.

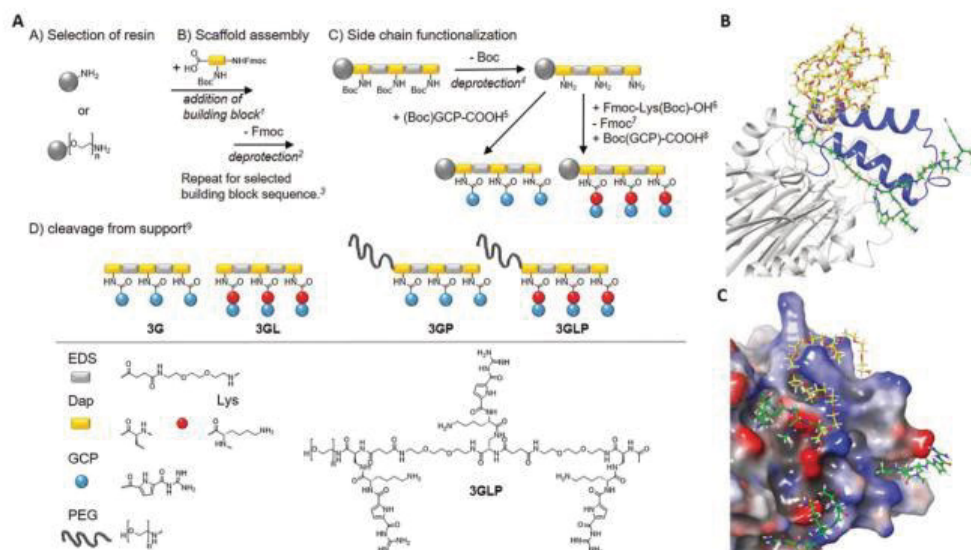


Fig. 1 Synthesis of GCP macromolecules using solid phase polymer synthesis (left) and a model of a supramolecular ligand blocking the NLS of Taspase1 (right). (A) Reaction conditions: ¹5 eq. building block, 5 eq. PyBOP, 10 eq. DIPEA in DMF, 90 min, ²25v% piperidine in DMF, 20 min, ³Next Fmoc-deprotection and acetylation of N-terminus (Ac₂O, 20 min), ⁴4 M HCl in dioxane, 20 min (on-resin cleavage of Boc), ⁵5 eq. (Boc)GCP-COOH, 5 eq. PyBOP, 10 eq. DIPEA in DMF, 90 min (double coupling), ⁶5 eq. Fmoc-Lys(Boc)-OH, 5 eq. PyBOP, 10 eq. DIPEA in DMF, 90 min (double coupling), ⁷25v% piperidine in DMF, 20 min, ⁸5 eq. (Boc)GCP-COOH, 5 eq. PyBOP, 10 eq. DIPEA in DMF, 90 min (double coupling), ⁹TentaGel® S RAM: 5% triisopropylsilane, 95% TFA, 90 min, TentaGel® PAP: TFA/thioanisole (95:5), 24 hours. PEG chain *n* = 70 (MW = 3106.7 g mol⁻¹). (B) Model of a supramolecular ligand blocking the NLS of Taspase1. (C) Schematic illustration of **3GLP** (green) as it addresses carboxylates near the loop (blue) while the PEG (yellow) masks the cationic loop. (bottom): the carboxylates (red) are addressed with GCP (green) and the cationic loop (blue) is masked by the PEG chain (yellow). The model is based on the literature.²⁸

autoproteolysis, and the two subunits reassemble to form the active Taspase1 heterodimer.^{12,21} Thus, interaction of the Taspase1 NLS with Importin α is pivotal for activation. Here, we aim at developing ligands that effectively block the NLS and thereby inhibit Importin α -complex formation as the first step of Taspase1 activation. Since basic amino acid clusters constituting the bipartite NLS of Taspase1 are flanked by multiple anionic amino acids such as aspartic and glutamic acids (see Fig. 1C), we envision that macromolecules presenting multiple oxo-anion binding motifs, GCP, should allow for binding to this site of the protein. It was previously shown that multivalent GCP ligands allow for the design of high affinity ligands by addressing multiple binding sites within a protein structure and can be used for stabilization of protein-protein complexes.²² Here we now want to realize both high affinity binding to the NLS and at the same time effective inhibition of binding to Importin α . We rationalize that in order to achieve both, we require two features of the macromolecular ligand – one segment presenting multiple GCP motifs able to address anionic amino acids in the NLS domain but that do not mediate binding with Importin α , and a second segment, ideally non-binding and sterically demanding to shield the NLS domain from any further interaction. This design is thus based on the general concept of sterical shielding for multivalent ligands to achieve inhibition.^{3,23}

For the first segment, we employ the previously established synthesis of sequence-controlled macromolecules (Fig. 1A).^{24,25} *Via* stepwise addition on a solid support, a monodisperse, sequence-controlled scaffold is assembled and used for site selective attachment of GCP motifs.²⁶ Here we used a previously developed EDS building block (4-((2-(2-(2-aminoethoxy)ethoxy)ethyl)-amino)-4-oxobutanoic) introducing hydrophilic ethylene glycol units within the backbone.²⁵ Fmoc-Dap(Boc)-OH (N_ε-Fmoc-N_α-Boc-L-2,3-diaminopropionic acid) was applied for attachment of GCP on the side chains: Dap side chains were deprotected on the solid support cleaving the Boc protecting groups and releasing primary amines for further functionalization with carboxylated GCP-derivative (see the ESI†). In order to further increase the affinity of GCP towards anionic amino acids, lysine as a cationic amino acid was added next to the GCP side chain by including an additional Fmoc-Lys(Boc)-OH during side chain assembly. Two different macromolecules were synthesized introducing three GCP side chains (**3G**) as well as Lys-GCP side chains (**3GL**). Model calculations suggest that multiple amino acids could be addressed *via* trivalent GCP macromolecules with one EDS as a spacer in between the binding motifs (Fig. 1). As our second segment in order to create GCP macromolecule inhibitors, we chose poly(ethylene glycol) (PEG) of 3 kDa that can be easily installed by starting the solid phase assembly from a PEG-preloaded resin giving PEGylated GCP



macromolecules **3GP** and **3GLP**. PEG is well known as a so-called stealth polymer to minimize non-specific interaction with proteins and to act as a steric shield blocking protein–protein interactions.²⁷ All macromolecules were cleaved off the resin, purified by preparative HPLC, isolated by freeze drying with relative purities >95% (as determined by RP-HPLC) and further characterized by ¹H-NMR, UHRMS and MALDI-ToF analysis (see the ESI†).

First, we looked at the direct binding of our ligands to Taspase1 by successfully setting up a surface plasmon resonance (SPR) assay (see the ESI†). Applying isothermal calorimetry was not successful at this time (see the ESI†). Monovalent macromolecules presenting only one GCP unit showed no binding and thus were omitted from any further testing (see the ESI†). For the trivalent macromolecules, binding is in the μM range as was expected based on previous GCP ligands (Fig. 2).²⁹

We observe a clear increase in binding upon introduction of the lysine residues next to the GCP unit, indicating an increase in affinity through the additional cationic moieties. Surprisingly, for **3G** we see an increase in binding upon introduction of the PEG block (**3GP**) which might be attributed to the higher molecular weight of this ligand and slower diffusion, as PEG itself showed no binding (see the ESI†). However, we did not see such increase for **3GLP**.

We next performed an *in vitro* pull-down assay to investigate the proposed inhibitory effect on the interaction between Taspase1 and Importin α . For this, we used recombinant GST-Importin α protein bound to a GSH matrix and added Taspase1-His pre-incubated with the respective ligands (see the ESI†). Unbound protein was removed and the Taspase1 bound to the matrix *via* its interaction with Importin α eluted. The samples were then analyzed by SDS-PAGE and Western Blotting. To validate our working hypothesis that only the PEGylated compounds will disrupt the protein interaction, we first compared the ligands (**3GP**, **3GLP**) and the controls (PEG alone, the non-PEGylated ligands **3G** and **3GL**) directly (Fig. 3). Indeed, the interaction between Taspase1 and Importin α was effectively disrupted by the pre-incubation of Taspase1 with the PEGylated GCP-ligands. Interestingly, ligands missing the PEG stealth block failed to interfere with Taspase1–Importin α complex formation

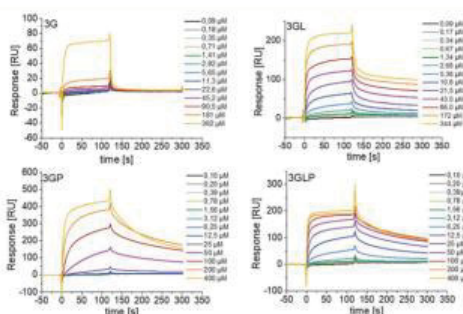


Fig. 2 SPR sensograms showing direct binding of trivalent GCP-ligands with and without PEG to immobilized Taspase1. Monovalent GCP-ligands showed no binding (see the ESI†).

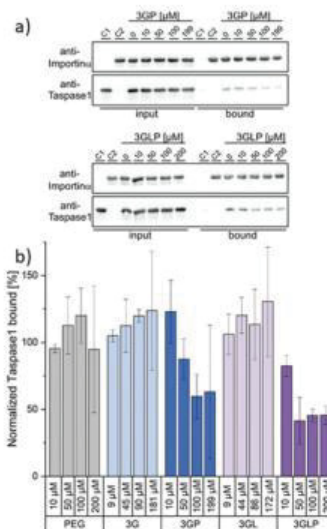


Fig. 3 The interaction between Taspase1 and Importin α is effectively disrupted by PEGylated GCP-ligands: (a) Exemplary blots from pull-down assays with increasing concentrations of the PEGylated GCP-ligands **3GP** and **3GLP** (see the ESI† for other samples). Column-bound protein fraction after the pull-down in comparison to the input initially present on the column. Controls: only Taspase1 (C1) or GST–Importin α (C2) were added to the column. (b) Densitometric quantification of pull-down assays, comprising the mean of three replicates \pm standard deviation.

and so did PEG itself. This suggests that the GCP-motif guides the ligand to Taspase1, but is not able to shield the NLS directly, in line with our model (Fig. 1). Furthermore, the PEG block itself does not affect the interaction and therefore does not ensnare the NLS while unguided. Thus, the introduction of the stealth block PEG to the guiding GCP-block is a necessary step for the ligands to act as inhibitors. Densitometric quantification of Western Blot analysis revealed a slightly increased effect of the lysine-containing ligand **3GLP** (40% Taspase1 bound) compared to **3GP** (55% Taspase1 bound) (see the ESI†). To further compare the PEGylated ligands that differ in their binding motifs (GCP and GCP plus lysine) **3GP** and **3GLP** were tested at different ligand concentrations ranging from 0 μM to 200 μM in the pull-down assay and the results were again quantified (Fig. 3). **3GP** effectively hampered the interaction already at 50 μM (87% Taspase1 bound). Increasing the concentration to more than 100 μM (59% Taspase1 bound) was not able to additionally fortify its effect. As seen in the direct binding study *via* SPR, addition of lysine next to the GCP motifs increased the apparent affinity. We hypothesize that this, when combined with the PEG segment, should also give more efficient inhibitors. Indeed, **3GLP** was effective already at 10 μM (82% Taspase1 bound), and its potency reached a limit at a concentration of 50 μM (41% Taspase1 bound). Importantly, we did not observe a comparable effect when using the PEG control or the non-PEGylated ligands



(see the ESI†), nor was the binding of Importin α to the column affected by the PEGylated ligand (see the ESI†).

In conclusion, we explored the concept of multivalent ligands for sterical shielding and developed structure-guided PEGylated sequence-controlled macromolecules for Taspase1 using GCP as a binding motif. We further showed that these ligands could effectively be used to disrupt the functionally relevant interaction with Importin α in a concentration-dependent manner, thereby exploiting a novel inhibition mechanism for this protease. Future studies will include investigations concerning the potential selectivity of the ligands as well as their potential for cellular studies. As a first prerequisite, the ligands were tested in a cell viability assay and showed no toxicity (see the ESI†).

The authors acknowledge the CRC 1093 funded by the "Deutsche Forschungsgemeinschaft"

Conflicts of interest

There are no conflicts to declare.

Notes and references

- H. Lu, Q. Zhou, J. He, Z. Jiang, C. Peng, R. Tong and J. Shi, *Signal Transduction Targeted Ther.*, 2020, **5**, 213.
- (a) E. Mahon and M. Barboiu, *Org. Biomol. Chem.*, 2015, **13**, 10590–10599; (b) C. T. Varner, T. Rosen, J. P. Martin and R. S. Kane, *Biomacromolecules*, 2015, **16**(1), 43–55.
- M. Mammen, S.-K. Choi and G. M. Whitesides, *Angew. Chem., Int. Ed.*, 1998, **37**, 2754–2794.
- (a) C. Fasting, C. A. Schalley, M. Weber, O. Seitz, S. Hecht, B. Koksch, J. Darnedde, C. Graf, E.-W. Knapp and R. Haag, *Angew. Chem., Int. Ed.*, 2012, **51**, 10472–10498; (b) C. R. Becer, *Macromol. Rapid Commun.*, 2012, **33**, 742–752.
- (a) S. C. Solleder, R. V. Schneider, K. S. Wetzel, A. C. Boukis and M. A. R. Meier, *Macromol. Rapid Commun.*, 2017, **38**, 1600711; (b) S. A. Hill, C. Gerke and L. Hartmann, *Chem. – Asian J.*, 2018, **13**, 3611; (c) J. F. Lutz, M. Ouchi, D. R. Liu and M. Sawamoto, *Science*, 2013, **341**(6146), 1238149.
- (a) L. Soria-Martinez, S. Bauer, M. Giesler, S. Schelhaas, J. Materlik, K. Janus, P. Pierzyna, M. Becker, N. L. Snyder, L. Hartmann and M. Schelhaas, *J. Am. Chem. Soc.*, 2020, **142**(11), 5252–5263; (b) S. Boden, F. Reise, J. Kania, T. K. Lindhorst and L. Hartmann, *Macromol. Biosci.*, 2019, **19**, 1800425; (c) L. Fischer, R. C. Steffens, T. J. Paul and L. Hartmann, *Polym. Chem.*, 2020, **11**, 6091–6096; (d) T. Freichel, V. Heine, D. Laaf, E. E. Mackintosh, S. Sarafova, L. Elling, N. L. Snyder and L. Hartmann, *Macromol. Biosci.*, 2020, **20**, 2000163.
- (a) C. Schmuck and M. J. Schwegmann, *J. Am. Chem. Soc.*, 2005, **127**, 3373–3379; (b) D. Maity, A. Gigante, P. A. Sánchez-Murcia, E. Sijbesma, M. Li, D. Bier, S. Mosel, S. Knauer, C. Ottmann and C. Schmuck, *Org. Biomol. Chem.*, 2019, **17**, 4359–4363.
- (a) C. Schmuck, *Coord. Chem. Rev.*, 2006, **250**, 3053–3067; (b) J. Matić, F. Šupljika, T. Tandarić, M. Dukši, P. Piotrowski, R. Vianello, A. Brozovic, I. Piantanida, C. Schmuck and M. R. Stojković, *Int. J. Biol. Macromol.*, 2019, **134**, 422–434.
- (a) C. Schmuck and M. Heil, *ChemBioChem*, 2003, **4**(11), 1232–1238; (b) X. Liu, K. Wang, M. Externbrink, J. Niemeyer, M. Giese and X. Y. Hu, *Chin. Chem. Lett.*, 2020, **31**(5), 1239–1242.
- C. López-Otin and L. M. Matrisian, *Nat. Rev. Cancer*, 2007, **7**, 800–808.
- C. López-Otin and J. S. J. Bond, *Biol. Chem.*, 2008, **283**, 30433–30437.
- J. J.-D. Hsieh, E. H.-Y. Cheng and S. J. Korsmeyer, *Cell*, 2003, **115**, 293–303.
- D. Y. Chen, Y. Lee, B. A. van Tine, A. C. Searleman, T. D. Westergard, H. Liu, H.-C. Tu, S. Takeda, Y. Dong and D. R. Piwnicka-Worms, *Cancer Res.*, 2012, **72**, 736–746.
- D. Y. Chen, H. Liu, S. Takeda, H.-C. Tu, S. Sasagawa, B. A. van Tine, D. Lu, E. H.-Y. Cheng and J. J.-D. Hsieh, *Cancer Res.*, 2010, **70**, 5358–5367.
- S. K. Knauer, V. Fetz, J. Rabenstein, S. Friedl, B. Hofmann, S. Sabiani, E. Schröder, L. Kunst, E. Proschak and E. Thines, *PLoS One*, 2011, **6**, 18253.
- J. T. Lee, D. Y. Chen, Z. Yang, A. D. Ramos, J. J.-D. Hsieh and M. Bogoy, *Bioorg. Med. Chem. Lett.*, 2009, **19**, 5086–5090.
- J. van den Boom, M. Mamić, D. Baccelliere, S. Zweerink, F. Kaschani, S. Knauer, P. Bayer and M. Kaiser, *ChemBioChem*, 2014, **15**, 2233–2237.
- Y. Miyamoto, K. Yamada and Y. Yoneda, *J. Biochem.*, 2016, **160**, 2728–2735.
- B. Bier, S. K. Knauer, D. Docter, G. Schneider, O. H. Kramer and R. H. Stauber, *Traffic*, 2011, **12**, 703–714.
- D. Wunsch, A. Hahnbrock, S. Jung, T. Schirmeister, J. van den Boom, O. Schilling, S. K. Knauer and R. H. Stauber, *Oncogene*, 2016, **35**, 3351–3364.
- A. Corbett, K. Mills, B. A. Lange, M. Stewart, E. Devine and J. C. J. Lange, *Biol. Chem.*, 2007, **282**, 5101–5105.
- L. Bartsch, M. Bartel, A. Gigante, J. Iglesias-Fernández, Y. B. Ruiz-Blanco, C. Beuck, J. Briels, N. Toetsch, P. Bayer, E. Sanchez-Garcia, C. Ottmann and C. Schmuck, *ChemBioChem*, 2019, **20**(23), 2921–2926.
- F. Jacobi, D. Wilms, T. Seiler, T. Queckbörner, M. Tabatabai, L. Hartmann and S. Schmidt, *Biomacromolecules*, 2020, **21**(12), 4850–4856.
- (a) F. Wojcik, S. Mosca and L. Hartmann, *J. Org. Chem.*, 2012, **77**(9), 4226–4234; (b) D. Ponader, F. Wojcik, F. Beceren-Braun, J. Darnedde and L. Hartmann, *Biomacromolecules*, 2012, **13**(6), 1845–1852.
- C. Gerke, M. F. Ebbesen, D. Jansen, S. Boden, T. Freichel and L. Hartmann, *Biomacromolecules*, 2017, **18**, 787–796.
- C. Schmuck, V. Bickert, M. Merschky, L. Geiger, D. Rupprecht, J. Dudaczek, P. Wich, T. Rehm and U. Machon, *Eur. J. Org. Chem.*, 2008, 324–329.
- (a) S. Schöttler, G. Becker, S. Winzen, T. Steinbach, K. Mohr, K. Landfester, V. Mailänder and F. R. Wurm, *Nat. Nanotechnol.*, 2016, **11**, 372–377; (b) S. De Santis, R. Chiaraluce, V. Consalvi, F. Novelli, M. Petrosino, P. Punzi, F. Sciubba, C. Giordano, G. Masci and A. Scipioni, *ChemPlusChem*, 2017, **82**, 241–250; (c) S. Akocak, M. R. Alam, A. M. Shabana, R. Kishore, K. Sanku, D. Vullo, H. Thompson, E. R. Swenson, C. T. Supuran and M. A. J. Ilies, *Med. Chem.*, 2016, **59**, 5077–5088; (d) K. Chitphet, S. M. Geary, C. H. F. Chan, A. L. Simons, G. J. Weiner and A. K. Salem, *Biomater. Sci. Eng.*, 2020, **6**(5), 2659–2667.
- J. van den Boom, F. Trusch, L. Hoppstock, C. Beuck and P. Bayer, *PLoS One*, 2016, **11**(3), 1–13.
- C. Schmuck and V. Bickert, *J. Org. Chem.*, 2007, **72**(18), 6832–6839.

Supporting Information

PEGylated sequence-controlled macromolecules using supramolecular binding to target the Taspase1/Importin α interaction

Peter Pasch^{a†}, Alexander Höing^{b†}, Serap Ueclue^a, Matthias Killa^c, Jens Voskuhl^c, Shirley K. Knauer^{b*} and Laura Hartmann^{a*}

- Department for Organic Chemistry and Macromolecular Chemistry, Heinrich Heine University Düsseldorf, Universitätsstraße 1, Düsseldorf 40225, Germany.
- Department for Molecular Biology II, Center of Medical Biotechnology (ZMB), University Duisburg-Essen, Universitätsstrasse 5, Essen, 45117, Germany.
- Faculty of Chemistry (Organic Chemistry), University of Duisburg-Essen, Universitätsstraße 7, 45117 Essen, Germany.

†These authors contributed equally.

* Corresponding authors.

Materials:

Diethyl ether (with BHT as inhibitor, $\geq 99.8\%$), triisopropylsilane (TIPS) (98%), concentrated hydrochloric acid (pa), acetic anhydride (pa) and formic acid (pa) were purchased from Sigma Aldrich. N,N-Diisopropylethylamine (DIPEA) ($\geq 99\%$) was purchased from Carl Roth. N,N-Dimethylformamide (DMF) (99.8%, for peptide synthesis), piperidine (99%) were obtained from Acros Organics. Dichloromethane (DCM) (99.99%), ethyl acetate (analytical reagent grade) and 1,4-dioxane (analytic reagent grade) were purchased from Fisher Scientific. Acetonitrile was purchased from AppliChem. Trifluoroacetic acid (TFA) (99%), (benzotriazol-1-yl-oxy)tripyrrolidinophosphonium hexafluorophosphate (PyBOP), and triethylsilane (analytical reagent grade) were purchased from Fluorochem. TentaGel® S RAM (Rink Amide) and TentaGel® PAP resins (loading: 0.23 mmol / g) were purchased from RAPP Polymer. N α -Fmoc-N ϵ -Boc-L-lysine ($\geq 98.0\%$) was purchased from Iris Biotech. N α -Fmoc-N β -Boc-L-2,3-diaminopropionic acid ($\geq 98.0\%$) was purchased from TCI. Polyethylene glycol 3000 was purchased from Merck.

Analytical Methods:

Preparative Reversed Phase- High Pressure Liquid Chromatography (prep RP-HPLC)

An Agilent 1260 Infinity device was used to purify the oligo(amidoamines), which is coupled to a variable wavelength detector (VWD) (set to 214 nm) and an automated fraction collector. The RP HPLC column, CAPCELL PAK C18 (20 x 250 mm, 5 μ m), was used. The mobile phases A and B were H₂O and acetonitrile, each containing 0.1 vol% formic acid. The flow rate was set at 15 ml/min.

Reversed Phase- High Pressure Liquid Chromatography- Mass Spectrometry (RP-HPLC-MS)/Electron Spray Ionization- Mass Spectrometry (ESI-MS)

RP-HPLC-MS was carried out on an Agilent 1260 Infinity instrument coupled to a variable wavelength detector (VWD) (set to 214 nm) and a 6120 Quadrupole LC/MS containing an Electrospray Ionization (ESI) source (operation mode positive, m/z range from 200 to 2000). A MZ-AquaPerfect C18 (3.0 x 50 mm, 3 μ m) RP column from Mz-Analysentechnik was used. As eluent system water/acetonitrile containing 0.1 vol% formic acid was applied. The mobile phases A and B were: System A) H₂O/acetonitrile (95/5, v/v); System B) H₂O / acetonitrile (5/95, v/v). The samples were analyzed at a flow rate of 0.4 ml/min using a linear gradient,

starting with 100% of system A) and reaching 100% system B) within 30 min. The temperature of the column room was set to 40 °C. All purities were determined using the OpenLab ChemStation software for LC/MS from Agilent Technologies.

Electron Spray Ionization- Mass Spectrometry (ESI-MS) measurements were performed with the above mentioned ESI source and quadrupole detector.

Ultra High Resolution - Mass Spectrometry (UHR-MS)

UHR-MS measurements were performed with a Bruker UHR-QTOF maXis 4G instrument with a direct inlet via syringe pump, an ESI source and a quadrupole followed by a Time of Flight (QTOF) mass analyzer.

Matrix-Assisted Laser Desorption Ionization-Time of Flight–Mass Spectrometry

(MALDI-TOF-MS) Compounds were detected using a Bruker MALDI-TOF Ultraflex I system with 2,5-dihydroxybenzoic acid (DHB) as matrix. The matrix to compound ratio of was 10:1. Spectra were acquired for reflector mode for a m/z range 2000-20000. The reflector mode was calibrated using a protein mixture.

Nuclear Magnetic Resonance Spectroscopy (NMR)

The ¹H-NMR spectra were recorded on a Bruker Avance III 600 (600 MHz). These spectra were evaluated according to the following scheme: (frequency in MHz, deuterated solvent), chemical shift in ppm (multiplicity, coupling constant, integral, signal assignment). The chemical shift is given in relation to the ¹H signals of the deuterated solvents used (D₂O: 4.79 ppm). The multiplicities of the signals were abbreviated as follows: s (singlet), d (doublet), t (triplet), m (multiplet).

Freeze dryer

The final oligomers were lyophilized with an Alpha 1-4 LD plus instrument from Martin Christ Freeze Dryers GmbH. The drying method was set to -40 °C and 0.1 mbar.

Docking

Maestro 11.5 Schrodinger was used for the images.

DAPGCP, DAPLysGCP and PEG700 were used for the docking. The molecules were prepared with LigPrep. A model of the Taspase1 crystal structure extended by a NMR based structure of the loop (Taspase1_40-420_van_den_Boom [1][2]) was used for the grids.

A grid around the amino acids Arg190/201 Lys 225/218 with a size of 36 Å (Loop), Asp233 with a size of 15 Å, Asp337 with a size of 15 Å and Glu207 with a size of 10 Å were generated with glide grid generator.

The prepared molecules and grids were used for Docking. The method was XP (extra precise) and the sampling was flexible. The following conditions were chosen: sample nitrogen inversions, bias sampling of torsions for amides.

Visualisation of Ligand and Loop

The three DapLysGCPs were dragged to the Asp233, Asp337 and Glu207. The PEG3000 was coiled by hand and put at the loop. After that a minimization was performed.

Cloning

The plasmid for the inactive Taspase1_{D233/T234A} mutant was generated as previously described [3].

The gene for Importina was amplified from a "pc3DNA-Importina-HA" plasmid and the ends modified via PCR (Forward primer: CAGGGGCCCTCCACCAACGAGAATGCTAAT, Reverse primer: TTCGGATCCTTAGAGAAAGTTAAAGGTCCC). The gene, now with overhangs for Apal/BamHI digestion, was cloned in a blunt pJET1.2 vector (Thermo Fisher) according to the CloneJET PCR cloning kit (Thermo Fisher). After transfection of *E. coli* NEB-10 β (New England BioLabs), the plasmid was amplified using the NucleoBond Xtra Midi kit (Macherey-Nagel). The sequence for Importina was then Apal/BamHI cloned into a modified pET-41b vector containing an N-terminal GST tag and a PreScission protease cleavage site (GeneArt). The plasmid was then again amplified using *E. coli* NEB10- β and isolated with the NucleoBond Xtra Midi kit. The sequence was verified by sequencing.

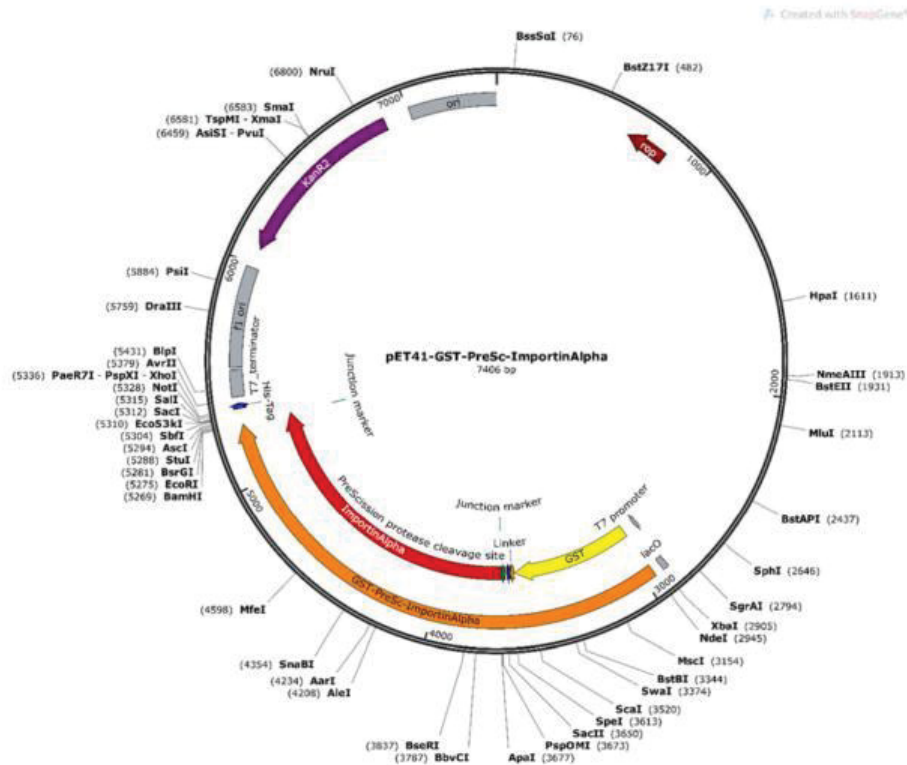


Figure S 1: Map of the plasmide pET41-GST-PreSc-Importina generated by cloning. The map was created using "Gene Construction Kit" (Texco Biosoftware) and visualized with "Snap Gene Viewer" (GSL Biotech).

Purification of recombinant proteins

pET22-Taspase1_{D233A/T234}-His was expressed in *E. coli* BL21 (DE3). The cells were lysed using ultrasonic sheering and enzymatic lysis by lysozyme. The protein was purified using the His tag for affinity chromatography with a HisTrap FF (GE Healthcare). After imidazole elution the Taspase1-His containing fractions were pooled and loaded onto a Superdex 200 HiLoad16/600 column (GE Healthcare) for size exclusion chromatography.

pET41-GST-PreScn-Importin α was expressed in *E. coli* BL21 (DE3), the cells were lysed using sonication and enzymatic lysis by lysozyme and the soluble fraction obtained with centrifugation and filtration. The protein was purified using the GST tag for affinity chromatography with a GSTrap 4B (GE Healthcare). After glutathione elution, the GST-Importin α containing fractions were pooled and loaded onto a Superdex 200 HiLoad16/600 column (GE Healthcare) for size exclusion chromatography. GST-Importin α containing fractions were pooled, frozen in liquid nitrogen and stored at -20°C .

Pull-down assay

For this assay, all solutions were prepared with Dulbecco's Phosphate Buffered saline (Sigma-Aldrich) containing 0,1 % (v/v) Triton X-100 (Carl Roth) and 1 mM DTT (Carl Roth) (PBST), all incubation steps were carried out at 4°C to preserve the proteins, all centrifugation steps were carried out at 400 xG and samples taken for later analysis were mixed with 5x sample buffer and heated to 95°C for 5 Min. 50 μM Glutathione Sepharose 4 B (Merck) were transferred to a Spin Column (IBA Lifescience), equilibrated with 500 μL PBST followed by centrifugation. 500 μL 2,5 μM GST-Importin α were added to the column, a sample for the "Input" fraction was taken and the column then incubated for 2 h on a rotator. Unbound protein was then removed by three washing steps with PBST followed by centrifugation. 500 μL 2,2 μM inactive Taspase1-His with the respective concentration of compound were pre-incubated for 1 h on a rotator and a sample for the "Input" fraction was taken. The free binding sites on the column were blocked with 1 % (w/v) BSA (Carl Roth) in PBST for 30 Min on a rotator. The blocking solution was removed from the column by centrifugation for 1 Min. After that, the inactive Taspase1-His pre-incubated with the compound was added to the column and allowed to bind for 1 h on a rotator. A sample from the "Unbound" fraction was taken and unbound protein was then removed by three washing steps with PBST followed by centrifugation for 1 Min. 500 μL 1x sample Buffer were added to the column and heated to 95°C for 10 Min. The proteins were eluted by centrifugation for 2 Min.

SDS-PAGE and Western Blotting

For these assays, we used the standard recipes for SDS-PAGE according to Laemmli [4] and for Western Blotting according to Towbin [5]. For SDS-PAGE, Tris-glycine gels with 10 % (v/v) acrylamide in the stacking gel and 4 % (v/v) acrylamide in the separating gel were cast according. For the electrophoresis, we used the TetraCell system (BioRad) set to 200 V for 45 Min. The proteins were then transferred to a nitrocellulose membrane using a wet blot tank (PeqLab) set to 360 mA for 90 Min at 4°C . To detect the different proteins, the membrane was first reversibly stained with Ponceau S (AppliChem) and then cut between the protein bands according to the was cut according to the Spectra Multicolor Broad Range Protein Ladder (Thermo Fisher). Free binding sites were blocked with 5 % (w/v) powdered milk (Carl Roth) in Tris buffered saline with Tween-20 (TBST) (Carl Roth) for 30 Min at room temperature. After that, the membranes were incubated with the respective primary antibodies rabbit anti-Taspase1 1:2000 (sc-85945, Santa Cruz) and mouse anti-Karyopherin α 2 1:1000 (sc-55538, Santa Cruz) in 5 % (w/v) powdered milk in TBST for 1 h at room temperature. Unbound antibodies were removed by three washing steps with TBST. The membranes were incubated with the respective secondary antibodies donkey anti-rabbit HRP-coupled 1:10000 (NA934,

GE Healthcare) and sheep anti-mouse HPR-coupled 1:10000 (NXA931, GE Healthcare) in 5 % w/v) powdered milk with TBST for 1 h. Unbound antibodies were removed by four washing steps in TBST. For the detection of chemiluminescence, we used Pierce ECL Plus Western Blotting Substrate (Thermo Fisher) and the ChemidocImaging System (BioRad).

The signal was quantified with "Fiji" [6]. If necessary, the signal of Taspase1 in the eluted fraction was corrected for the Taspase1 stuck to the column without Importina. To correct possible loading differences the signal of Taspase1 in the eluted fraction was then normalized for the signal of Importina in the eluted fractions. The data was evaluated using "Origin2019" (OriginLab).

Toxicity Assay

1 x 10⁴ cells were cultured in Corning 96 Well microplates (Sigma-Aldrich) in 100 µl Dulbecco's modified eagle medium (DMEM) (Thermo Fisher Scientific) supplied with 10 % (v/v) fetal calf serum (FCS) (Life Technologies GmbH), Antibiotic-Antimycotic (Life Technologies GmbH) and the respective compound concentration. The cells were then cultivated at 37 °C and 5 % CO₂ for 24 h. After that, the compound-containing medium was removed, and cells were washed with PBS once. 100 µL fresh DMEM with 10 % FCS and Antibiotic-Antimycotic were added to each well. After the following addition of 20 µL Cell Titer Aqueous One (Promega), absorption at 490 nm was recorded with the plate reader Promega Glow Max (Promega) after 30 min of incubation. Since the compounds were dissolved in water, the results were then normalized to a water treated control to correct for the dilution of the media. The data are the mean of at least three replicates ± standard deviation.

Isothermal titration calorimetry (ITC)

ITC was performed with MicroCal ITC2000 (Malvern Pananalytical). The proteins were rebuffed five times into a tenfold volume of assay buffer and then concentrated using Vivaspin 6, 10000 MWCO (Sartorius) at 4900 xg and 4 °C. The rebuffed samples were degassed immediately before ITC with MicroCal ThermoVac (Malvern Pananalytical). The experimental setup was 18 injections of 2.0 µL with 1-1.5 mM ligand to 200 µL 70-80 µM inactive Taspase1-His with an injection time of 4 s and 180 s spacing between each injection at 25 °C and with constant stirring at 750 rpm. The first injection set to 0.4 µL to remove air and mixed reactants from the tip. For each experiment, we performed a ligand-to-buffer (LtB) titration as well as a buffer-to-protein (BtP) titration with the same experimental setup to correct for possible heat of dilution introduced by the ligand or protein. The data was analysed using MicroCal Analysis (OriginLab). The first injection peak was discarded and the isotherms of the LtB and BtP controls were subtracted from the experimental isotherm.

At this time, ITC experiments were not successful (see titration curves below). At this point we attribute this to the challenge in stabilizing Taspase1 at high concentrations which requires high ionic strength, which in turn is expected to affect interaction of the GCP units.

Surface Plasmon Resonance (SPR)

The measurements were performed on a Biacore X100 from GE Healthcare Life Sciences, Uppsala, Sweden. The sensograms were recorded with the Biacore X100 Control Software and evaluated with the Biacore X100 Evaluation Software.

For the measurements a C1 sensor chip from GE Healthcare Life Science was used. Before immobilization the sensor chip surface was activated by twofold injection of 0.1 M glycine-NaOH + 0.3 % Triton X 100, pH 12 and followed by washing with HBS-P⁺ buffer. Taspase1 was immobilized on the sensor chip surface on flow cell 2 via carbodiimide chemistry by the wizard

template for immobilization. Therefore, a 126 μM stock solution of Taspase1 in PBS buffer was diluted in 10 mM acetate buffer (pH 5.5, GE Healthcare) to get a final protein concentration of 1.26 μM . For flow cell 2 an immobilization level of 1391,6 RU was reached. The flow cell 1 was blocked by a solution of ethanolamine (1 M, pH 8.5, GE Healthcare) and an immobilization level of 1.6 RU was obtained. As running buffer HBS-P⁺ buffer (pH 7.4, GE Healthcare) at a flow rate of 5 $\mu\text{L min}^{-1}$ was used.

After immobilization the system was primed with the running buffer and two startup cycles were performed. The PEGylated and non-PEGylated GCP macromolecules were injected in concentrations of 0.10 – 400 μM in HBS-P⁺ buffer with a dilution factor of 2. A flow rate at 5 $\mu\text{L min}^{-1}$ and the contact and dissociation time were 120 s, respectively 180 s were used. After each measurement, the sensor chip was regenerated by injection of 0.1 M arginine in HBS-P⁺ buffer at a flow rate of 5 $\mu\text{L min}^{-1}$ with a contact time of 90 s to ensure that all sample was washed out and to achieve a stable baseline for the following measurements. For each sample the measurements were repeated three times.

To test for reproducibility, the assay was performed on a second chip prepared as described above giving an immobilization level of 1282,6 RU for flow cell 2 and an immobilization level of 144,6 RU for flow cell 1. Due to different immobilization levels, different absolute values are determined that are, however, in the same range [μM] and show the same trend for the different ligands as observed for the first chip. These measurements were repeated two times.

Measurements for monovalent ligands as well as only PEG were performed on the second chip and repeated two times.

Macromolecule Synthesis:

Synthesis EDS and GCP

(4-((2-(2-(2-aminoethoxy)ethoxy)ethyl)- amino)-4-oxobutanoic)[7] as well as N-Boc-protected 5-(guanidinocarbonyl)-1H-pyrrole-2-carboxylic acid (GCP) as triethylamine salt [8] were synthesized according to literature procedures. The free acid of the GCP was obtained by crystallization from methanol.

General

Oligomer synthesis were carried out manually in 10 ml polypropylene syringe reactors with a polyethylene frit and a Luer stopper from MultisynTech GmbH. All oligomers were synthesized on the TentaGel® S RAM (Rink Amide) or TentaGel® PAP resin with a loading of 0.23 mmol/g. Batch size of all oligomers was 0.15 mM.

Fmoc cleavage

The resin was swollen in DCM for 30 min and subsequently washed three times with DMF. Secondly the Fmoc protecting group of the resin as well as from the coupled building blocks or amino acids was cleaved by means of a 25% solution of piperidine in DMF achieving an amine end group. The deprotection was carried out twice for 20 min. Afterwards the resin was washed 10 times with DMF.

Coupling protocol

First the resin was swollen in DCM for 30 min and then washed three times with DMF. The Fmoc protecting group has to be removed before further couplings!

For the building block, amino acid or GCP (5 eq.), 5 eq. PyBOP and 10 eq. DIPEA were dissolved in 5 ml DMF, drawn into the reactor syringe and shaken for 90 min, followed by washing ten times with DMF. A double coupling, adding fresh building block and coupling reagents, was performed each time the GCP motif was coupled.

Capping of N-terminal primary amine

With scaffold completion of the oligomer the N-terminal amine group was acetylated with 8 ml of acetic anhydride, shaking for 20 min. After that, the resin was washed 5 times with DMF.

Boc-Cleavage

For Boc-deprotection, 6 ml of a 4 M HCl in dioxane solution (2 ml HCL conc. and 4 ml dioxane) was drawn into the reactor syringe and shaken for 10 min. Afterwards the reaction mixture was washed 3 times with dioxane and again 6 ml fresh 4 M HCl dioxane solution was drawn into the syringe and shaken for 20 min. Subsequently the solution was removed and the resin washed three times alternately with dioxane and DCM. To neutralize the resin, a 10 volume percent ice-cold DIPEA DCM solution was drawn up twice and shaken for 10 min. Last the resin was washed alternately three times with dioxane and DCM and finally 10 times with DMF.

Cleavage from solid phase

The oligomers were cleaved from the TentaGel® S RAM resin by drawing up a solution of 5 vol% triisopropylsilane (TIPS) and 95 vol% TFA into the syringe and shaking for 1.5 hours. The TentaGel® PAP cleavage was achieved with TFA/thioanisole (95/5, v/v) for 24 hours at room temperature.

Afterwards the solution was placed in ice cooled diethyl ether. The resulting precipitate was centrifuged off and the supernatant was decanted off. The pellet was washed 3 times with diethyl ether.

The product was dried and dissolved in MilliQ water. The entire solution was collected in a falcon tube and freeze-dried to isolate the product. Subsequently, the products were purified by means of preparative HPLC. Due to the purification by preparative HPLC and the added 0.1 vol% formic acid in the mobile phases, the structures are present as formates. The number of formates was quantified by ¹H NMR spectra. Further information can be found in the respective ¹H NMR data.

Analytical data for macromolecules:

Macromolecule **3G**

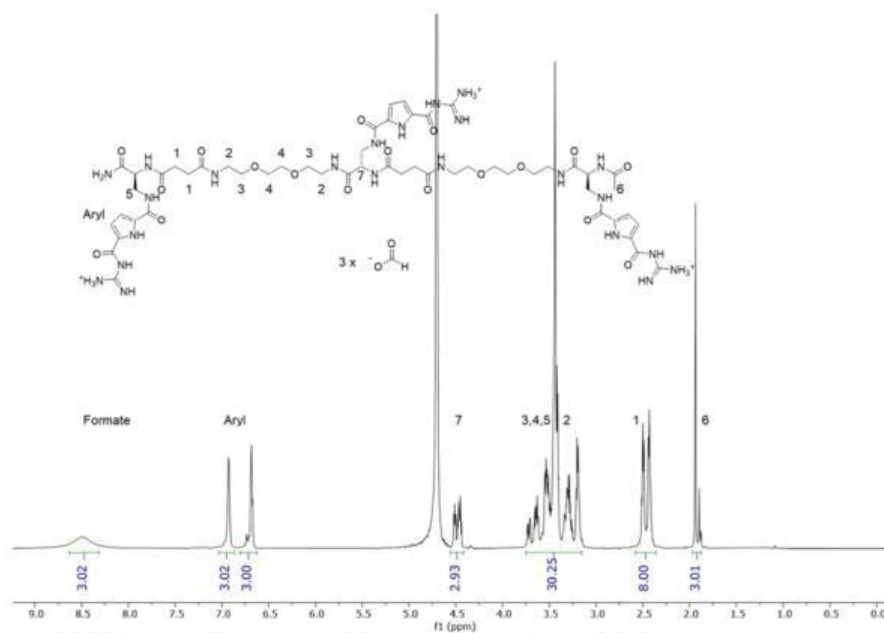


Figure S 2: 600 MHz ^1H NMR spectrum of **3G** as formate salt in D_2O at 25°C .

^1H -NMR (600 MHz, D_2O , 25°C): δ (ppm) = In the range from 8.25 to 8.75 signal of the formate (s, 3H, **3G** is present with three formate anions), 7.09-6.85 (m, 3H, Ar-H), 6.79-6.24 (m, 3H, Ar-H), 4.50-4.40 (m, 3H, H7), 3.51-3.16 (m, 30H, H2-H5), 2.63-2.37 (m, 8H, H1), 1.94 (s, 3H, H6, second small signal cannot be assigned).

The effective molar mass for **3G** with three formates is 1450.4 g/mol.

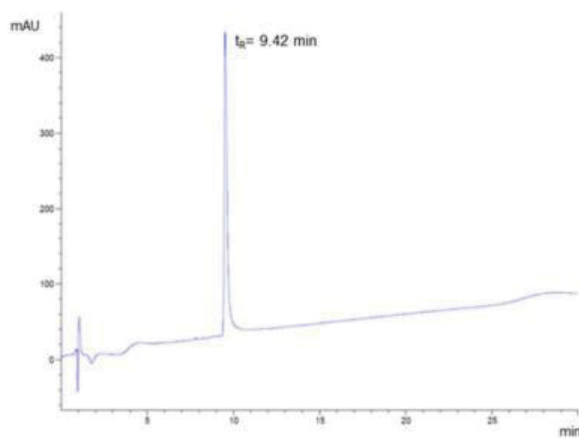


Figure S 3: **3G** detected with relative purities >95% by RP-HPLC analysis (linear gradient from 5 – 50 vol% eluent H₂O/acetonitrile) in 30 min at 40 °C.

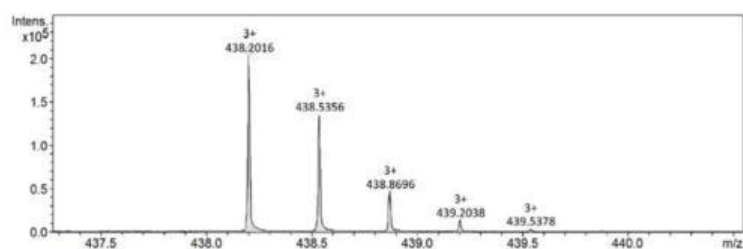


Figure S 4: HR-ESI-MS of **3G**.

HR-ESI-MS: for C₅₂H₈₀N₂₃O₁₈ m/z [M+3H]³⁺ calcd.: 438.2012, found: 438.2016, mass accuracy -0.9 ppm.

Macromolecule 3GL

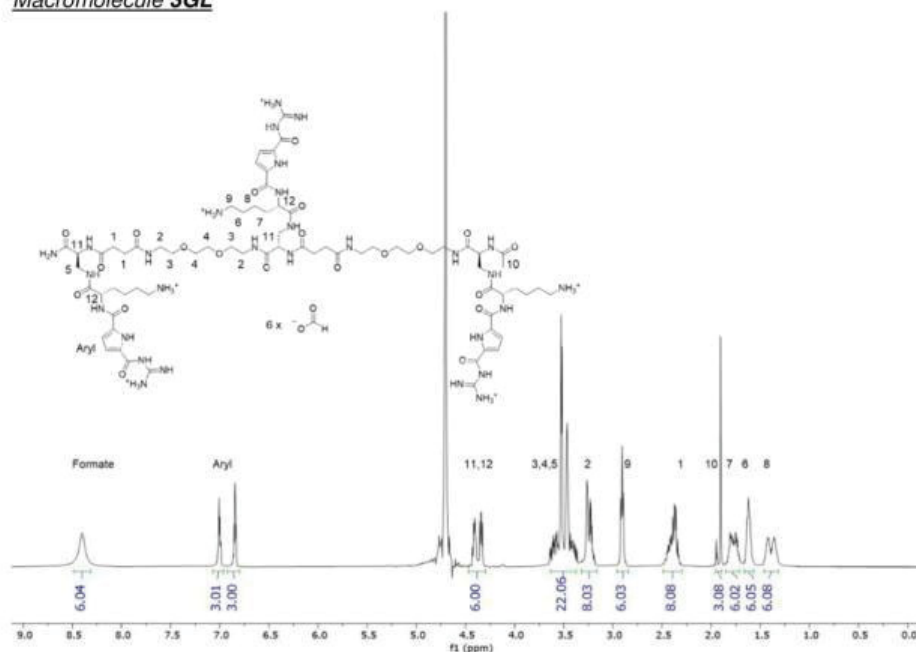


Figure S 5: 600 MHz ^1H NMR spectrum of **3GL** as formate salt in D_2O at 25°C

^1H -NMR (600 MHz, D_2O , 25°C): δ (ppm) = In the range from 8.30 to 8.50 signal of the formate (s, 6H, **3GL** is present with six formate anions), 7.12-6.92 (m, 3H, Ar-H), 6.87-6.79 (m, 3H, Ar-H), 4.48-4.27 (m, 6H, H11, H12), 3.69-3.38 (m, 22H, H3-H5), 3.33-3.19 (m, 8H, H2), 2.91-2.82 (m, 6H, H9), 2.49-2.27 (m, 8H, H1), 1.91 (s, 3H, H10, second small signal cannot be assigned), 1.82-1.71 (m, 6H, H7), 1.68-1.59 (m, 6H, H6), 1.45-1.31 (m, 6H, H8).

The effective molar mass for **3GL** with six formates is 1971.7 g/mol.

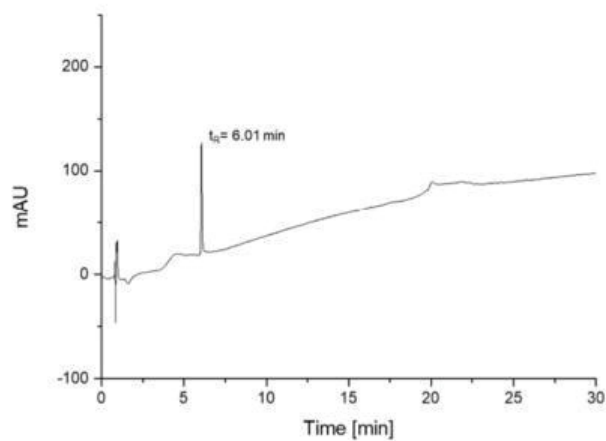


Figure S 6: **3GL** detected with relative purities >95% by RP-HPLC analysis (linear gradient from 5 – 50 vol% eluent H_2O /acetonitrile) in 30 min at 40 °C.

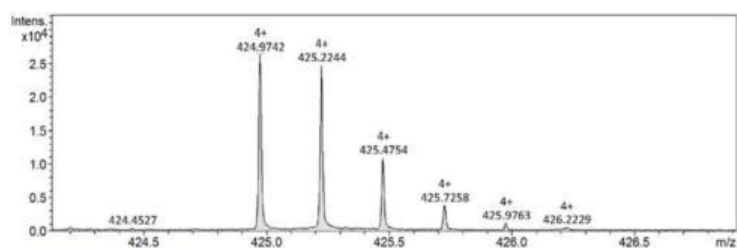


Figure S 7: HR-ESI-MS of **3GL**.

HR-ESI-MS: for $\text{C}_{70}\text{H}_{117}\text{N}_{29}\text{O}_{21}$ m/z $[\text{M}+4\text{H}]^{4+}$ calcd.: 424.9739, found: 424.9742, mass accuracy -0.6 ppm.

Macromolecule **3GP**

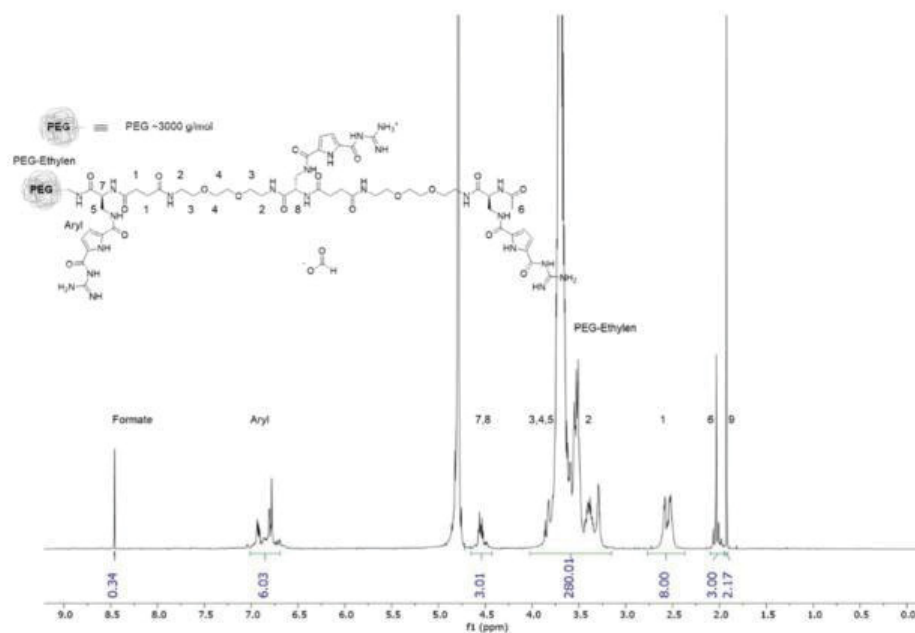


Figure S 8: 600 MHz ¹H NMR spectrum of **3GP** as formate salt in D₂O at 25°C.

¹H-NMR (600 MHz, D₂O, 25°C): δ (ppm) = In the range from 8.40 to 8.50 signal of the formate (s, 0.34H, **3GP** is present at an average of 0.34 formate anion per molecule), 7.08-6.65 (m, 6H, Ar-H), 4.70-4.39 (m, 3H, H7, H8), 4.06-3.19 (m, 280H, HPEG, H2-H5), 2.78-2.36 (m, 8H, H1), 2.11-1.97 (m, 3H, H6), 1.94 (s, 2H, H9, signal of the end group of the PEG chain).

The effective molar mass for **3GP** with formate is 4413.4 g/mol.

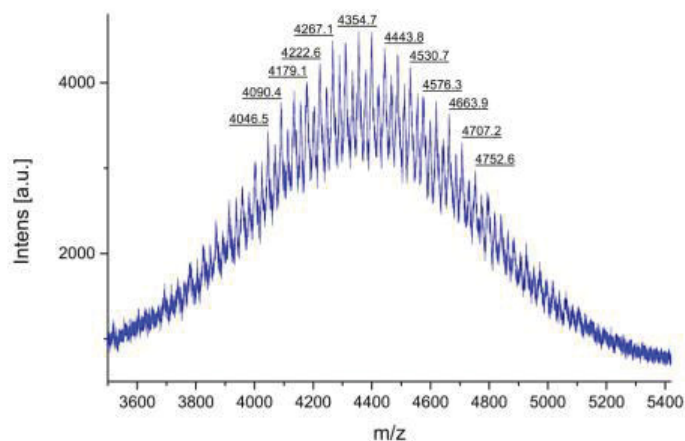


Figure S 9: MALDI-TOF-MS of **3GP** in a m/z range using DHB as matrix in a compound to matrix ratio of 1:5.

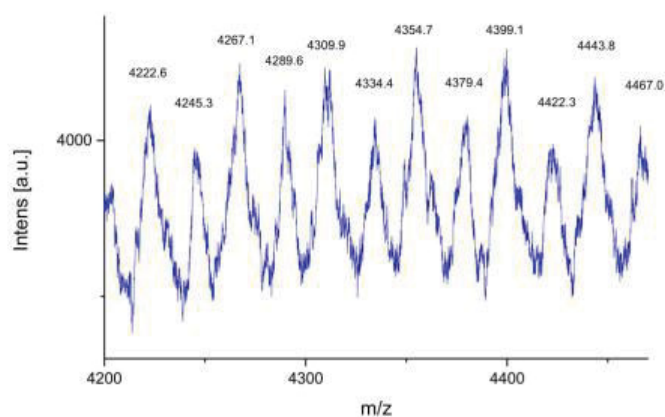


Figure S 10: Detailed view on MALDI-TOF-MS of **3GP**, focusing on PEG-repeating units (every second signal corresponds to one PEG unit more, intermediate signal corresponds to one additional sodium ion).

Mass analysis MALDI-TOF-MS of **3GP**: m/z found 4399.1- 3106.8 (PEG-Part) = 1292.3
(m/z calcd. Oligomer Part: 1311.6).

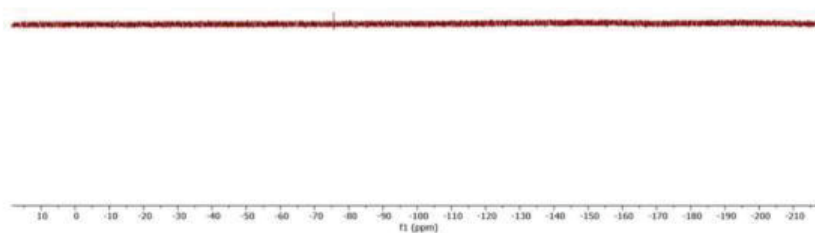


Figure S 11: Exemplary 600 MHz ^{19}F NMR spectrum of **3GP** in D_2O at 25°C showing that no TFA counterions are present.

Macromolecule **3GLP**

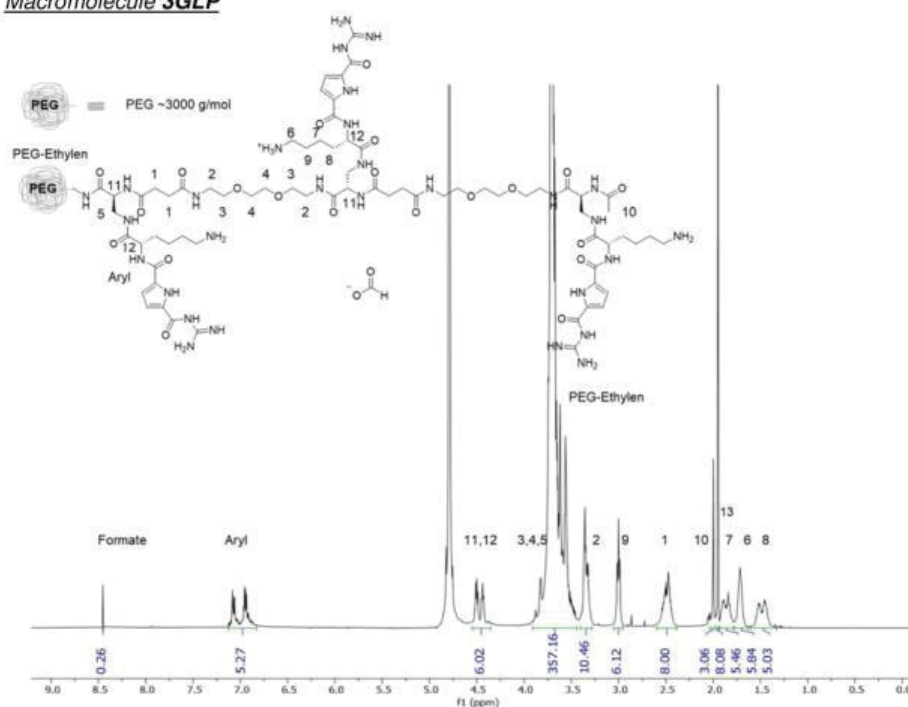


Figure S 12: 600 MHz ¹H NMR spectrum of **3GLP** as formate salt in D₂O at 25°C.

¹H-NMR (600 MHz, D₂O, 25°C): δ (ppm) = In the range from 8.40 to 8.50 signal of the formate (s, 0.26H, **3GLP** is present at an average of 0.26 formate anion per molecule), 7.18-6.79 (m, 6H, Ar-H), 4.57-4.32 (m, 6H, H11, H12), 3.82-3.46 (m, 357H, HPEG, H3-H5), 3.41-3.27 (m, 10H, H2), 3.08-2.90 (m, 6H, H9), 2.61-2.31 (m, 8H, H1), 2.04 (m, 3H, H10). 2.00-1.93 (m, H13, signal of the end group of the PEG chain) 1.90-1.78 (m, 6H, H7), 1.76-1.62 (m, 6H, H6), 1.59-1.30 (m, 6H, H8).

The effective molar mass for **3GLP** with formate is 4818.8 g/mol.

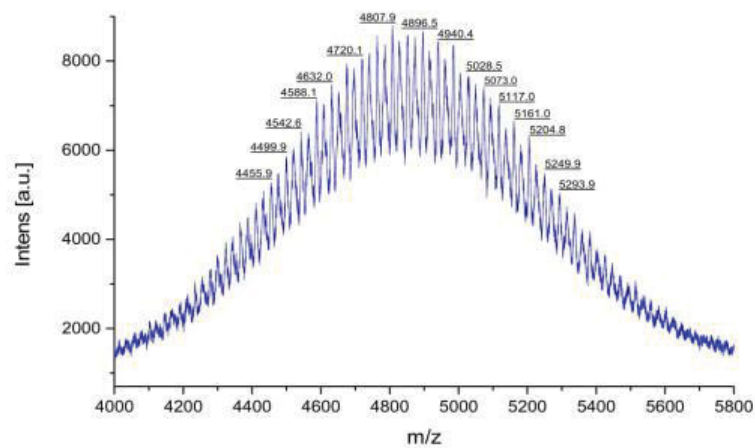


Figure S 13: MALDI-TOF-MS of **3GLP** in a m/z range using DHB as matrix in a compound to matrix ratio of 1:10.

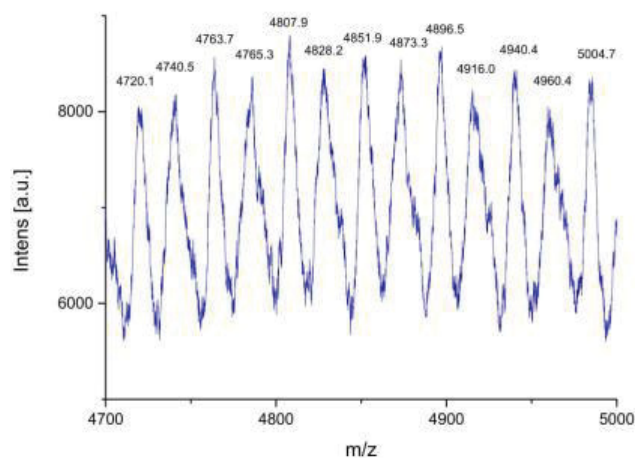


Figure S 14: Detailed view on MALDI-TOF-MS of **3GLP**, focusing on PEG-repeating units (every second signal corresponds to one PEG unit more, intermediate signal corresponds to one additional sodium ion).

Mass analysis MALDI-TOF-MS of **3GLP**: m/z found 4807.9- 3106.8 (PEG-Part) = 1701.2
(m/z calcd. Oligomer Part: 1695.7).

Macromolecule G

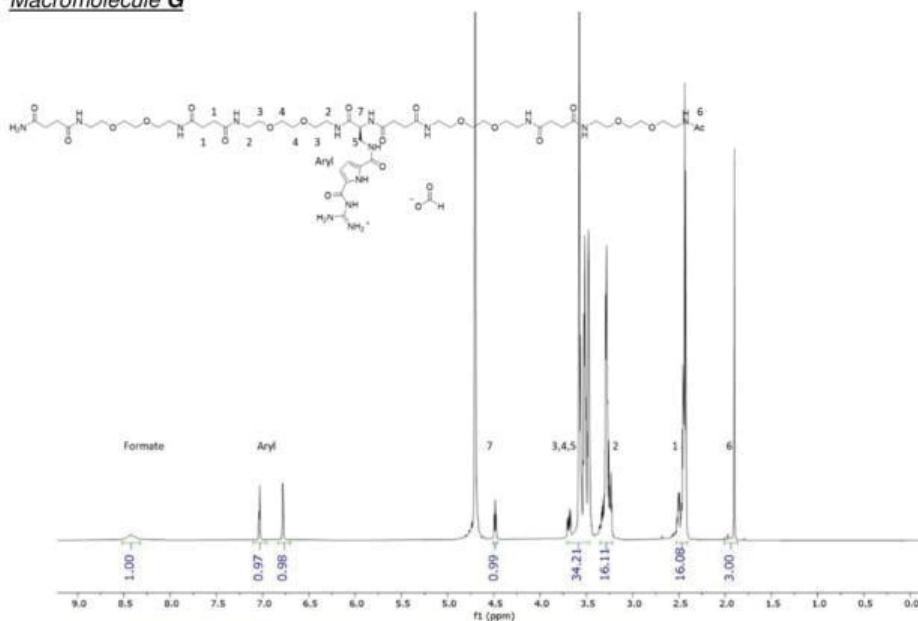


Figure S 15: 600 MHz ^1H NMR spectrum of **G** as formate salt in D_2O at 25°C .

$^1\text{H-NMR}$ (600 MHz, D_2O , 25°C): δ (ppm) = In the range from 8.30 to 8.50 signal of the formate (s, 1H, **G** is present with one formate anion), 7.08 (s, 1H, Ar-H), 6.78 (s, 1H, Ar-H), 4.52-4.44 (m, 1H, H7), 3.69-3.41 (m, 34H, H3-H5), 3.35-3.23 (m, 16H, H2), 2.56-2.39 (m, 16H, H1), 1.92 (s, 3H, H6).

The effective molar mass for **G** with one formate is 1291.42 g/mol.

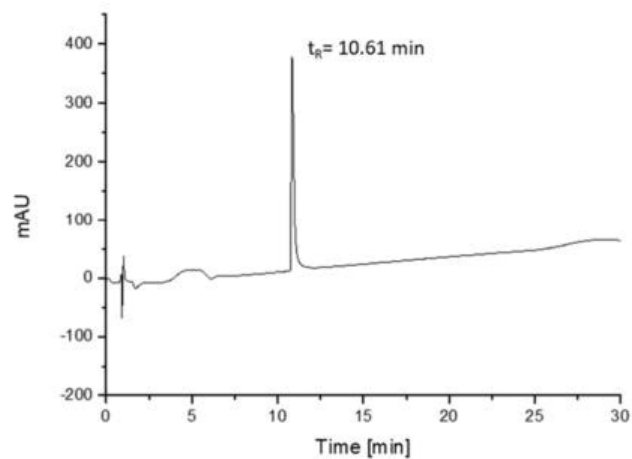


Figure S 16: **G** detected with relative purities >95% by RP-HPLC analysis (linear gradient from 5 – 50 vol% eluent H₂O/acetonitrile) in 30 min at 40 °C.

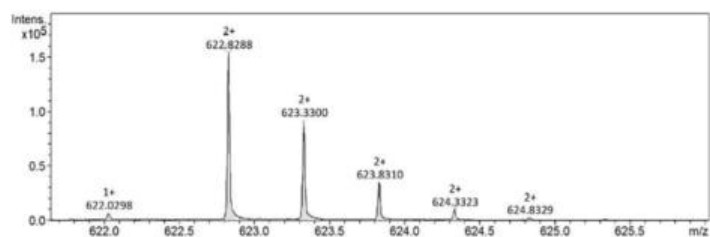


Figure S 17: HR-ESI-MS of **G**.

HR-ESI-MS: for C₅₂H₉₉N₁₅O₂₀ m/z [M+2H]²⁺ calcd.: 622.8277, found: 622.8288, mass accuracy -1.7 ppm.

Macromolecule GL

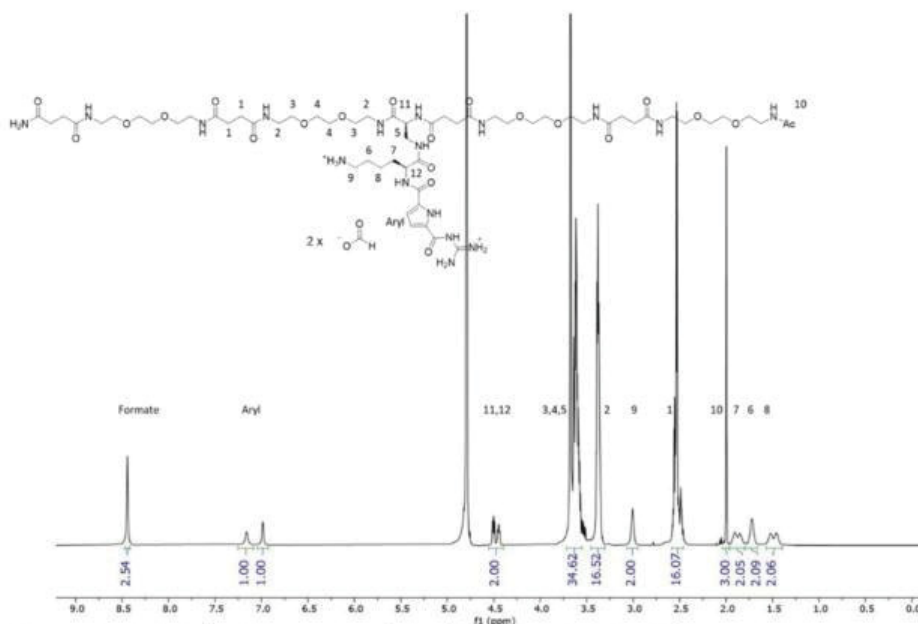


Figure S 18: 600 MHz ^1H NMR spectrum of **GL** as formate salt in D_2O at 25°C.

^1H -NMR (600 MHz, D_2O , 25°C): δ (ppm) = In the range from 8.40 to 8.50 signal of the formate (s, 2H, **GL** is present with two formate anions) amide, guanidino functionalities occur, 7.17 (s, 1H, Ar-H), 7.01 (s, 1H, Ar-H), 4.56-4.40 (m, 2H, H11, H12), 3.73-3.54 (m, 34H, H3-H5), 3.36-2.27 (m, 16H, H2), 3.07-2.95 (m, 2H), H9), 2.59-2.44 (m, 16H, H1), 2.01 (s, 3H, H10), 1.93-1.80 (m, 2H, H7), 1.76 (s, 2H, H6), 1.57-1.40 (m, 2H, H8).

The effective molar mass for **GL** with two formates is 1457.7 g/mol.

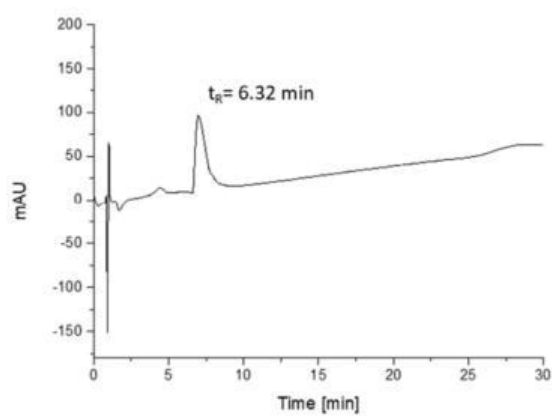


Figure S 19: **GL** detected with relative purities >95% by RP-HPLC analysis (linear gradient from 5 – 50 vol% eluent H₂O/acetonitrile) in 30 min at 40 °C.

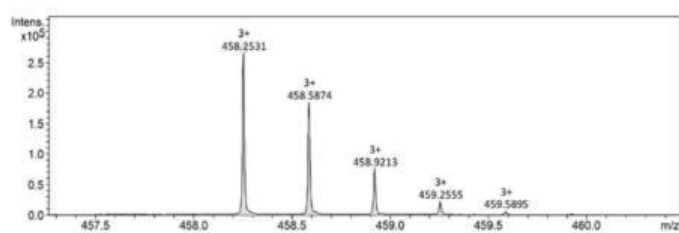


Figure S 20: HR-ESI-MS of **1GL**.

HR-ESI-MS: for C₅₈H₁₀₁N₁₇O₂₁ m/z [M+3H]²⁺ calcd.: 458.2525, found: 458.2531, mass accuracy -1.2 ppm.

PEG

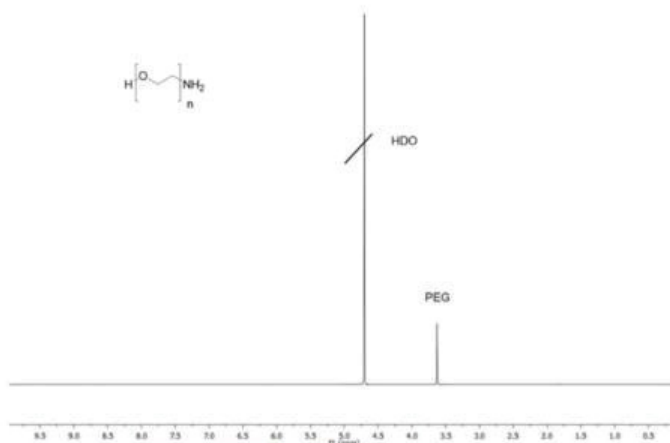


Figure S 21: 600 MHz ^1H NMR spectrum of PEG in D_2O at 25°C.

^1H -NMR (600 MHz, D_2O , 25°C): δ (ppm) = 3.64 (s, HPEG).

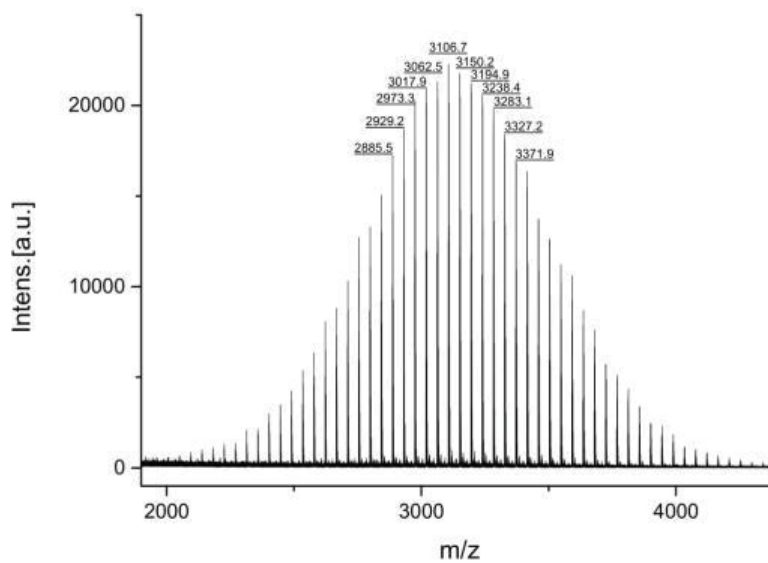


Figure S 22: MALDI-TOF-MS of PEG in a m/z range using DHB as matrix in a compound to matrix ratio of 1:10. The value 3106.7 g/mol corresponds to 70 polyethylene glycol repeating units.

Binding to Taspase1: SPR Assay

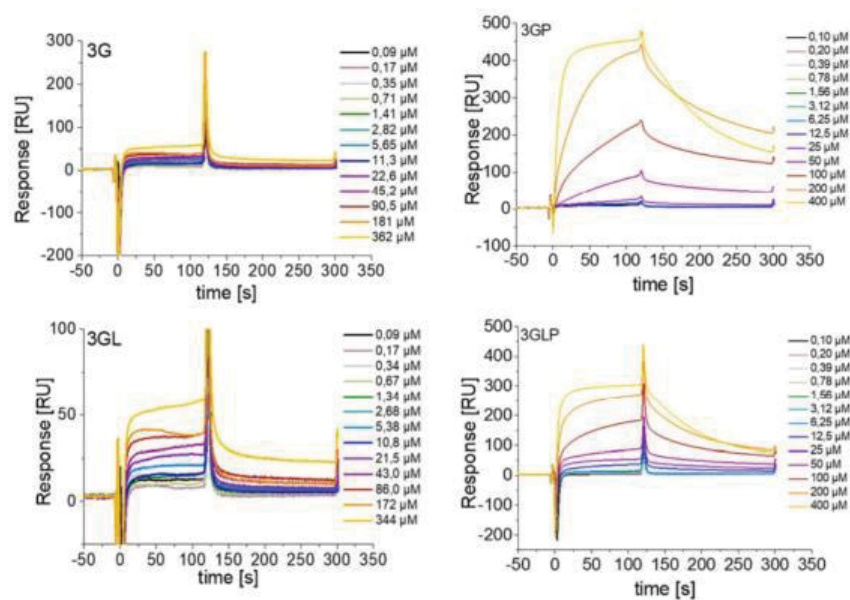


Figure S 23: SPR-Sensograms for PEGylated and non-PEGylated GCP macromolecules for the second C1 sensor chip. Each measurement was repeated two times.

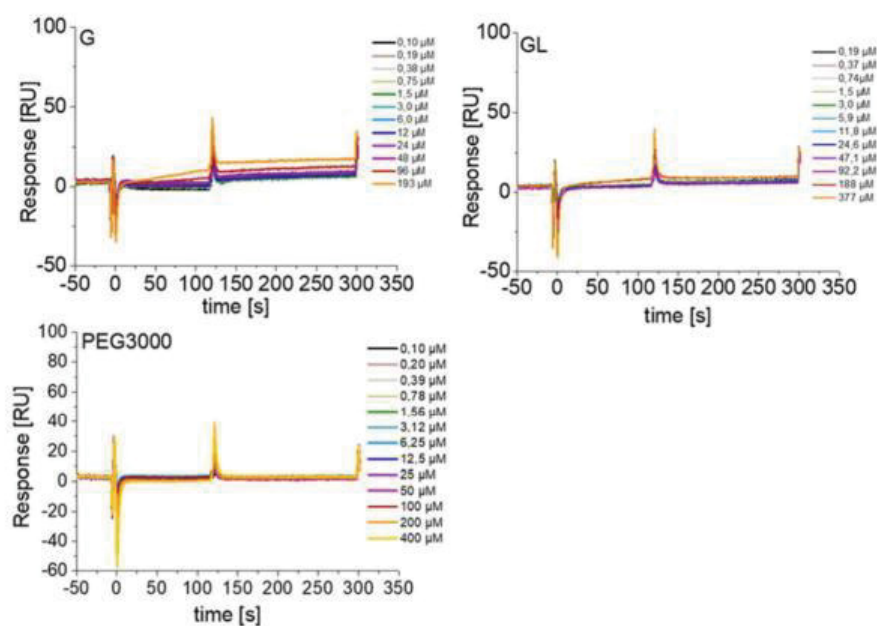


Figure S 24: SPR-Sensograms for monovalent non-PEGylated GCP macromolecules (top) and PEG3000 (bottom). The measurements showed no binding to Taspase1. Each measurement was repeated two times on the second C1 sensor chip.

Binding to Taspase1: Pull-down assay

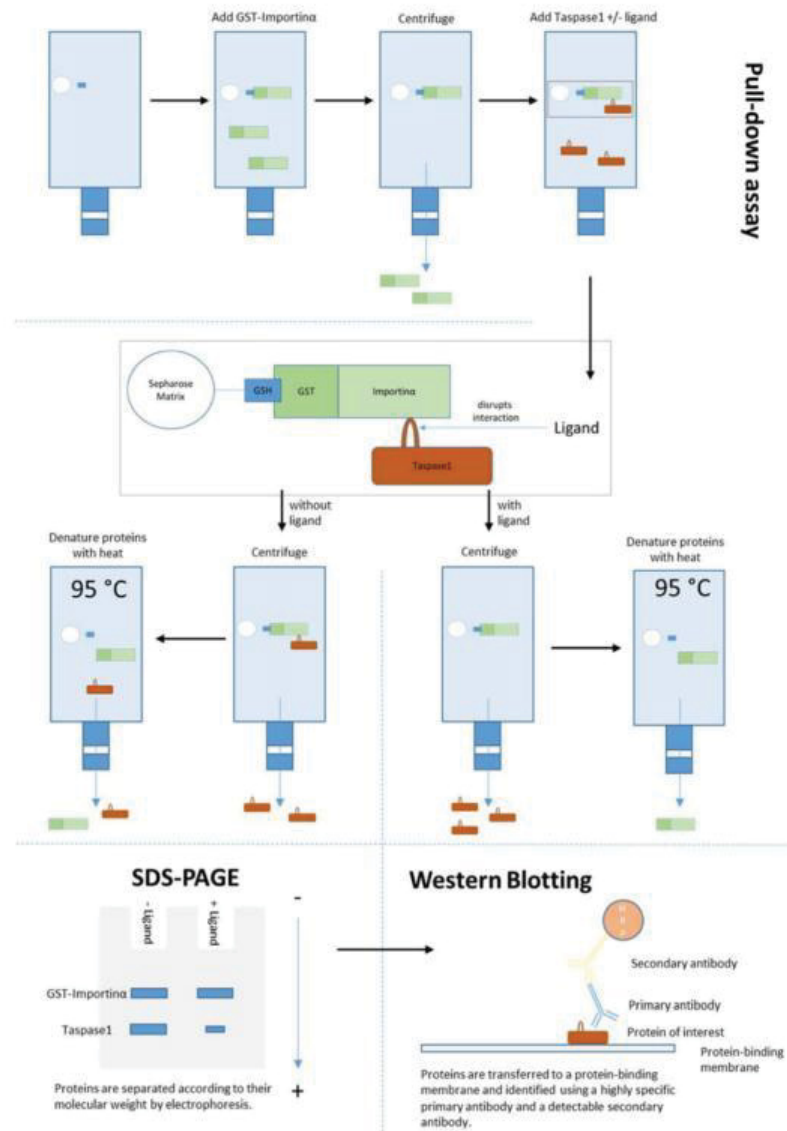


Figure S 25: Workflow of the modified pull-down assay. A spin column was used to fix GST-Importin α on a Sepharose matrix coated with glutathione. First, GST was allowed to bind to glutathione with high affinity, and unbound protein was removed by centrifugation. Then, Taspase1-His was pre-incubated with ligand or left untreated as indicated, subsequently added to the column, and unbound protein was again removed by centrifugation. Next, a buffer containing ionic detergents as well as reducing agents was applied to the column and heated to 95 °C to denature and thus dissociate all protein from the matrix. Finally, the proteins were separated according to their molecular weight by SDS page and analyzed by Western Blot analysis for quantification.

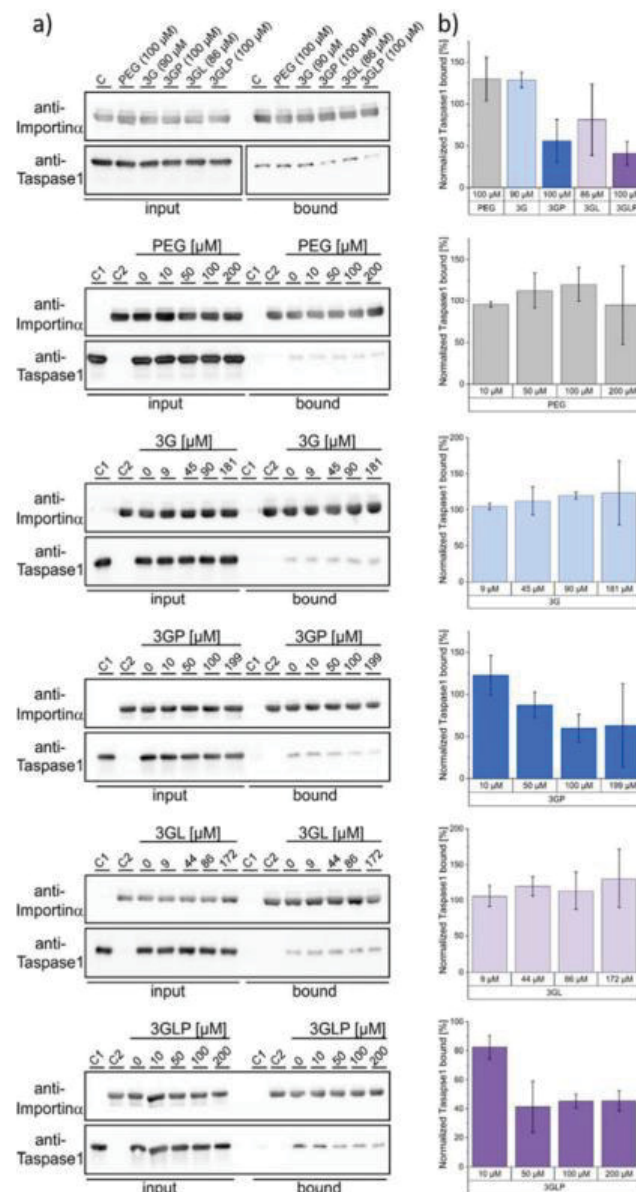


Figure S 26: a) Representative Western Blot analyses from the pull-down assays performed with the different compounds. The input fraction contains samples of the complete protein preparation added to the column, the bound fraction contains the respective portion bound to the column. The latter comprises GST-Importin α directly associated with the column and Taspase1 indirectly bound via its interaction with Importin α . C = Untreated control, C1 = Control with only Taspase1, C2 = Control with only Importin α . b) Densitometric quantification of the respective pull-down assays, comprising three replicates \pm standard deviation. **Please note:** originally concentrations were calculated not considering the counterions present in the structures. This was corrected leading to the here shown concentrations.

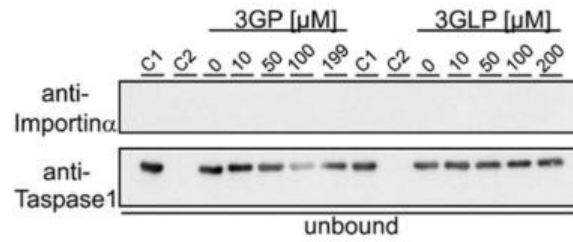


Figure S 27: Binding of Importin α to the column was not affected by the PEGylated ligands during the assay. Western Blot of the unbound fraction after incubation of the Importin α -loaded column with Taspase1 in the presence of the indicated ligands. C1 = Control with only Taspase1, C2 = Control with only Importin α .

Binding to Taspase1: ITC measurements

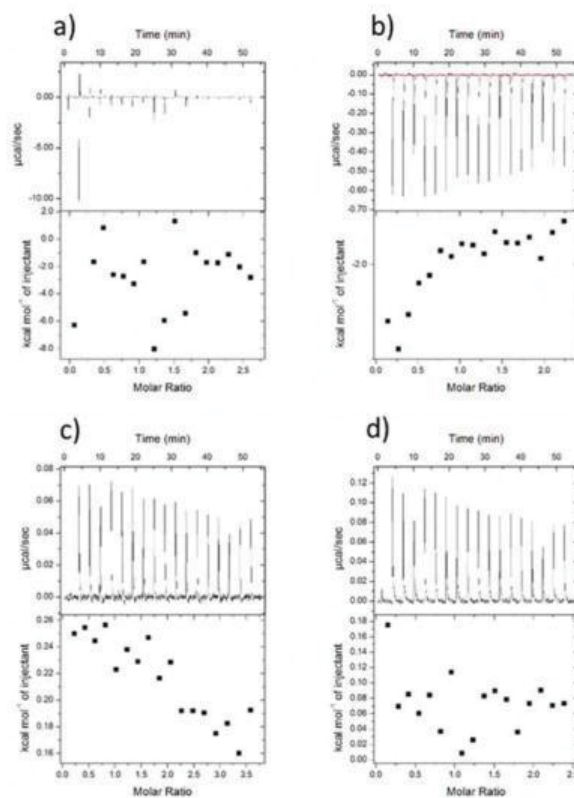


Figure S 28: Test of different ITC conditions with inactive Taspase1 and the respective ligands. a) 1 mM GLP to 70 μ M inactive Taspase1, buffer: 150 mM NaCl, 50 mM NaH_2PO_4 , pH 7,4. b) 1 mM GLP to 80 μ M inactive Taspase1, buffer: 10 % (w/v) Sucrose, 50 mM NaH_2PO_4 , pH 7,4. c) 1,5 mM GLP to 75 μ M inactive Taspase1, buffer: 10 % (w/v) Sucrose, 50 mM NaH_2PO_4 , pH 7,4. d) 1 mM GP to 75 μ M inactive Taspase1, buffer: 10 % (w/v) Sucrose, 50 mM NaH_2PO_4 , pH 7,4. e) 1 mM GL to 75 μ M inactive Taspase1, buffer: 10 % (w/v) Sucrose, 50 mM NaH_2PO_4 , pH 7,4.

Toxicity study

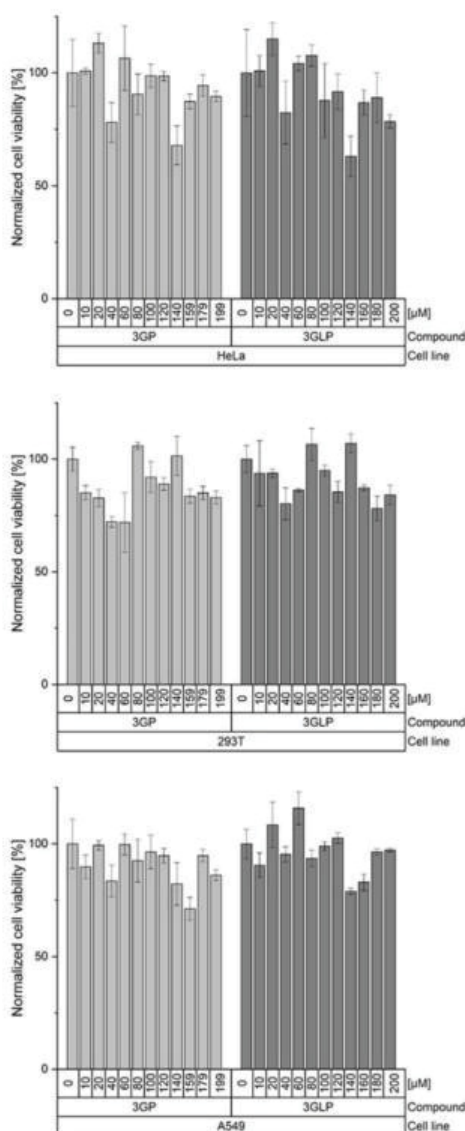


Figure S 29: The compounds do not affect the cell viability of various tumor cell lines. 293T (a), A549 (b) and HeLa (c) cells were cultivated in cell culture medium supplied with the respective concentrations of compound for 24 h. After that, we performed an MTS assay to determine the cell viability. The data points are the mean of triplicates \pm standard deviation. **Please note:** originally concentrations were calculated not considering the counterions present in the structures. This was corrected leading to the here shown concentrations.

References:

- [1] J. van den Boom, F. Trusch, L. Hoppstock, C. Beuck, P. Bayer, *PloS one* **2016**, 11 (3), 1-13.
- [2] J. A. Khan, B. M. Dunn, L. Tong. *Structure*. **2005**, 13(10), 1443-1452.
- [3] J. van den Boom, A. Hensel, F. Trusch, A. Matena, S. Siemer, D. Guel, D. Docter, A. Höing, P. Bayer, R. H. Stauber, S. K. Knauer, *Nanoscale* **2020**, 12, 19093-19103.
- [4] S. Ramakrishnan, K. N. Sulochana, R. Punitham, K. Arunagiri, *Glycoconj. J.* **1996**, 13, 519-523.
- [5] H. Towbin, T. Staehelin, J. Gordon, *PNAS* **1979**, 76 (9), 4350-4354.
- [6] J. Schindelin, I. Arganda-Carreras, E. Frise, V. Kaynig, M. Longair, T. Pietzsch, A. Cardona, *Nat. Methods* **2012**, 9 (7), 676-682.
- [7] M. F. Ebbesen, C. Gerke, P. Hartwig, L. Hartmann, *Polym. Chem.* **2016**, 7 (46), 7086-7093.
- [8] C. Schmuck, V. Bickert, M. Merschky, L. Geiger, D. Rupprecht, J. Dudaczek, P. Wich, T. Rehm, U. Machon, *Eur. J. Org. Chem.* **2008**, 2, 324-329.





5.2 Take your Positions and Shine: Effects of Positioning Aggregation-Induced Emission Luminophores within Sequence-Defined Macromolecules

Peter Pasch, Matthias Killa, Hauke Lukas Junghans, Kateryna Loza, Jens Voskuhl, Laura Hartmann

Own Contribution:

Collaborative conceptualisation and design of the project. Synthesis and purification of all building blocks (except GCP building blocks). Supervision of oligomer synthesis performed by Hauke Lukas Junghans within his bachelor thesis. Oligomer characterization (LC-MS, NMR, UHR). Evaluation of fluorescence studies. Collaborative manuscript writing.

FULL PAPER

 <p>Hello AIEs</p> <p>Sequence-defined oligo (amidoamines) are employed to develop supramolecular ligands with AIE properties for detection of binding. Special focus is devoted to varying the position of the AIE luminophore within the scaffold and in</p>	 <p>Take your Position!</p> <p>relation to the supramolecular binding motif. A strong influence of the position on the resulting AIE properties is shown and evaluated for the ligand binding to various natural and synthetic polyanions.</p>	 <p>Who will shine?</p> <p><i>P. Pasch, M. Killa, H. L. Junghans, M. Schmidt, Jun.-Prof. Dr. S. Schmidt, Jun.-Prof. Dr. J. Voskuhl*, Prof. Dr. L. Hartmann*</i></p> <p>1 – 8</p> <p>Take your Positions and Shine: Effects of Positioning Aggregation-Induced Emission Luminophores within Sequence-Defined Macromolecules</p> 
--	--	---

Take your Positions and Shine: Effects of Positioning Aggregation-Induced Emission Luminophores within Sequence-Defined Macromolecules

Peter Pasch,^[a] Matthias Killa,^[b] Hauke Lukas Junghans,^[a] Melanie Schmidt,^[a] Stephan Schmidt,^[a] Jens Voskuhl,^{*,[b]} and Laura Hartmann^{*,[a]}

In memory of Carsten Schmuck

Abstract: A luminophore with aggregation-induced emission (AIE) is employed for the conjugation onto supramolecular ligands to allow for detection of ligand binding. Supramolecular ligands are based on the combination of sequence-defined oligo(amidoamine) scaffolds and guanidinocarbonyl-pyrrole (GCP) as binding motif. We hypothesize that AIE properties are strongly affected by positioning of the luminophore within the ligand scaffold. Therefore, we system-

atically investigate the effects placing the AIE luminophore at different positions within the overall construct, for example, in the main or side chain of the oligo(amidoamine). Indeed, we can show that the position within the ligand structure strongly affects AIE, both for the ligand itself as well as when applying the ligand for the detection of different biological and synthetic polyanions.

Introduction

The concept of aggregation-induced emission (AIE) was introduced by Tang in 2001.^[1–3] In contrast to the well-known quenching of fluorescence by aggregation of a fluorophore, AIE luminophores do not emit in the dissolved state but only when restricting their intramolecular rotation or vibration (RIR or RIV), for example through aggregation or in the solid state.^[4] Today, a wide range of AIE luminophores has been developed and explored in various applications such as in high-performance OLEDs^[5,6] or organic lasers.^[7,8] Another interesting area of application is the use of AIE luminophores as optical sensor or marker: binding or complex formation of the AIE with the compound that is supposed to be detected leads to RIR and thus to an increase in emission. This can then be detected and

correlated to the binding event. Such AIE sensors have been developed towards the recognition of chemicals compounds such as explosives^[9] or vapors^[10] and bioamines.^[11] Furthermore, they can be applied as biosensors for the detection of amino acids and proteins or for monitoring conformational changes of DNA or proteins^[4,12] as well as bioimaging.^[13] Along those lines, AIEs can also serve as a biomarker for diagnosing diseases as recently demonstrated by Lou and Xia for a real-time quantitative light detection of telomerase in the urine of bladder cancer patients with a cationic AIE tetraphenylethene derivative.^[14]

When developing such novel biomarkers or biosensors, the luminophore has to be modified in a way that allows for strong and ideally specific binding to the target molecule. Usually this is achieved either by bioconjugation for example of a peptide or antibody, or by introducing non-natural recognition motifs such as charged groups or supramolecular binding motifs.^[15] In comparison to bioconjugation, non-natural recognition motifs potentially can address new or alternative binding sites of the target molecule and avoid the risk of side effects for example through immunological or cytotoxic responses when used in vitro or in vivo.

In 1999 Schmuck and coworkers introduced the guanidinocarbonyl-pyrrole (GCP) as supramolecular binding motif.^[16,17] The GCP is an arginine mimetic and binds oxyanions such as anionic amino acids on protein surfaces via a hydrogen-bond-assisted ion pairing.^[18,19] They have also already demonstrated that by combining multiple GCP motifs on a scaffold, higher affinity and selectivity can be achieved.^[20] However, one of the major challenges remains in the detection and analysis of binding of such supramolecular ligands on the target. Therefore, in this work, we combine the use of AIEs for detection of

[a] P. Pasch, H. L. Junghans, M. Schmidt, Jun.-Prof. Dr. S. Schmidt, Prof. Dr. L. Hartmann
Department for Organic Chemistry and Macromolecular Chemistry
Heinrich Heine University Düsseldorf
Universitätsstraße 1, Düsseldorf 40225 (Germany)
E-mail: laura.hartmann@hhu.de

[b] M. Killa, Jun.-Prof. Dr. J. Voskuhl
Faculty of chemistry (Organic chemistry) and CENIDE
University of Duisburg Essen
Universitätsstrasse 7, 45141 Essen (Germany)
E-mail: jens.voskuhl@uni-due.de

Supporting information for this article is available on the WWW under <https://doi.org/10.1002/chem.202101086>

© 2021 The Authors. Chemistry – A European Journal published by Wiley-VCH GmbH. This is an open access article under the terms of the Creative Commons Attribution Non-Commercial License, which permits use, distribution and reproduction in any medium, provided the original work is properly cited and is not used for commercial purposes.

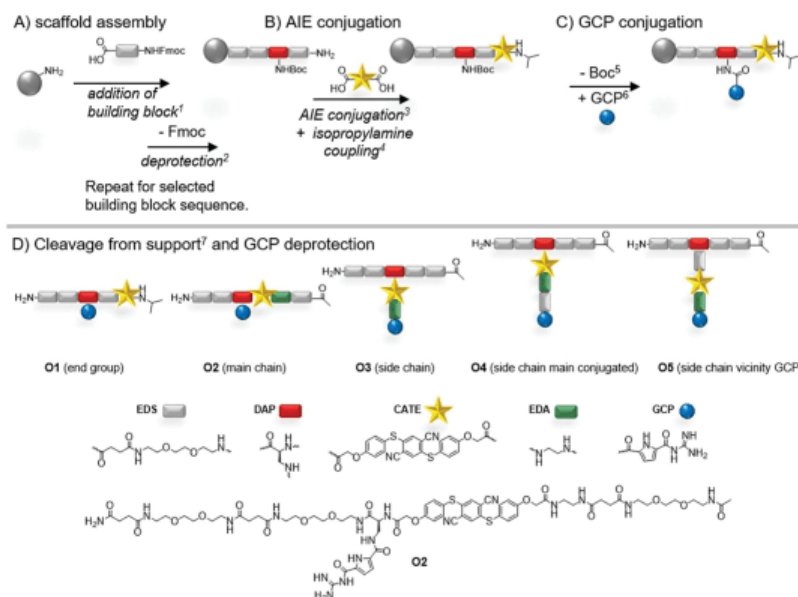
binding with the GCP functionalized scaffolds as supramolecular binding unit.

For a luminophore construct to be used as an AIE-based sensor, it should be flexible or completely dissolved without the presence of the target molecule, thereby giving no AIE response. Only upon binding to the target or aggregation, the motion is restricted giving rise to AIE and thereby read-out of the binding event. Therefore, we chose flexible, sequence-defined macromolecules^[21] as scaffolds, specifically oligo(amidoamines) accessible via so-called solid-phase polymer synthesis^[22–25] and allowing for site-specific introduction of both AIE and GCP motifs. We have recently demonstrated that such sequence-defined GCP-functionalized oligo(amidoamines) can act as inhibitors of protein-protein interactions.^[26] Since the AIE properties and specifically its emission upon aggregation can be expected to be strongly affected by attachment to the scaffold, in this study we systematically investigate the effects of the position of the AIE within the overall construct. Based on our findings, in the future, GCP oligomers could be designed allowing for both, inhibition of protein-protein interactions and direct read-out of ligand-protein binding via the AIE luminophore.

Results and Discussion

Overall five AIE modified GCP functionalized oligomers (**O1–O5**) were synthesized. The AIE luminophore, based on aromatic thioethers described by Voskuhl et al.,^[27,28] varies in its position from the direct vicinity of the binding motif to the middle of the side chain or main chain to the position as end group of the oligomer (Scheme 1). All oligomers were synthesized using previously established solid phase polymer synthesis protocols, combining tailor-made building blocks such as EDS (4-((2-(2-(2-aminoethoxy)ethoxy)ethyl)-amino)-4-oxobutanoic),^[25] commercially available amino acids such as N_α -Fmoc- N_β -Boc-L-2,3-diaminopropionic acid (DAP), carboxy-functionalized GCP building block and carboxylated aromatic thioether (CATE) as AIE.^[29]

In short, the synthesis started from an amine functionalized resin and employed the stepwise addition of building blocks, which carried a free carboxy-group for attachment onto the resin and a protected amine group. Upon successful coupling of the first building block, the protecting group, here fluorenylmethoxycarbonyl (Fmoc), was released and the next building block can be coupled. For the introduction of side chains and attaching GCP and/or AIE motifs, *tert*-butoxycarbonyl (Boc-) protected DAP was used. Boc can be selectively cleaved on solid phase by using 4 M HCl in dioxane solution,



Scheme 1. Synthesis of AIE- and GCP-functionalized oligomers 1–5 using solid phase polymer synthesis. Reaction conditions: 1) 5 equiv. building block, 5 equiv. PyBOP, 10 equiv. DIPEA in DMF, 90 min/2) 25 v% piperidine in DMF, 20 min, 3) 10 equiv. CATE, 10 equiv. PyBOP, 20 equiv. DIPEA in DMF, 48 h, 4) 5 equiv. Isopropylamine, 5 equiv. PyBOP, 10 equiv. DIPEA in DMF, 90 min/ Ac2O, 20 min (acetylation of N-terminus), 5) 4 M HCl in dioxane, 20 min (on-resin cleavage of Boc), 6) 5 equiv. (Boc)GCP-COOH, 5 equiv. PyBOP, 10 equiv. DIPEA in DMF, 90 min (double coupling), 7) TentaGel® S RAM; 5% triisopropylsilane, 95% TFA, 90 min.

thus allowing for coupling of building blocks and constructing the side chain at this position.

Since CATE, synthesized in a three step reaction sequence,^[29] carries two carboxylic groups, it can either be placed within the scaffold, as a side chain, or end group. When placed within the scaffold, the remaining carboxylic groups after coupling was activated on solid support and coupled with ethylene diamine to give an amine group for attachment of the next building block. All oligomers were isolated after cleavage from the resin and purification by preparative HPLC as their formate salts with relative purities > 95 % (as determined by RP-HPLC) and further characterized by ¹H NMR and UHR-MS (see Supporting Information).

With these molecules in hand, we investigated their fluorescence properties in solid state in order to know the initial fluorescence of the compounds as a powder. All compounds showed emission maxima in the range of 455 nm ± 5 nm, meaning for our five compounds the AIE position has no influence on the emission behavior in the solid state (see Supporting Information, Figure S20).

We then looked at the AIE behavior in solution. For this purpose, we examine their fluorescence properties first without the presence of a potential binder but already looking at conditions typical for later biological testing (10 mM HEPES buffer at pH 7.4 and 6.5). The selected two pH values allow us to study the start fluorescence in uncharged and charged state of the binding motif, GCP (pK_a = 6.6). At a pH value of 7.4 the GCP is uncharged and at 6.5 it is mostly cationic. In general, for oligomers **O1–O5**, the AIE luminophore absorbed at 380 nm and emitted in the range of 425–575 nm (see concentration series in water Supporting Information). First, we look at the fluorescence of the oligomers at pH 7.4 at a concentration of 9.71 to 9.77 μM (Figure 1A). We observed weak fluorescence signals of the oligomers with an emission maximum at 450 nm. Compound **O4** had the lowest starting fluorescence suggesting that the AIE luminophore is not or only to a very minor degree restricted in its motion. In general, all oligomers where the luminophore was incorporated in the side chain (**O3–O5**) showed a lower starting fluorescence intensity than the derivatives where the luminophore was conjugated in the main chain (**O1, O2**). In comparison, **O1**, where the luminophore was incorporated at the end of the main chain, showed the highest fluorescence intensity, indicating AIE-effects. We attribute this to differences in the inter- and intramolecular interactions of the different structural units such as H-bonds of the amide groups, π-π stacking as well as cationic-aromatic interactions of the luminophore and the GCP motif based on their position within the oligomer. To evaluate this further, we reduced the pH value to 6.5. Figure 1B shows the emission maxima of **O1–O5** at pH 7.4 compared to 6.5 at identical fluorescence settings. In general, the emission intensity of all compounds at pH 6.5 increased. We attribute this to additional cationic-aromatic interactions caused by the cationic charge of the GCP^[30] that lead to more pronounced inter- and intramolecular interactions. The fluorescence at lower pH is thus a first insight into a potential bound or aggregated state of the AIE oligomers and thus their ability to change fluorescence upon interaction with

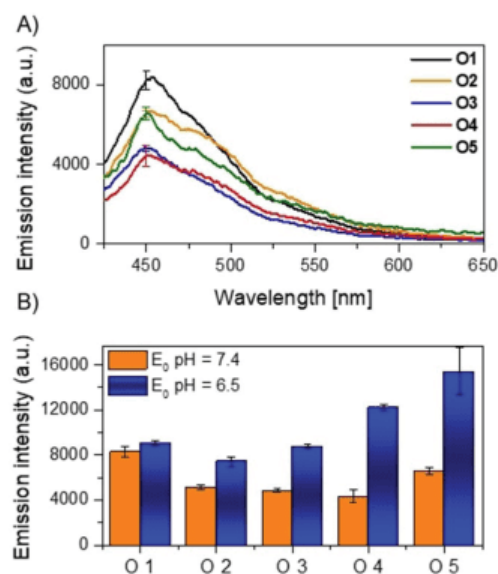


Figure 1. A) Starting fluorescence spectra of **O1–O5** (9.74 μM; 9.71 μM; 9.75 μM; 9.77 μM; 9.77 μM) in 10 mM HEPES buffer at pH = 7.4, (Triplicates, λ_{exc} = 380 nm). B) Starting fluorescence maxima at 450 nm of **O1–O5** in 10 mM HEPES buffer at pH = 7.4 and 6.5 (Triplicates, λ_{exc} = 380 nm).

a target structure. The increase in fluorescence was more pronounced for oligomers where the luminophore was side chain conjugated (**O3–O5**). This indicates that side chain conjugated oligomers could be more beneficial to allow for AIE behavior in solution as the luminophore remains less restricted by the scaffold itself when positioned in the side chain. Comparing compounds **O4** and **O5** carrying an additional hydrophilic building block in the side chain, this effect was more pronounced than for **O3**, supporting the idea that more flexibility in the non-bound state of the AIE-oligomer gives more pronounced AIE effects upon binding and/or aggregation.

In order to further evaluate the AIE behavior when bound to a potential target structure and to explore the potential use of the AIE oligomers as biosensors, we screened for potential binding partners. In our ligand design we applied GCP as binding unit. GCP is known to bind to oxyanions of various types, for example carboxylates^[16] or phosphates^[31] therefore we chose a range of anionic molecules and materials: bovine serum albumin (BSA), concanavalin A (Con A), esterase and 14-3-3_ζ were selected as proteins with an isoelectric point at or even below pH 5.^[32] Additionally trypsin with an isoelectric point of almost 11 was selected for comparison.^[33] In addition to the proteins, heparin and RNA as natural and poly(acrylic acid) (PAA) as non-natural polyanions were tested. Phosphate-buffered saline (PBS) was used as a small molecule anion along with sodium dodecyl sulfate (SDS) above its critical micelle concentration to give anionic micelles. As larger materials with

sizes on the order of 500 nm, poly(*N*-isopropylacrylamide) microgels (MGs) containing 2% or 5% methacrylic acid as anionic comonomer (MG 2% and MG 5%) were included in this study.^[34] Overall this offers a range of anionic materials of different size as well as charge density. AIE GCP oligomers were titrated against the different anionic compounds and emission was measured at 450 nm. Figure 2 depicts the differences observed for emission of the pure oligomers (E_0) divided by the emission detected for the mixture with the according anionic compound (E). Values for $E/E_0 = 1$ showed no AIE effect, values > 1 showed an increased emission upon mixing with the anionic compound and thus an AIE effect. Values that go below

1 would indicate fluorescence quenching. Surprisingly, we observed only very little AIE response, if at all, for oligomers **O1**–**O3** and **O5**. Only **O4** showed a clear increase in emission upon mixing with anionic MGs and PAA, less pronounced in mixtures with BSA, esterase, heparin, PBS, 14-3-3 ζ and RNA. It is noticeable that **O4** could achieve an AIE effect with anionic phosphates presented on RNA or in PBS as well as anionic amino acids on protein surfaces though these effects are not as pronounced. This can probably be attributed to the higher density of anionic groups within the polyanions in comparison to the proteins, as we also observed a stronger AIE effect for the MGs with a higher density of anionic groups, i.e. when comparing MG 5% vs. MG 2%. Overall, the AIE effect observed for our oligomers is not extremely high yet significant and well in the range of other ligands described in literature that have successfully used emission changes to detect ligand binding.^[35,36]

Figure 3 highlights the differences between **O4** (Figure 3B), and **O5** (Figure 3C) as exemplary non-AIE oligomer when binding to MGs and PAA. Also optically, the AIE effects were clearly visible for **O4** in contrast to **O5** with no increase in emission upon mixing with any of the anionic compounds. When looking at the emission maxima (Figure 3A), of **O4** when binding to MGs or PAA, we saw a slight shift to higher wavelengths from 450 nm for pure **O4** up to 462 nm by addition of MG 5%. This red-shift in the emission spectra could be attributed to the close proximity of the AIE fluorophore to the polar carboxylates when the oligomer binds to the anionic material. For anionic microgels we even observed turbidity which indicates a screening of the stabilizing charges and aggregation of MGs which would in turn further promote AIE effects.

Next, we looked at the resulting changes for the AIE effect of **O4** with selected materials at pH 6.5 instead of pH 7.4. We selected MGs, PAA and 14-3-3 ζ , as they already showed AIE effects at pH 7.4. For 14-3-3 ζ , **O4** showed no more AIE effect at pH 6.5. We attribute this to the increased number of cationic amino acids on the protein surface, which interfered with the binding of cationic GCP of **O4** to 14-3-3 ζ .

For MGs and of PAA, on the other hand, we still observed a clear AIE effect also at pH 6.5. Again, the most pronounced AIE effects in this series were achieved with MG 5%. Interestingly, as the PAA fluorescence intensity is higher at pH 6.5, this system seems to profit more from the increased cationic charge of the GCP units. This could potentially be a concentration dependent effect, where the ratio of anionic groups to GCP motifs could also affect the complex formation and thus AIE read out.

To further investigate the concentration dependence of the AIE effect, we looked at two titration series of PAA to the oligomer **O4**. Figure 4A shows the AIE effects of the titration of PAA. We started at a ratio of 1 μ M PAA to 9.77 μ M oligomer, which corresponds to about 10 molecules of **O4** per PAA chain with an average of 6250 acrylic acid side chains. Next, we further increased the amount of PAA thereby diluting the ratio of oligomer per PAA. Within the error margins of these experiments, we saw a slight decrease in AIE with increasing concentration of PAA but the AIE effect remained indicating

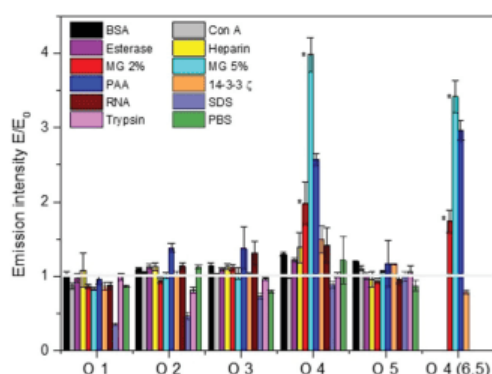


Figure 2. Change in fluorescence emission of **O1**–**O5** (9.74 μ M; 9.71 μ M; 9.75 μ M; 9.77 μ M; 9.77 μ M) in the presence of different anionic molecules, aggregates and materials measured in 10 mM HEPES buffer at pH = 7.4. (Triplicates, λ_{exc} = 380 nm, λ_{em} = 450 nm, E = Final Emission, E_0 = Start; BSA, Con A, Heparin, PAA, PBS, Trypsin and 14-3-3 ζ 10 μ M; Esterase and Micro gel (NIPAM-co-MAA Copolymer) 2 and 5%, RNA 100 μ g/ml and SDS 10 mM) and **O4** (6.5) (10 mM HEPES buffer at pH = 6.5) PAA, Micro gel (NIPAM-co-MAA Copolymer) 2 and 5%. Samples that showed turbidity are marked with *.

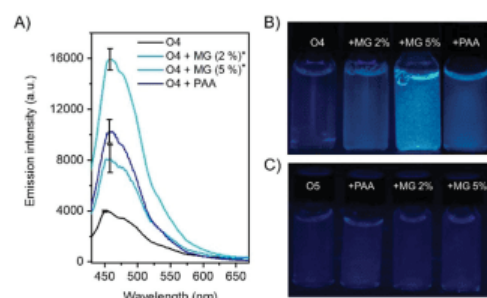


Figure 3. A) Fluorescence spectra of **O4** (9.77 μ M) pure (black) and in the presence of MG 2% 100 μ g/ml, MG 5% 100 μ g/ml and PAA 10 μ M (triplicates, λ_{exc} = 380 nm, λ_{em} = 450 nm). Samples that showed turbidity are marked with *. Comparison of fluorescence emission of B) **O4** and C) **O5** (both 9.77 μ M) with and without anionic binders. Reflection effects on the glass surface were removed using GIMP 2.10 software.

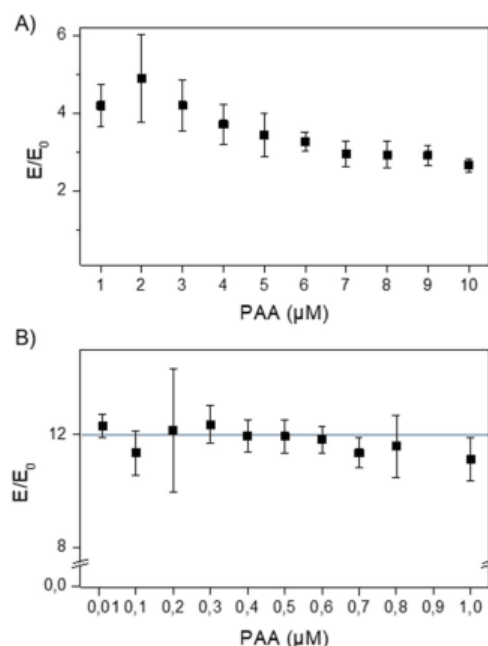


Figure 4. Change in fluorescence emission of **O4** (9.77 μM) in the presence of PAA A) 1–10 μM and B) 0.01–1 μM ; both assays in 10 mM HEPES buffer at pH = 7.4, (triplicates, λ_{exc} = 380 nm, λ_{em} = 450 nm, E = Final Emission, E_0 = Start). In concentration series B, turbidity was observed for all samples.

that interaction of the oligomer and the polyanion lead to some change in vibrational and/or rotational freedom of the fluorophore. When performing the titration starting from a higher ratio of oligomer per PAA chain, 0.01 to 1 μM of PAA (Figure 4B), we observed a stronger AIE effect that was accompanied by turbidity in all samples. Higher concentrations of **O4** more effectively shield the anionic charge of the PAA chains, leading to destabilization and aggregation. As could be expected, for these samples an overall higher AIE effect was observed. Overall, these experiments demonstrate that **O4** showed AIE behavior over a wide range of concentrations. For a potential application in biological settings this could indeed be an important feature as concentrations of a target protein for

example inside a cell or cellular compartment might not be known.

The oligomer fluorescence properties without the presence of an anionic binder, indicate that intra- and intermolecular interactions of the oligomers in solution affect their AIE properties. In order to investigate intermolecular interactions in more detail, we analyzed the oligomer aggregation behavior in water via atomic force microscopy (AFM) and scanning electron microscopy (SEM).

All samples were prepared from 100 μM aqueous solution and dried by spincoating prior to sample analysis. Figure 5 shows representative AFM data for all oligomers (for detailed zoomed in data see Supporting Information). Similar structures for the different samples were also observed by SEM (see Supporting Information). Indeed, we saw clear differences between the different oligomers. Particularly oligomer **O2** formed network like structures whereas **O3–O5** showed shorter linear structures and **O1** showed spherical aggregates. We hypothesize that when positioning the AIE at the end of the main chain end, as in **O1**, we induce an amphiphilic character of the overall oligomer which in turn could lead to the formation of spherical aggregates, similar to micelles. When moving the AIE more towards the middle of the scaffold, amphiphilicity seems to be reduced and we observed network formation of **O2**. Similar effects have been already described for other AIE luminophore systems, for example Gonzalez-Rodriguez et al. as well as B. Z. Tang showed the occurrence of network formation induced by π - π interactions of the AIE luminophores, which are supported by additional hydrogen bonds to large defined superstructures.^[37,38] When moving the AIE into the side chain of the oligomer, we still observed aggregates that were smaller and linear rather than larger networks. The stacking of oligomers is likely less ordered when going from linear to branched oligomers as is the case when moving from **O2** to **O3–O5**. This is in line with similar observations on linear and branched polymers, where an increase in branching reduces intermolecular interactions and thereby increases the free volume and flexibility of the chains.^[39] It is thus not surprising that a branched oligomer, **O4**, was the one oligomer that showed AIE behavior.

When comparing the three branched oligomers of this series, **O3–O5**, the main difference between **O3/O5** (showing no AIE) and **O4** (showing AIE) is the relative positioning of the AIE luminophore and the binding GCP unit. In **O3** and **O5**, luminophore and GCP were placed next to each other, while in **O4** we added a spacer building block introducing an additional diethyleneglycol linker in between. We originally rationalized

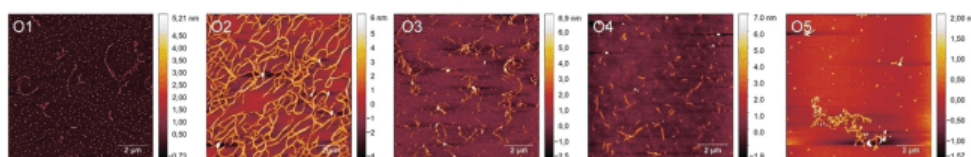


Figure 5. Atomic force microscope images of **O1–O5** (100 μM in Millipore water). Further AFM, SEM images and their analysis see the Supporting Information.

that a closer proximity of luminophore and binding unit should be beneficial for the AIE effect, in order to enable a more pronounced change in rotational and vibrational freedom upon binding of the GCP unit. However, unexpectedly, only the introduction of an additional linker between luminophore and binding unit leads to an AIE active oligomer. Future studies will explore this effect further by synthesizing oligomers with additional linker units of different length and flexibility as well as for oligomers presenting multiple GCP motifs, thereby looking more closely at the interplay of inter- and intramolecular interactions.

Conclusion

In summary, we realized the sequence-defined positioning of an AIE luminophore within oligomers presenting the supramolecular binding motif GCP. Surprisingly, we found that only one of the oligomeric structures of this study showed an AIE effect in solution when interacting with anionic structures. The fluorescence results demonstrate that indeed the positioning of AIE luminophore and binding motif (here GCP) within an oligomeric ligand affect the ability of the luminophore to show AIE behavior. None of the oligomers that has the AIE luminophore in the main chain and directly attached the GCP motif to the main chain show AIE behavior in solution. However, also for the side chain constructs, a fine differentiation was observed in terms of the relative positioning of AIE and GCP. It seems that directly linking AIE and GCP motifs through the ethylene diamine linker does not allow for AIE behavior, while introducing an additional EDS building block lead to **O4** and clear AIE properties. Based on our findings we can now further develop sequence-defined oligomers carrying both, supramolecular binding motifs and AIE luminophores, and explore their potential as biosensors.

Acknowledgements

The authors acknowledge funding from the DFG through the collaborative research center 1093 (projects A10, A11 and A1). We thank Christian Ottmann for providing 14-3-3 ζ and Tobias Wilcke and Henning Berens for taking the photos for Figure 3. We thank Steffen Riebe for helping with the initial synthesis of the AIE luminophore. We thank Tobias Bochmann for scanning electron microscopy. Open access funding enabled and organized by Projekt DEAL.

Conflict of Interest

The authors declare no conflict of interest.

Keywords: aggregation induced emission • biosensors • sequence-defined oligomers • solid phase polymer • supramolecular synthesis

- [1] H. Fang, S. Xu, Bin Liu, *Adv. Mater.* **2018**, *30*, 1801350.
- [2] Y. Hong, *Methods Appl. Fluoresc.* **2016**, *4*, 022003.
- [3] J. Luo, Z. Xie, J. W. Y. Lam, L. Cheng, H. Chen, C. Qiu, H. S. Kwok, X. Zhan, Y. Liu, D. Zhuc, B. Z. Tang, *Chem. Commun.* **2001**, *18*, 1740–1741.
- [4] J. Liang, B. Z. Tang, B. Liu, *Chem. Soc. Rev.* **2015**, *44*, 2798–2811.
- [5] Z. Zhao, J. W. Y. Lam, B. Z. Tang, *J. Mater. Chem.* **2012**, *22*, 23726–23740.
- [6] Z. Zhao, B. He, B. Z. Tang, *Chem. Sci.* **2015**, *6*, 5347–5365.
- [7] X. Gu, J. Yao, G. Zhang, Y. Yan, C. Zhang, Q. Peng, Q. Liao, Y. Wu, Z. Xu, Y. Zhao, H. Fu, D. Zhang, *Adv. Funct. Mater.* **2012**, *22*, 4862–4872.
- [8] X. Gu, J. Yao, G. Zhang, C. Zhang, Y. Yan, Y. Zhao, D. Zhang, *Chem. Asian J.* **2013**, *8*, 2362–2369.
- [9] H. Zhou, M. H. Chua, B. Z. Tang, J. Xu, *Polym. Chem.* **2019**, *10*, 3822–3840.
- [10] M. Gao, S. Li, Y. Lin, Y. Geng, X. Ling, L. Wang, A. Qin, B. Z. Tang, *ACS Sens.* **2016**, *1*, 179–184.
- [11] M. Hayduk, S. Riebe, K. Rudolph, S. Schwarze, F. van der Vight, C. G. Daniliuc, G. Jansen, J. Voskuhl, *Isr. J. Chem.* **2018**, *58*, 927–931.
- [12] R. T. K. Kwok, C. W. T. Leung, J. W. Y. Lam, B. Z. Tang, *Chem. Soc. Rev.* **2015**, *44*, 4228–4238.
- [13] S. Riebe, C. Vallet, F. van der Vight, D. Gonzalez-Abadelo, C. Wölper, C. A. Strassert, G. Jansen, S. Knauer, J. Voskuhl, *Chem. Eur. J.* **2017**, *23*, 13660–13668.
- [14] I. M. Khan, S. Niazi, M. K. Iqbal Khan, I. Pasha, A. Mohsin, J. Haider, M. W. Iqbal, A. Rehman, L. Yue, Z. Wang, *TrAC Trends Anal. Chem.* **2019**, *119*, 115637.
- [15] a) L. A. Logsdon, C. L. Schardon, V. Ramalingam, S. K. Kwee, A. R. Urbach, *J. Am. Chem.* **2011**, *133*, 17087–17092; b) F. Trusch, K. Kowski, K. Bravo-Rodriguez, C. Beuck, A. Sowislok, B. Wellig, A. Matena, E. Sanchez-Garcia, H. Meyer, T. Schrader, P. Bayer, *Chem. Commun.* **2016**, *52*, 14141–14144; c) J. Matic, F. Supljika, N. Tir, P. Piotrowski, C. Schmuck, M. Abramic, I. Plantanida, S. Tomic, *RSC Adv.* **2016**, *6*, 83044.
- [16] C. Schmuck, *Chem. Eur. J.* **2000**, *6*, 709–718.
- [17] C. Schmuck, J. Lex, *Org. Lett.* **1999**, *1*, 1779–1781.
- [18] C. Schmuck, *Coord. Chem. Rev.* **2006**, *250*, 3053–3067.
- [19] J. Matic, F. Supljika, T. Tandarić, M. Dukši, P. Piotrowski, R. Vianello, A. Brozovic, I. Plantanida, C. Schmuck, M. R. Stojković, *Int. J. Biol. Macromol.* **2019**, *134*, 422–434.
- [20] M. Giese, J. Niemeyer, J. Voskuhl, *ChemPlusChem* **2020**, *85*, 985.
- [21] a) M. A. R. Meier, C. Barner-Kowollik, *Adv. Mater.* **2019**, *31*, 1806027; b) W. Konrad, F. R. Bloesser, K. S. Wetzel, A. C. Boukis, M. A. R. Meier, C. Barner-Kowollik, *Chem. Eur. J.* **2018**, *24*, 3413.
- [22] D. Ponader, F. Wojcik, F. Beceren-Braun, J. Darnedde, L. Hartmann, *Biomacromolecules* **2012**, *13*, 1845–1852.
- [23] C. Gerke, F. Jacobi, L. E. Goodwin, F. Pieper, S. Schmidt, L. Hartmann, *Macromolecules* **2018**, *51*, 5608–5619.
- [24] S. Boden, F. Reise, J. Kania, T. K. Lindhorst, L. Hartmann, *Macromol. Biosci.* **2019**, *19*, 1800425.
- [25] a) C. Gerke, M. F. Ebbesen, D. Jansen, S. Boden, T. Freichel, L. Hartmann, *Biomacromolecules* **2017**, *18*, 787–796; b) M. F. Ebbesen, C. Gerke, P. Hartwig, L. Hartmann, *Polym. Chem.* **2016**, *7*, 7086–7093.
- [26] P. Pasch, A. Höing, S. Ueclue, M. Killa, J. Voskuhl, S. K. Knauer, L. Hartmann, *Chem. Commun.* **2021**, *57*, 3091–3094.
- [27] a) J. Stelzer, C. Vallet, A. Sowa, D. Gonzalez-Abadelo, S. Riebe, C. G. Daniliuc, M. Ehlers, C. A. Strassert, S. K. Knauer, J. Voskuhl, *ChemistrySelect* **2018**, *3*, 985–991; b) P. Ahlers, C. Götz, S. Riebe, M. Zirbes, M. Jochem, D. Spitzer, J. Voskuhl, T. Basché, P. Besenius, *Polym. Chem.* **2019**, *10*, 3163–3169.
- [28] a) S. Riebe, C. Wölper, J. Balszuweit, M. Hayduk, M. E. Gutierrez Suburu, C. A. Strassert, N. L. Doltsinis, J. Voskuhl, *ChemPhotoChem* **2020**, *4*, 383–384; b) H. Frisch, D. Spitzer, M. Haase, T. Basché, J. Voskuhl, P. Besenius, *Org. Biomol. Chem.* **2016**, *14*, 5574–5579.
- [29] a) C. Schmuck, V. Bickert, M. Merschky, L. Geiger, D. Rupprecht, J. Dudaczek, P. Wich, T. Rehm, U. Machon, *Eur. J. Org. Chem.* **2008**, *2*, 324–329; b) M. Externbrink, S. Riebe, C. Schmuck, J. Voskuhl, *Soft Matter* **2018**, *14*, 6166–6170.
- [30] J. Hatai, C. Schmuck, *Acc. Chem. Res.* **2019**, *52*, 1709–1720.
- [31] S. Junghänel, S. Karczewski, S. Bäcker, S. K. Knauer, C. Schmuck, *ChemBioChem* **2017**, *18*, 2268–2279.
- [32] a) W. S. Ang, M. Elimelech, *J. Membr. Sci.* **2007**, *296*, 83–92; b) G. Entlicher, J. V. Koštil, J. Kocourek, *Biochim. Biophys. Acta* **1971**, *236*, 795–797; c) D. Wynne, Y. Shalitin, *Arch. Biochem.* **1973**, *154*, 199–203.
- [33] M. Bier, F. F. Nord, *Arch. Biochem.* **1951**, *33*, 320–332.
- [34] a) S. Schmidt, T. Hellweg, R. von Klitzing, *Langmuir* **2008**, *24*, 12595–12602; b) S. Schmidt, H. Motschmann, T. Hellweg, R. von Klitzing, *Polymer* **2008**, *49*, 749–756; c) T. Hoare, R. Pelton, *Langmuir* **2004**, *20*,

- 2123–2133; d) A. Strzelczyk, T. J. Paul, S. Schmidt, *Macromol. Biosci.* **2020**, *20*, 2000186.
- [35] D. Maitly, A. Gigante, P. A. Sánchez-Murcia, E. Sijbesma, M. Li, D. Bler, S. Mosel, S. Knauer, C. Ottmann, C. Schmuck, *Org. Biomol. Chem.* **2019**, *17*, 4359–4363.
- [36] Y. Liu, C. Deng, L. Tang, A. Qin, R. Hu, J. Z. Sun, B. Z. Tang, *J. Am. Chem. Soc.* **2011**, *133*, 660–663.
- [37] D. Gonzalez-Rodriguez, A. P. H. J. Schenning, *Chem. Mater.* **2011**, *23*, 310–325.
- [38] J. Li, J. Wang, H. Li, N. Song, D. Wang, B. Z. Tang, *Chem. Soc. Rev.* **2020**, *49*, 1144–1172.
- [39] a) L. J. Markoski, J. S. Moore, I. Sendjarevic, A. J. McHugh, *Macromolecules* **2001**, *34*, 2695; b) J. Peter, A. Khalyavina, J. Kriz, M. Bleha, *Eur. Polym. J.* **2009**, *45*, 1716.

Manuscript received: March 25, 2021

Accepted manuscript online: April 20, 2021

Version of record online: May 28, 2021

Chemistry–A European Journal

Supporting Information

Take your Positions and Shine: Effects of Positioning Aggregation-Induced Emission Luminophores within Sequence-Defined Macromolecules

Peter Pasch, Matthias Killa, Hauke Lukas Junghans, Melanie Schmidt, Stephan Schmidt, Jens Voskuhl,* and Laura Hartmann*

Materials:

Diethyl ether (with BHT as inhibitor, $\geq 99.8\%$), triisopropylsilane (TIPS) (98%), concentrated hydrochloric acid (pa), acetic anhydride (pa) methacrylic acid (MAA, 99%) ammonium peroxodisulfate (APS, 98%), poly(acrylic acid) [$M_v \sim 450,000$], bovine serum albumin (BSA), esterase from porcine, ribonucleic acid (RNA) from yeast, heparin, phosphate buffered saline powder (PBS) and formic acid (pa) were purchased from Sigma Aldrich. Concanavalin A was purchased from LKT Laboratories. N,N-Diisopropylethylamine (DIPEA) ($\geq 99\%$) was purchased from Carl Roth. N,N-dimethylformamide (DMF) (99.8%, for peptide synthesis), N-isopropylacrylamide (NIPAM) and piperidine (99%) were obtained from Acros Organics. Dichloromethane (DCM) (99.99%), ethyl acetate (analytical reagent grade), 1 M sodium hydroxide and 1,4-dioxane (analytic reagent grade) were purchased from Fisher Scientific. Acetonitrile was purchased from AppliChem. Trifluoroacetic acid (TFA) (99%), benzotriazol-1-yl-oxytripyrrolidinophosphonium hexafluoro phosphate (PyBOP), and triethylsilane (analytical reagent grade) were purchased from Fluorochem. TentaGel® S RAM (Rink Amide) (loading: 0.23 mmol / g) was purchased from RAPP Polymer. N_α -Fmoc- N_β -Boc-L-2,3 - diaminopropionic acid ($\geq 98.0\%$) was purchased from TCI. N,N - methylenebisacrylamide was purchased from Merk (MBA, $\geq 98\%$) and sodium dodecyl sulfate from Serva (SDS).

Methods:

Preparative RP-HPLC: An Agilent 1260 Infinity device coupled to a variable wavelength detector (VWD) (set to 214 nm) and an automated fraction collector was used to purify the oligo(amidoamines). An RP-HPLC column, CAPCELL PAK C18 (20 x 250 mm, 5 μ m), was used. The mobile phases A and B were H₂O and acetonitrile, each containing 0.1 vol% formic acid. The flow rate was set at 15 ml/min.

Reversed Phase - High Pressure Liquid Chromatography- Mass Spectrometry (RP- HPLC-MS)/Electron Spray Ionization - Mass Spectrometry (ESI-MS): RP-HPLC-MS was carried out on an Agilent 1260 Infinity instrument coupled to a variable wavelength detector (VWD) (set to 214 nm) and a 6120 Quadrupole LC/MS containing an Electrospray Ionization (ESI) source (operation mode positive, m/z range from 200 to 2000). A MZ-AquaPerfect C18 (3.0 x 50 mm, 3 μ m) RP column from Mz-Analysentechnik was used. As eluent system water/acetonitrile containing 0.1 vol% formic acid was applied. The mobile phases A and B were: System A) H₂O/acetonitrile (95/5, v/v); System B) H₂O / acetonitrile (5/95, v/v). The samples were analyzed at a flow rate of 0.4 ml/min using a linear gradient, starting with 100% of system A) and reaching 100% system B) within 30 min. The temperature of the column room was set to 40 °C. All relative purities were determined using the OpenLab ChemStation software for LC/MS from Agilent

Technologies. ESI-MS measurements were performed with the above mentioned ESI source and quadrupole detector.

Ultra High Resolution - Mass Spectrometry (UHR-MS): UHR-MS measurements were performed with a Bruker UHR-QTOF maXis 4G instrument with a direct inlet via syringe pump, an ESI source and a quadrupole followed by a Time of Flight (QTOF) mass analyzer.

Nuclear Magnetic Resonance Spectroscopy (NMR): The ^1H -NMR spectra were recorded on a Bruker Avance III 600 (600 MHz). These spectra were evaluated according to the following scheme: (frequency in MHz, deuterated solvent), chemical shift in ppm (multiplicity, coupling constant, integral, signal assignment). The chemical shift is given in relation to the ^1H signals of the deuterated solvents used ((δ 2.50 [DMSO- d_6])). The multiplicities of the signals were abbreviated as follows: s (singlet), d (doublet), t (triplet), m (multiplet).

Freeze dryer: Oligomers were lyophilized with an Alpha 1-4 LD plus instrument from Martin Christ Freeze Dryers GmbH. The drying method was set to -40 °C and 0.1 mbar.

Fluorescence: Emission spectra were recorded at 298 K on CLARIOstar BMG LABTECH microplate reader. For sample preparation, the compounds were freeze-dried and stock solutions were prepared in Millipore water for each. Based on these, the respective concentrations were adjusted with buffer systems (10 mM HEPES buffer) and the pH values of 6.5 or 7.4. Subsequently, the samples were measured using Cell Culture microplate, 96 well, F-bottom from greiner bio-one. The excitation wavelength was 380 nm and triplicates were measured. Emission and excitation spectra in the solid state were measured on a Shimadzu RF 6000 spectrometer using a solid sample holder. The pure sample was placed between two quartz plates and measured in a 90° angle.

Atomic force microscopy (AFM): 10 μL of a 100 μM solution of the molecules in water were dropped onto a freshly cleaved mica surface (Plano) and dried by spin-coating (30 rps) for 15 min. The AFM images were taken in tapping mode using a NanoDrive Controller with an Innova Scanning Probe Microscope (Veeco) and N-type silicon cantilever (Olympus AC 160TS). The AFM-images were analysed with the Gwyddion-2.49 software.

Scanning Electron Microscope (SEM): 10 μL of a 100 μM solution of molecules in water were dropped onto a spinning (30 rps) mica surface (Plano). After 15 min of spinning, the dried surface was sputtered with a Sputter Coater Cressington MTM 10 (sputter source $\text{Au}_{80}\text{Pd}_{20}$, 12 positions for 13 mm SEM

samples). The SEM images were taken with Apreo S LoVac (Thermo Fisher Scientific). The SEM-images were analysed with ImageJ.

Solid phase synthesis procedures:

General: The oligo(amidoamines) synthesis were carried out manually in 10 ml polypropylene syringe reactors with a polyethylene frit and a Luer stopper from MultisynTech GmbH. All oligo(amidoamines) were synthesized on the TentaGel® S RAM (Rink Amide) resin with a loading of 0.23 mmol/g. Batch sizes of all oligo(amidoamines) were 0.15 mM.

Coupling protocol: First the resin was swollen in DCM for 30 min and then washed three times with DMF. The Fmoc protecting group has to be removed before further couplings! For the building block, amino acid or GCP coupling, respectively, 5 eq., 5 eq. PyBOP and 10 eq. DIPEA were dissolved in 5 ml DMF, drawn into the reactor syringe and shaken for 90 min, followed by washing ten times with DMF. A double coupling, adding fresh building block and coupling reagents, was performed each time the GCP motif was coupled. For the coupling of the diacid AIE chromophore 10 eq. of the AIE building block, 10 eq. PyBOP and 20 eq. DIPEA were used in 6 ml DMF. In addition, a double coupling was carried out.

Fmoc cleavage: The resin was swollen in DCM for 30 min and subsequently washed three times with DMF. Secondly the Fmoc protecting group of the resin as well as from the coupled building blocks or amino acids was cleaved by means of a 25% solution of piperidine in DMF (7mL) achieving an amine end group. The deprotection was carried out twice with the mentioned cleavage solution for 20 min. Afterwards the resin was washed 10 times with DMF.

Boc-cleavage: For Boc-deprotection, 6 ml of a 4 M HCl in dioxane solution (2 ml HCl conc. and 4 ml dioxane) was drawn into the reactor syringe and shaken for 10 min. Afterwards the reaction syringe was washed 3 times with dioxane and again 6 ml fresh 4 M HCl dioxane solution was drawn into the syringe and shaken for 20 min. Subsequently the solution was removed and the resin washed three times alternately with dioxane and DCM. To neutralize the resin, a 10 volume percent ice-cold DIPEA DCM solution was drawn up twice and shaken for 10 min. Last the resin was washed alternately three times with dioxane and DCM and finally 10 times with DMF.

Capping of N-terminal primary amine: With scaffold completion of the oligo(amidoamine), the N-terminal amine group was acetylated with 8 ml of acetic anhydride, shaking for 20 min. After that, the resin was washed 5 times with DMF.

Cleavage from solid phase: The oligo(amidoamines) were cleaved from the TentaGel® S RAM resin by drawing up a solution of 5 vol% triisopropylsilane (TIPS) and 95 vol% TFA into the syringe and shaking

for 1.5 hours. Afterwards the solution was poured into ice cooled diethyl ether. The resulting precipitate was centrifuged off and the supernatant was decanted off. The pellet was washed 3 times with diethyl ether. The product was dried and dissolved in Millipore water. The entire solution was collected in a falcon and freeze-dried to isolate the product. Subsequently, the products were purified by means of preparative HPLC. Due to the purification by preparative HPLC and the added 0.1 vol% formic acid in the mobile phases, the structures are present as formate salts. For more information, please refer to the respective ^1H NMR data.

Synthesis of EDS, AIE, GCP and microgels: (4-((2-(2-(2-aminoethoxy)ethoxy)ethyl)-amino)-4-oxobutanoic) was synthesized according to literature.^[1] AIE building block was synthesized according to literature.^[2] N-Boc-protected 5-(guanidinocarbonyl)-1H-pyrrole-2-carboxylic acid was synthesized according to literature^[3] and recrystallized from methanol yielding the free carboxylic acid of GCP. Microgels were synthesized and characterized according to literature.^[4]

Analytical data of oligomers O1-O5:

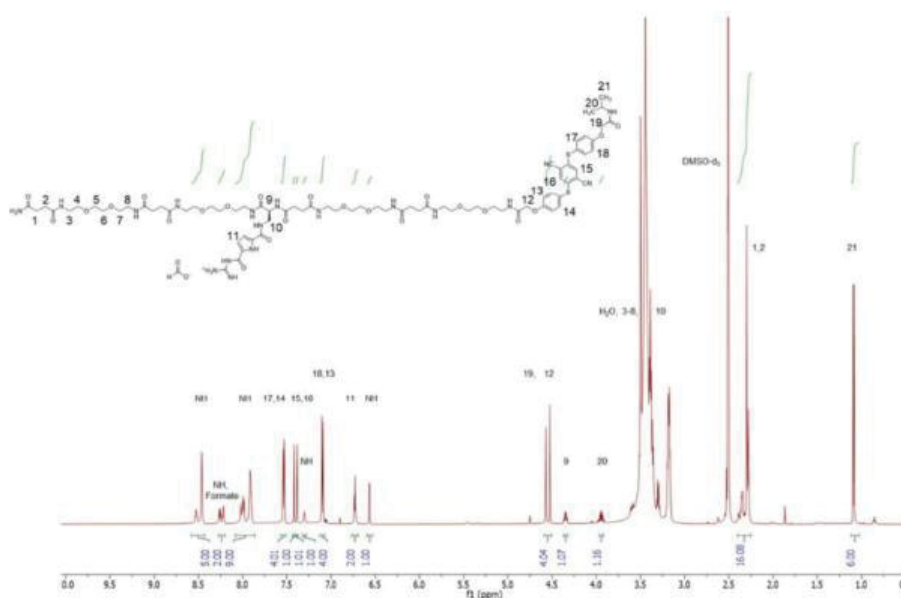


Figure S 1: ^1H -NMR (600 MHz, $\text{DMSO}-d_6$) of **O1** as formate at RT.

^1H -NMR (600 MHz, $\text{DMSO}-d_6$): δ (ppm) = 8.62-8.42 (m, 5H, NH), 8.29-8.20 (m, 2H, NH and formate) 8.15-7.82 (m, 9H, NH) 7.53 (d, 3J = 8.60 Hz, 4H, H17,14), 7.44 (s, 1H, H15), 7.39 (s, 1H, H16), 7.33 (s, 1H, NH)

7.05 (d, $^3J = 8.54$ Hz, 4H, H18,13), 7.27-7.21 (m, 2H, H11), 6.59 (s, 1H, NH), 4.53 (d, $^2J = 5.51$ Hz, 4H, H19,12), 4.40-4.31 (m, 1H, H9), 3.99-3.90 (m, 1H, H₂O), water signal covers signals H3-H8 and H10, 2.41-2.23 (m, 16H, H1,2), 1.10 (s, 6H, H21).

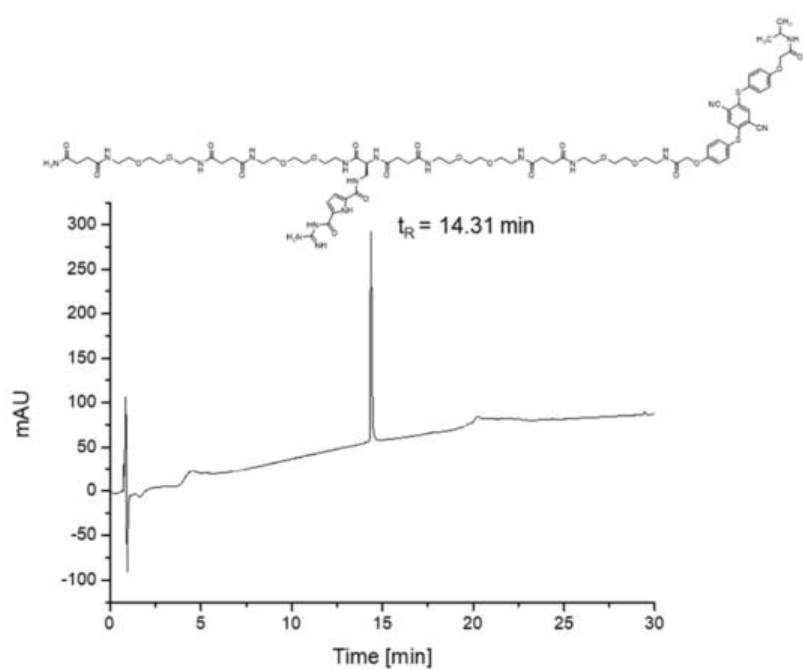


Figure S 2: RP-HPLC analysis of **O1** with relative purities >95% (linear gradient from 5-95% acetonitrile in Millipore water in 30 min at 40 °C).

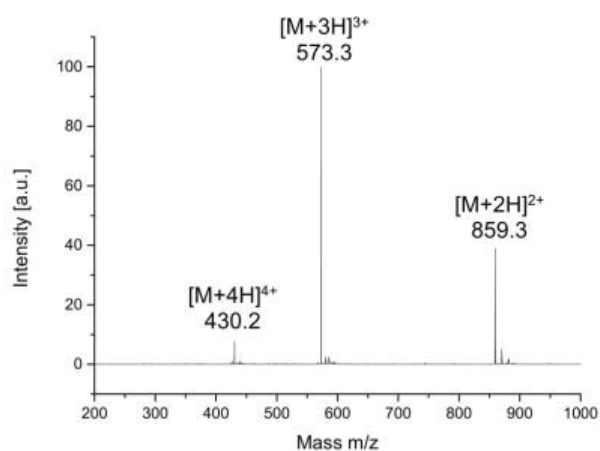


Figure S 3: ESI-MS (ESI⁺, single quadrupole) of **O1**.

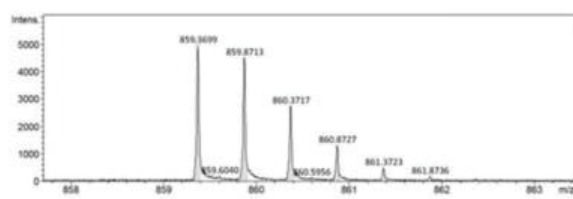


Figure S 4: HR-ESI-MS of **O1**.

HR-ESI-MS: for $C_{77}H_{108}N_{18}O_{23}S_2$ m/z $[M+2H]^{2+}$ calcd.: 859.3711, found: 859.3699, mass accuracy +1.4 ppm.

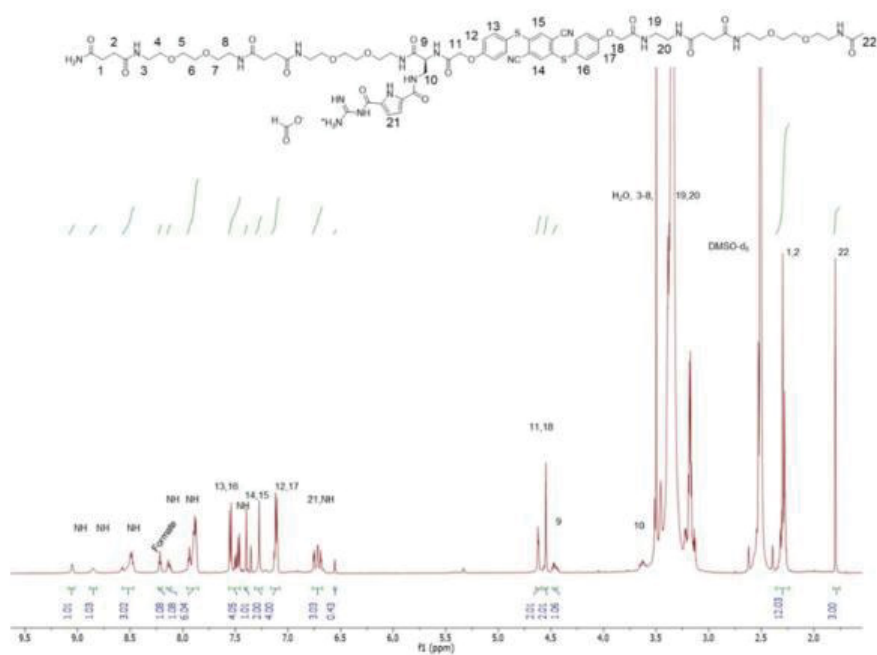


Figure S 5: ^1H -NMR (600 MHz, $\text{DMSO-}d_6$) of **O2** as formate at RT.

^1H -NMR (600 MHz, $\text{DMSO-}d_6$): δ (ppm) = 9.11 (s, 1H, NH), 8.59 (s, 1H, NH), 8.58-8.46 (m, 3H, H1), 8.25-8.20 (m, 1H, formate), 8.17-8.13 (m, 1H, NH), 7.94-7.82 (m, 6H, NH), 7.58-7.44 (m, 4H, H16,13), 7.40 (s, 1H, NH), 7.29-7.23 (m, 2H, H15,14), 7.20-7.11 (m, 4H, H17,12), 7.28-7.17 (m, 3H, H21, NH), 6.59 (s, 1H, NH), 4.63 (s, 2H, H11), 4.55 (s, 2H, H18), 4.46-4.40 (m, 1H, H9), water signal covers signals H3-H8, H10, H19, H20, 2.40-2.25 (m, 12H, H1,2), 1.77 (s, 3H, H22).

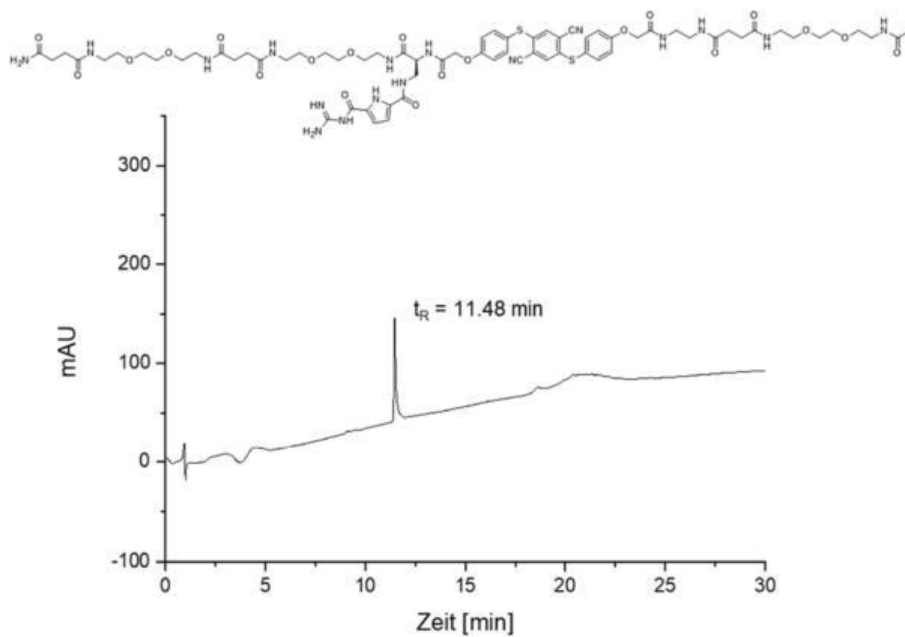


Figure S 6: RP-HPLC analysis of **O2** with relative purities >95% (linear gradient from 5-95% acetonitrile in Millipore water in 30 min at 40 °C).

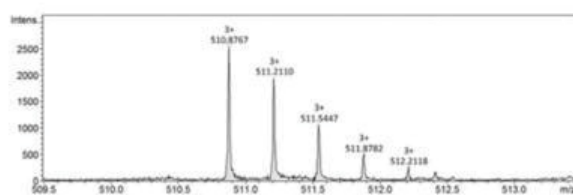


Figure S 7: HR-ESI-MS of **O2**.

HR-ESI-MS: for $C_{68}H_{91}N_{17}O_{20}S_2$ m/z $[M+3H]^{3+}$ calcd.: 510.8758, found: 510.8767, mass accuracy - 2.4 ppm.

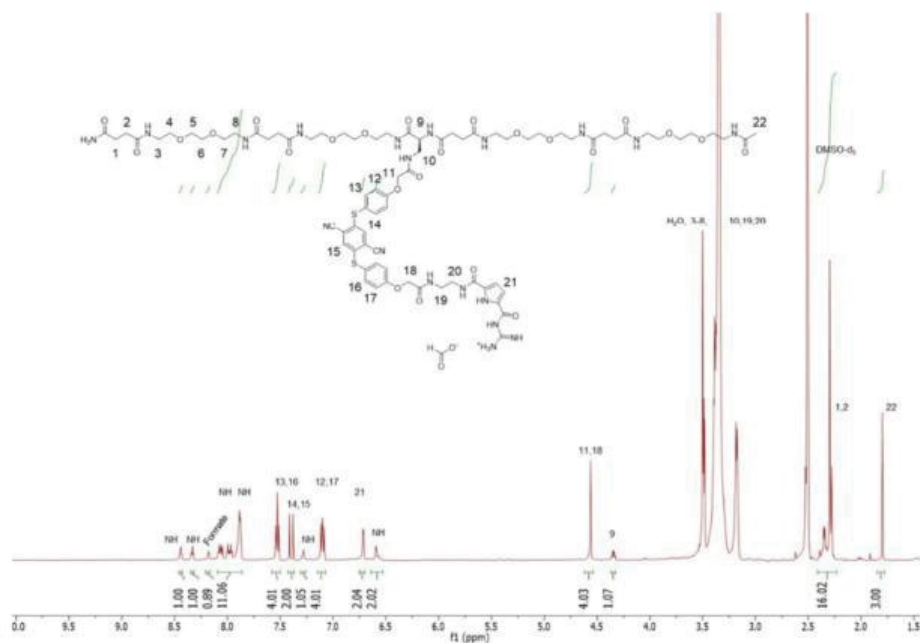


Figure S 8: ^1H -NMR (600 MHz, $\text{DMSO}-d_6$) of **O3** as formate at RT.

^1H -NMR (600 MHz, $\text{DMSO}-d_6$): δ (ppm) = 8.48-8.43 (m, 1H, NH), 8.36-8.32 (m, 1H, NH), 8.21 (s, 1H, formate), 8.15-7.82 (m, 11H, NH), 7.59-7.48 (m, 4H, H16,13), 7.41 (d, $^3J = 8.5$ Hz, 2H, H15,14), 7.27 (s, 1H, NH), 7.21-7.10 (m, 4H, H17,12), 7.26-7.19 (m, 2H, H21), 6.62-6.52 (m, 1H, NH), 4.55 (s, 4H, H18,11), 4.34-4.29 (m, 1H, H9), water signal covers signals H3-H8, H10, H19, H20, 2.46-2.21 (m, 16H, H1,2), 1.77 (s, 3H, H22).

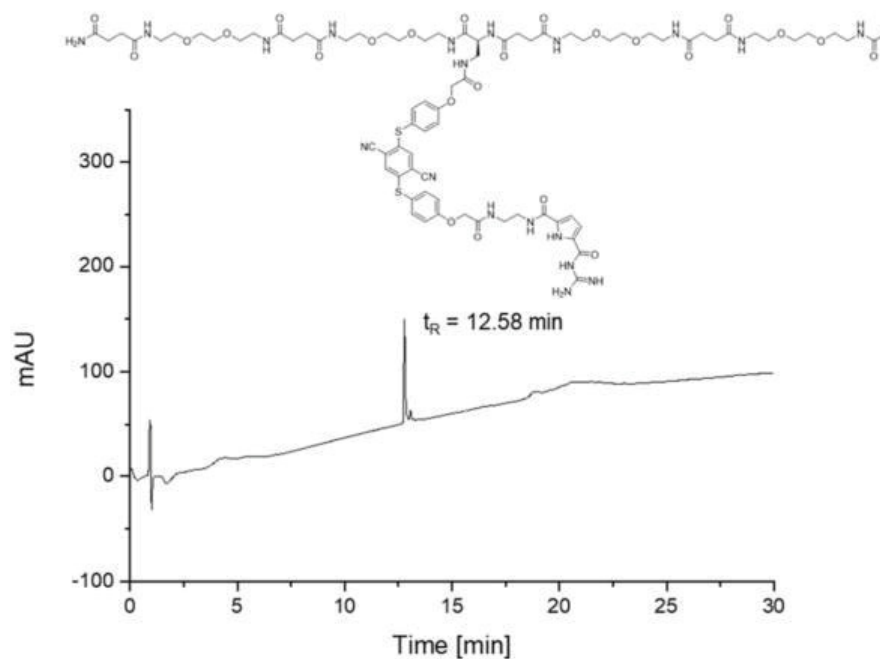


Figure S 9: RP-HPLC analysis of **O3** with relative purities >95% (linear gradient from 5–50% acetonitrile in Millipore water in 30 min at 40 °C).

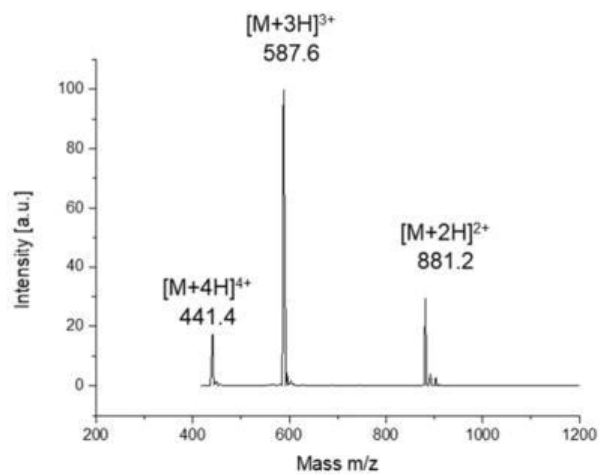


Figure S 10: ESI-MS (ESI⁺, single quadrupole) of **O3**.

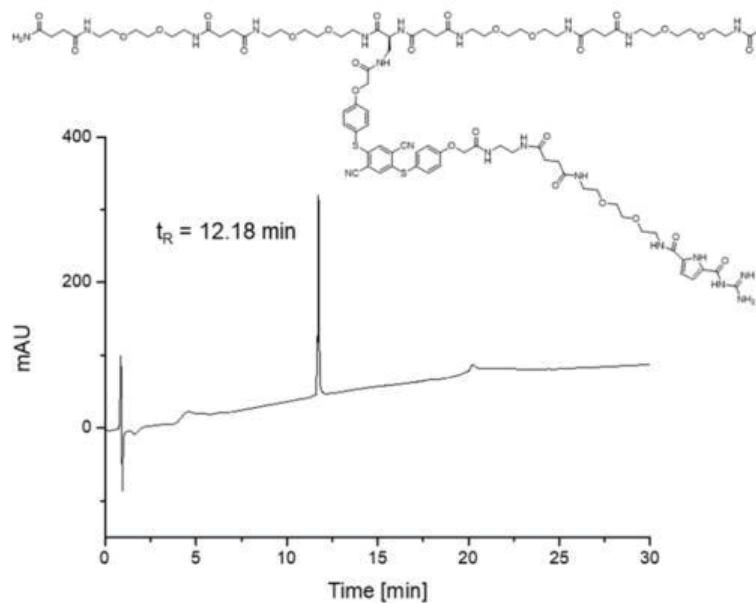


Figure S 13: RP-HPLC analysis of **O4** with relative purities >95% (linear gradient from 5-95% acetonitrile in Millipore water in 30 min at 40 °C).

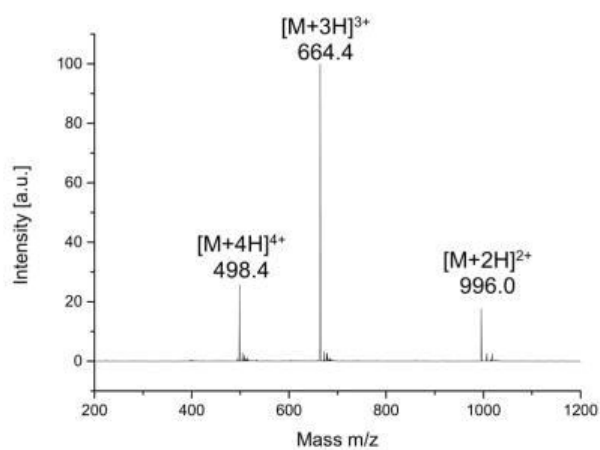


Figure S 14: ESI-MS (ESI+, single quadrupole) of **O4**.

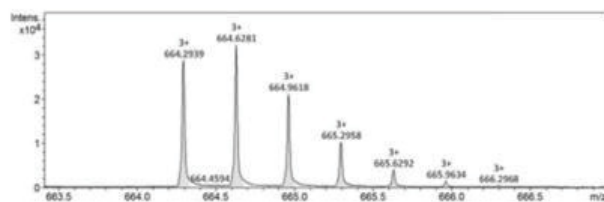


Figure S 15: HR-ESI-MS of **O4**.

HR-ESI-MS: for $C_{88}H_{127}N_{21}O_{28}S_2$ m/z $[M+3H]^{3+}$ calcd.: 664.2940, found: 664.2939, mass accuracy +0.1 ppm.

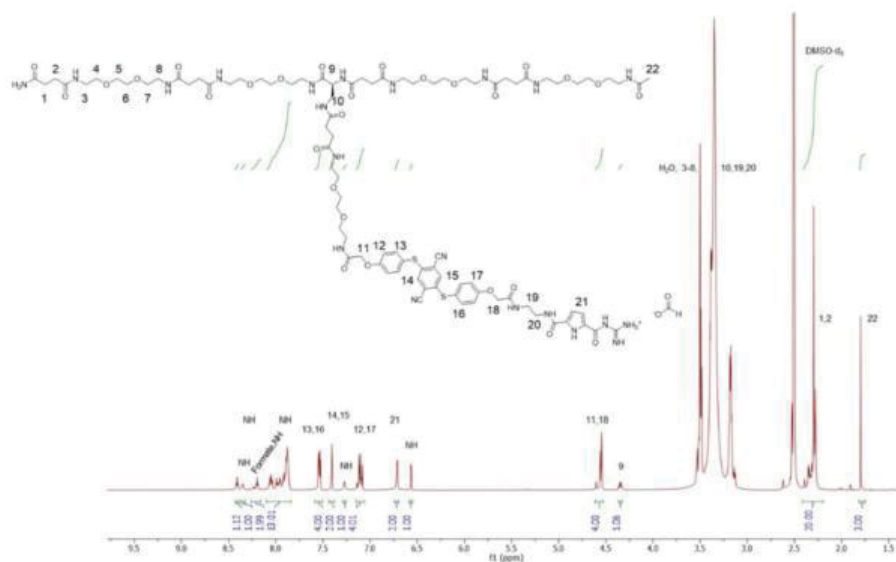
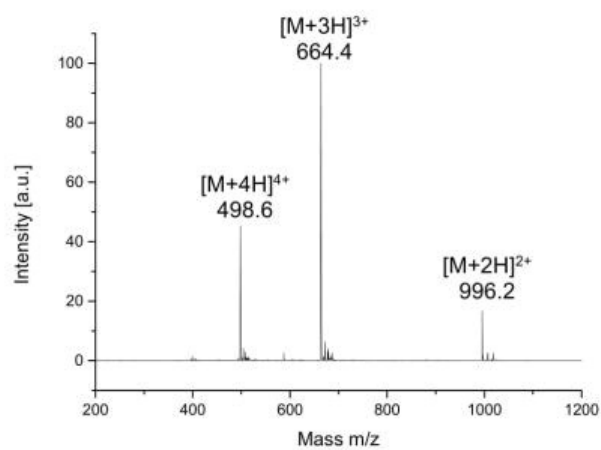
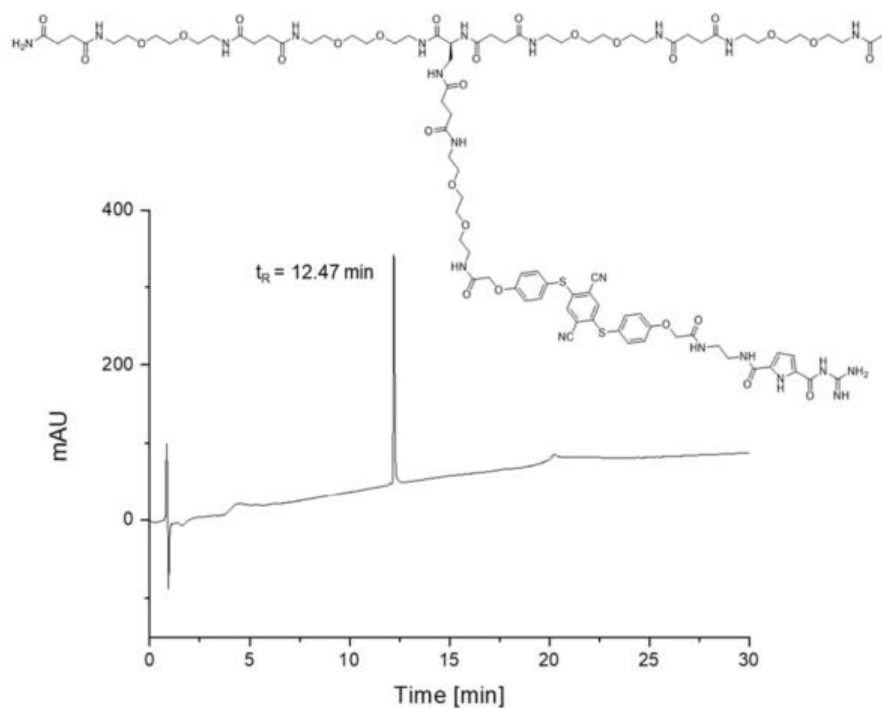


Figure S 16: 1H -NMR (600 MHz, $DMSO-d_6$) of **O5** as formate at RT.

1H -NMR (600 MHz, $DMSO-d_6$): δ (ppm) = 8.48-8.42 (m, 1H, NH), 8.32 (s, 1H, NH), 8.25-8.20 (m, 2H, NH, formate), 8.24-7.79 (m, 13H, NH), 7.60-7.49 (m, 4H, H16,13), 7.41 (s, 2H, H15,14), 7.27 (s, 1H, NH), 7.20-7.10 (m, 4H, H17,12), 7.26-7.18 (m, 2H, H21), 6.59 (s, 1H, NH), 4.58-4.51 (m, 4H, H18,11), 4.33-4.26 (m, 1H, H9), water signal covers signals H3-H8, H10, H19, H20, 2.40-2.22 (m, 20H, H1,2), 1.77 (s, 3H, H22).



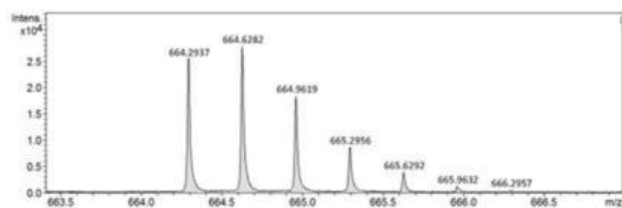


Figure S 19: HR-ESI-MS of **O5**.

HR-ESI-MS: for $C_{88}H_{127}N_{21}O_{28}S_2$ m/z $[M+3H]^{3+}$ calcd.: 664.2940, found: 664.2937, mass accuracy +0.4 ppm.

Additional fluorescence spectra:

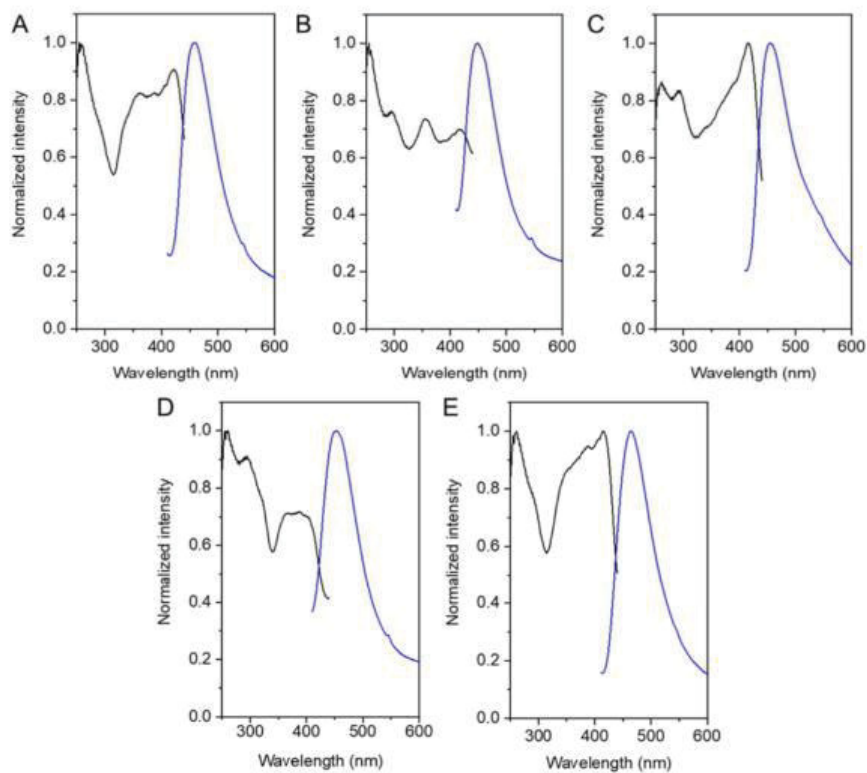


Figure S 20: Excitation-(black) and emission (blue) spectra of A) **O1**, B) **O2**, C) **O3**, D) **O4** and E) **O5** in the solid state are plotted with normalized intensities against wavelengths [nm].

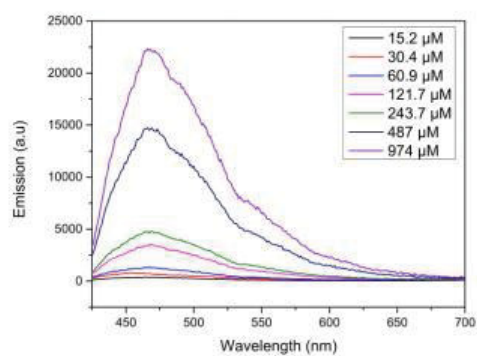


Figure S 21: Concentration series of **O1** in the range from 974 to 15.2 μM (Triplicates in water, λ_{ex} = 380 nm).

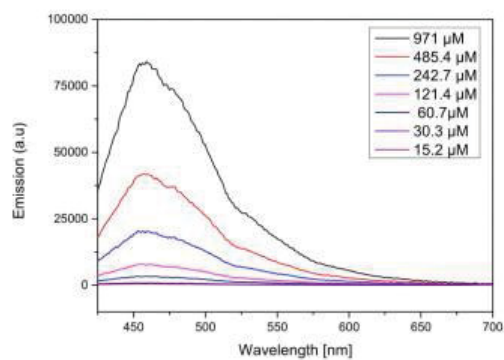


Figure S 22: Concentration series of **O2** in the range from 971 to 15.2 μM (Triplicates in water, λ_{ex} = 380 nm).

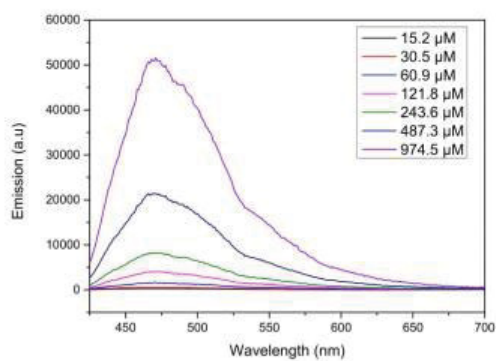


Figure S 23: Concentration series of **O3** in the range from 974.5 to 15.2 μM (Triplicates in water, $\lambda_{\text{ex}} = 380 \text{ nm}$).

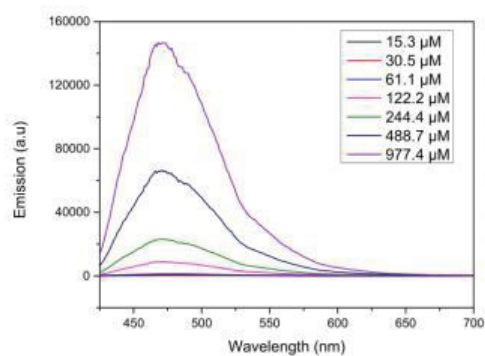


Figure S 24: Concentration series of **O4** in the range from 977.4 to 15.3 μM (Triplicates in water, $\lambda_{\text{ex}} = 380 \text{ nm}$).

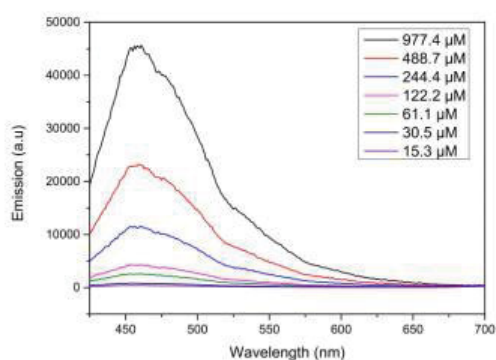


Figure S 25: Concentration series of **O5** in the range from 977.4 to 15.3 μM (Triplicates in water, $\lambda_{\text{ex}} = 380 \text{ nm}$).

Analytical data for studying oligomer aggregation via AFM and SEM:

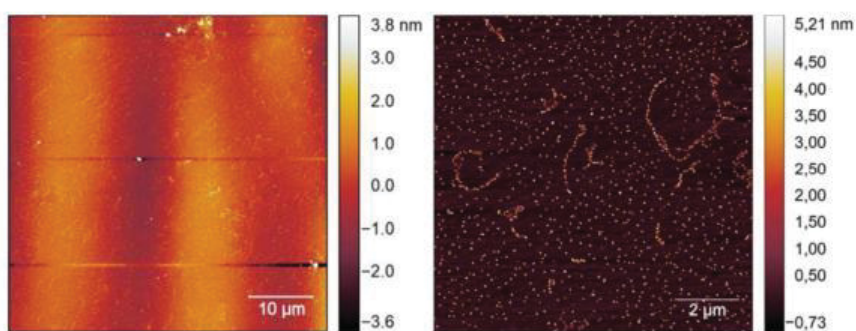


Figure S 26: Atomic force microscope image of **O1** (100 μM in Millipore water).

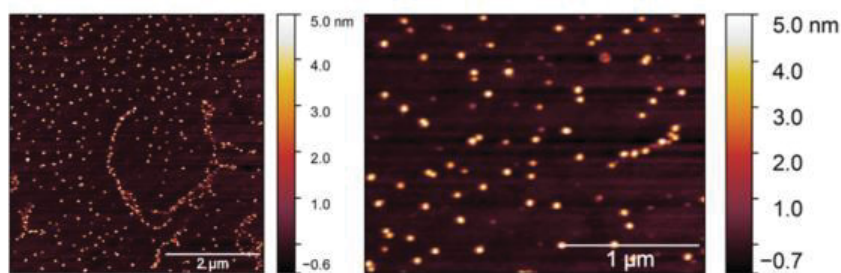


Figure S 27: Atomic force microscope image of **O1** in zoom (100 μM in Millipore water).

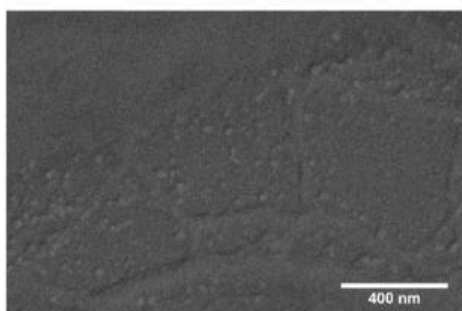


Figure S 28: SEM analysis of **O1** (100 μ M in Millipore water).

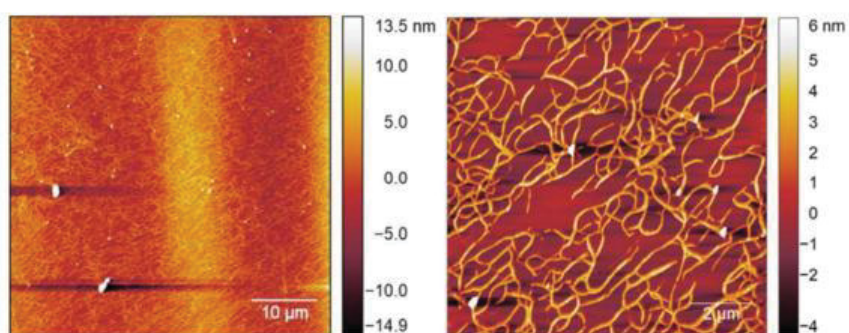


Figure S 29: Atomic force microscope images of **O2** (100 μ M in Millipore water).

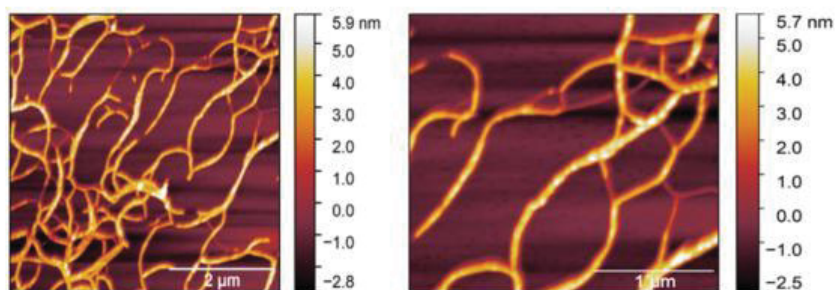


Figure S 30: Atomic force microscope image of **O2** in zoom (100 μ M in Millipore water).

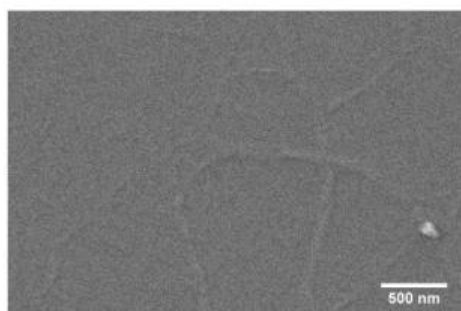


Figure S 31: SEM analysis of **O2** (100 µM in Millipore water).

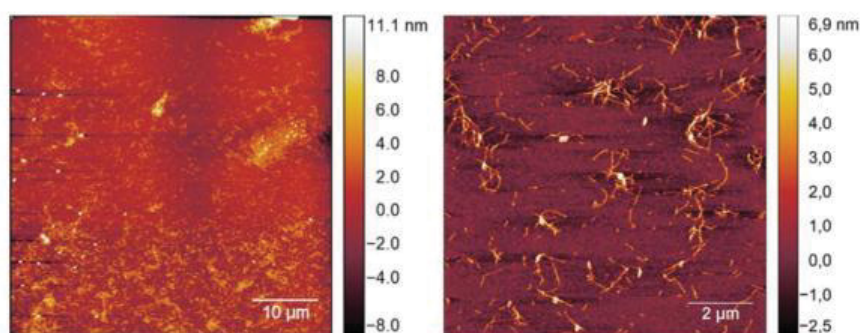


Figure S 32: Atomic force microscope images of **O3** (100 µM in Millipore water).

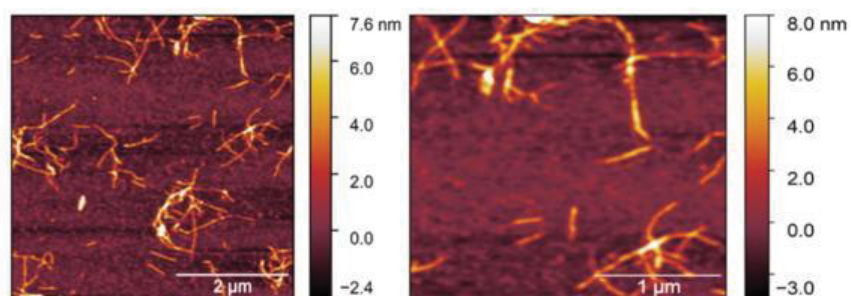


Figure S 33: Atomic force microscope image of **O3** in zoom (100 µM in Millipore water).

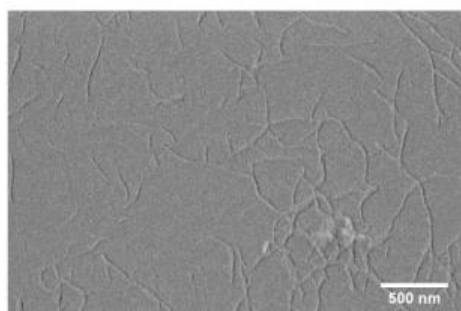


Figure S 34: SEM analysis of **O3** (100 μ M in Millipore water).

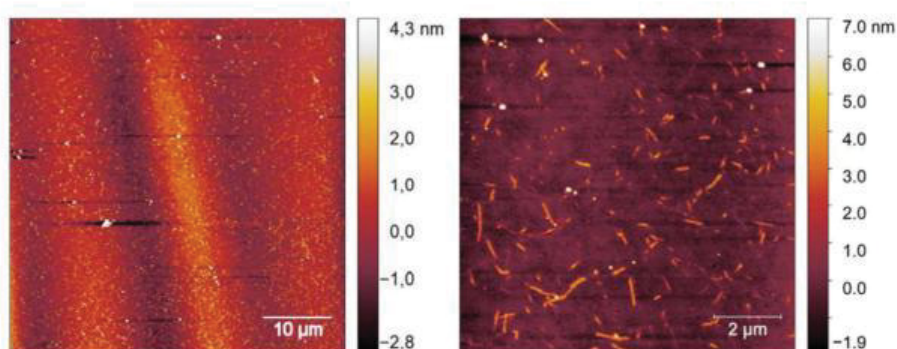


Figure S 35: Atomic force microscope images of **O4** (100 μ M in Millipore water).

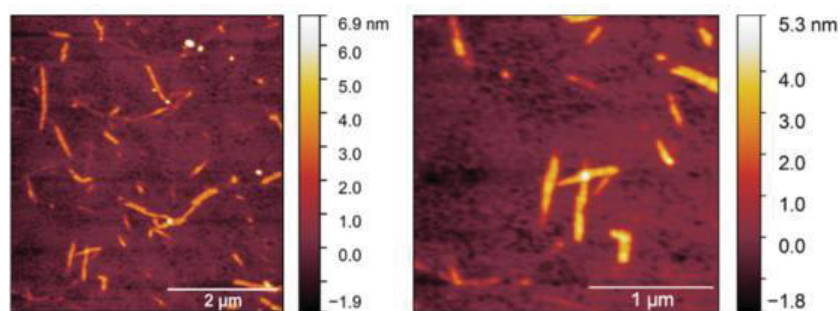


Figure S 36: Atomic force microscope image of **O4** in zoom (100 μ M in Millipore water).

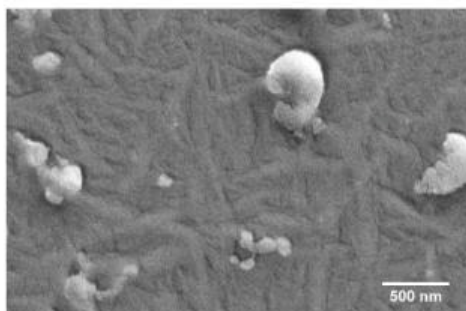


Figure S 37: SEM analysis of **O4** (100 μ M in Millipore water).

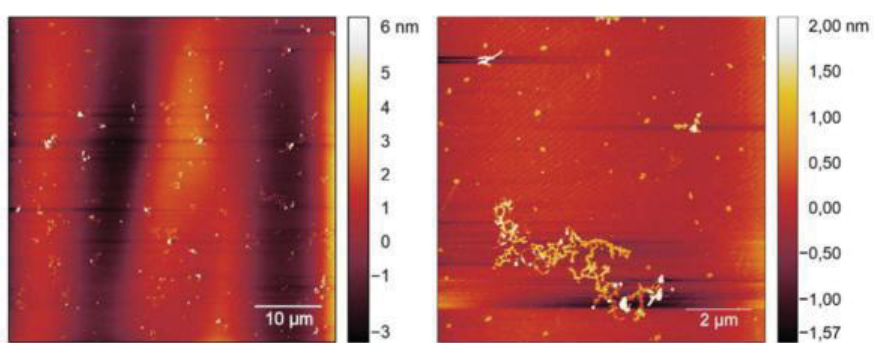


Figure S 38: Atomic force microscope images of **O5** (100 μ M in Millipore water).

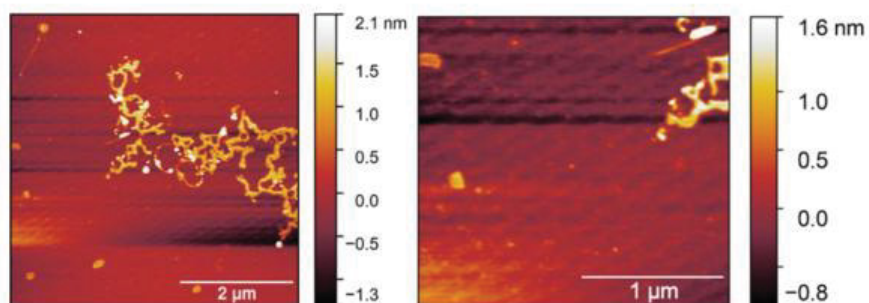


Figure S 39: Atomic force microscope image of **O5** in zoom (100 μ M in Millipore water).

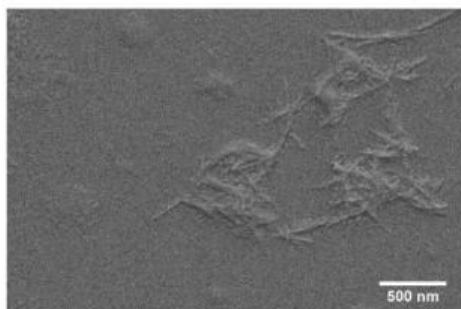


Figure S 40: SEM analysis of **O5** (100 μ M in Millipore water).

Microgel synthesis and characterization:

The PINPAM microgels were synthesized by the classic precipitation polymerization method developed by Pelton.^[5] In a 250 mL triple neck flask with reflux condenser, *N*-isopropylacrylamide (6.2 mmol), *N,N'*-methylenebisacrylamide (0.33 mmol), methacrylic acid (0.13 or 0.34 mmol) and (0.09 mmol) sodium dodecyl sulfate were added to 75 mL ultrapure water. The solution was stirred with a magnetic stirrer at 350 rpm and heated to 70 °C for at least 40 min under nitrogen purge to remove oxygen. The initiator ammonium peroxodisulfate (0.9 mmol) in 5 mL ultrapure water was then added to start the polymerization. During the reaction, the solution was continuously purged with nitrogen and stirred at 350 rpm. After 55 min the reaction was stopped by cooling in an ice bath. The reaction solution was filtered over glass wool and centrifuged at 20000 g to remove the reactants from the microgels. After several centrifugation/washing cycles the microgels were freeze dried and stored in a freezer until use.

The hydrodynamic radius of the microgels was determined by dynamic light scattering using Malvern Zetasizer nano ZS at 20 °C (backscattering angle of 171° at a wavelength of 633 nm). The zeta potential was determined with the same instrument. The concentration of carboxylic acid groups was quantified by titration with toluidine blue O.

Table 1: Results of the microgel properties

	RH20 [nm]	Zeta-potential [mV]	COOH conc. [μ mol/g]
PNIPAm-co-MAA 2mol%	499 \pm 8	-11.3 \pm 0.3	89 \pm 14
PNIPAm-co-MAA 5mol%	470. \pm 7	-13.3 \pm 0.3	121 \pm 24

The microgel morphology was additionally determined by atomic force microscopy (AFM) using a Nanowizard II (JPK instruments, Berlin, Germany) at intermittent contact mode using cantilevers with a

nominal spring constant of 300 N/m (μ mash, Sofia, Bulgaria). For AFM sample preparation, a droplet of a 0.1 wt% microgel dispersion was dried on a microgel surface.

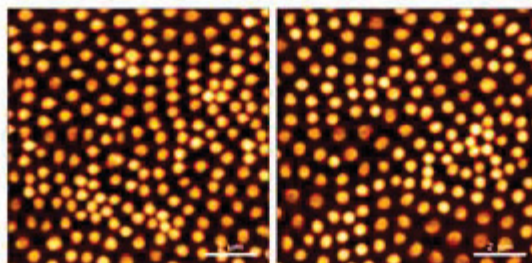


Figure S 41: Atomic force microscope of PNIPAM-co-MAA 2mol%.

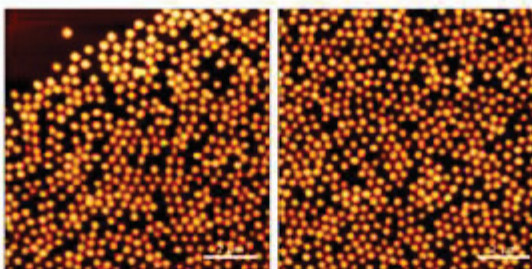


Figure S 42: Atomic force microscope of PNIPAM-co-MAA 5mol%.

References:

- [1] M. F. Ebbesen, C. Gerke, P. Hartwig, L. Hartmann, *Polym. Chem.* **2016**, *7*, 7086-7093.
- [2] M. Externbrink, S. Riebe, C. Schmuck, J. Voskuhl, *Soft Matter* **2018**, *14*, 6166-6170.
- [3] C. Schmuck, V. Bickert, M. Merschky, L. Geiger, D. Rupprecht, J. Dudaczek, P. Wich, T. Rehm, U. Machon, *Eur. J. Org. Chem.* **2008**, *2*, 324-329.
- [4] a) S. Schmidt, T. Hellweg, R. von Klitzing, *Langmuir* **2008**, *24*, 12595-12602; b) S. Schmidt, H. Motschmann, T. Hellweg, R. von Klitzing, *Polymer* **2008**, *49*, 749-756. c) T. Hoare, R. Pelton, *Langmuir* **2004**, *20*, 2123-2133; c) A. Strzelczyk, T. J. Paul, S. Schmidt, *Macromol. Biosci.* **2020**, *20*, 2000186.
- [5] R. Pelton, *Adv. Colloid Interface Sci.* **2000**, *85*, 1-33.

5.3 Sequence-defined glycomacromolecules using AIE for direct read-out of lectin binding

Peter Pasch, Jens Voskuhl, Laura Hartmann

Publication Draft

Own Contribution:

Collaborative project design. Synthesis and purification of building blocks and oligomers. Measurement and evaluation of all LC-MS experiments. Evaluation of all NMR and UHR experiments. Performance and evaluation of fluorescence and turbidity measurements. Collaborative writing of the manuscript.

Sequence-defined glycomacromolecules using AIE for direct read-out of lectin binding

Peter Pasch¹, Jens Voskuhl², Laura Hartmann^{*1}

Address: ¹Department for Organic Chemistry and Macromolecular Chemistry Heinrich Heine University Düsseldorf, Universitätsstraße 1, Düsseldorf 40225, Germany and ²Department, Institute of Organic Chemistry, University of Duisburg-Essen, Universitätsstraße 7, 45141 Essen, Germany.

Email: Laura.Hartmann@hhu.de

* Corresponding author

Abstract

The synthesis of sequence-defined, multivalent glycooligo(amidoamines) carrying TPE as AIE luminophore is achieved by solid-phase polymer synthesis. Carbohydrate units mediate binding to lectins such as ConA, GNA, LCA and PSA while AIE allows for direct read-out of the binding through fluorescence spectroscopy. Fluorescence and turbidity assays with four different lectins show structure-property correlations of oligomer design for effective AIE read-out: results demonstrate the necessity of a clustering effect to reach a pronounced aggregation-induced emission signal which is promoted by both, multivalency of the ligand as well as the protein. Formation of single ligand-protein complexes seem to not efficiently enough affect rotational and vibrational states and thereby leads to no AIE signal. This is supported by a dimeric lectin showing no clustering and inducing no AIE behavior.

Keywords

Aggregation-Induced Emission; Biosensor; Lectins; Solid-Phase-Synthesis; Tetraphenylethylene.

Introduction

Carbohydrates mediate many biological interactions such as cell growth, cell-cell recognition, cancer metastasis, inflammation, and bacterial and viral infections.^[1] Therefore, they can be used both as sensors and modulators of carbohydrate-protein interactions. While natural carbohydrate ligands are often weak binders, their multivalent presentation, e.g., on artificial scaffolds such as polymers, leads to a strong enhancement of binding.^[2] When using such glycomimetics, it is also important to be able to detect their binding directly and at low cost.

Therefore, fluorescent dyes have been explored for combination with glycomimetics to allow direct readout of ligand-receptor binding via fluorescence spectroscopy. However, when traditional fluorescent dyes are interacted in biomacromolecules and dispersed in aqueous media, aggregation-induced fluorescence quenching often occurs, limiting the efficiency and sensitivity of biosensors.^[3] This could be remedied by the phenomenon of aggregation-induced emission (AIE), which was first presented by Tang and co-workers.^[4] The special feature is that AIE fluorogens are not emissive when dissolved in solution, but by forming aggregates or restricting their intramolecular rotation, they become strongly emissive.^[5] The fluorescence quantum yields of AIE molecules are particularly pronounced in this regard, so they have rapidly gained applications as probes and bioprobes.^[6] One particular AIE is tetraphenylethylene (TPE) developed by Tang et al. which already has practical applications as OLEDs,^[7] chemosensors,^[8] and bioprobes,^[9] because it is easy to synthesize and functionalize.^[10] In recent years, combinations of the TPE luminophore with carbohydrates for detection have also been synthesized and explored. Among others, Jin-Xiang Wang et. al. used TPE luminophores conjugated with multiple Mannose units for Concanavalin A- detection.^[11] In this context, a TPE derivative with six conjugated Mannose units showed a stronger increase in emission with ConA than the same derivative with only two Mannose units. Overall, an elevenfold increase in emission intensity was demonstrated by ConA titrations. In addition, Takanobu Sanji et al. specifically detected ConA with synthesized TPE-containing Mannose ligands.^[12] Remarkably was, that the "turn-on" fluorescence sensor enabled detection with intense blue emission within a few seconds. Further in both projects, the high selectivity towards different lectins of the AIE Mannose derivatives was also demonstrated.^[11,12]

Based on these findings, this study aims at combining AIE read-out with sequence-defined glycooligo(amidoamines) as accessible via solid phase polymer synthesis.^[13] Glycooligo(amidoamines) have previously been introduced as a new class of multivalent glycomimetics that allow for the control over the number, type and density of carbohydrate ligands on a polymer scaffold.^[14] Furthermore, variations of the topology and combinations with non-natural binding motifs are easily accessible, giving access to new insights into the structure-property relations of glycomimetics.^[15] By combining glycooligo(amidoamines) with AIE luminophore a direct read-out of receptor binding should be realized, enabling also binding studies in complex setting e.g. in cells or mixtures of proteins that are challenging with classical binding assays such as SPR or ITC.

Synthesis

A) scaffold assembly

addition of building block¹

- Fmoc

deprotection²

Repeat for selected building block sequence.

B) sugar functionalization

sugar conjugation³

C) AIE conjugation

- Fmoc²

+ ADS⁴

+ TPE Click⁵

D) Deacetylation⁶ & cleavage from support⁷

Man-TPE

Gal-TPE

TDS

ADS

EDS

TPE

α -Man

β -Gal

Man-TPE

Figure 1: Step-by-step solid phase synthesis to give final oligomers **Man-TPE** and **Gal-TPE**. Reaction conditions: 1) 5 eq. building block, 5 eq. PyBOP, 10 eq. DIPEA in DMF, 90 min, 2) 25v% piperidine in DMF, 20 min, 3) 2 eq of acetyl protected 2-azidoethyl pyranoside (Mannose/Galactose) per alkyne group dissolved in 3 mL DMF plus 20 mol% sodium ascorbate and 20 mol% CuSO₄ dissolved in water, 24 h. 4) 5 eq. ADS, 5 eq. PyBOP, 10 eq. DIPEA in DMF, 90 min and subsequently deprotection step 2. 5) The implementations are identical to step 3, but using 2 eq. 1-ethynyl-4-(1,2,2-triphenylethenyl) benzene. 6) 0.2 M sodium methoxide in methanol, 1 hour. 7) TentaGel® S RAM: 5% triisopropylsilane, 95% TFA, 90 min.

All three building blocks presenting a free carboxy- and a temporary Fmoc-protected amine group are assembled on solid support using Fmoc peptide coupling chemistry. Upon achieving the desired

oligomer sequences, azido functionalized acetylated α -D Mannose (Man) or β -Galactose (Gal) are conjugated via copper(I)-catalysed alkyne azide cycloaddition (CuAAC). After releasing the terminal Fmoc-group, a terminal ADS building block is introduced and subsequently used for conjugation of TPE-luminophore alkyne derivative via a second CuAAC reaction. Finally, the carbohydrate groups of the synthesized TPE-glycooligomers are deacetylated, cleaved off the resin, purified by preparative HPLC and lyophilized. Both TPE-glyco oligomers **Man-TPE** and **Gal-TPE** were obtained with a high relative purity > 95 % structures were confirmed by UHR-MS and ^1H NMR (for further information and analytical data see SI).

Lectin Detection

As lectins for the following binding assays, Concanavalin A (Con A) isolated from Jack beans, Galanthus nivalis agglutinin (GNA) from snowdrop bulbs, Pisum sativum agglutinin (PSA) from peas and Lens culinaris agglutinin (LCA) from the lentil Lens culinaris were employed. All four lectins are α -D-Mannose-specific receptors thus Gal-TPE will serve as negative control presenting a non-binding sugar ligand. Con A and GNA are tetrameric thus presenting four binding sites.^[17] PSA and LCA lectin are dimeric presenting two receptor sites.^[17] In addition, all four lectins have different binding affinities to α -D mannose. Here, Con A shows the highest affinity followed by GNA, PSA and LCA.^[17]

First, **Man-TPE** and **Gal-TPE** were investigated for their AIE behavior upon addition of the different lectins, which was performed by titration experiments as in literature known.^[11,12] The fluorescence changes were detected by an excitation wavelength of 340 nm for TPE and the entire emission spectra from 400 to 700 nm were recorded (see SI for spectra).

For tetrameric Con A a pronounced increase in fluorescence is detectable already at low concentrations of **Man-TPE** (Fig. 2 A, detailed titration curves see SI). This observation is consistent with the literature, where an AIE effect can be obtained after only a few seconds with small amounts of sensor.^[11] The fluorescence increases stepwise until 22 μM Con A, reaching a plateau at higher concentrations. Finally, a fifteenfold increase in emission can be achieved, which is a strong AIE effect compared to similar structures from the literature.^[11,12] In addition to the fluorescence increase, turbidity can be observed by the solutions becoming cloudy. The negative control, **Gal-TPE**, shows no increase in fluorescence. (Photo Fig. 2 A) Titration of the GNA tetramer also shows a clear increase in fluorescence with the addition of a small amount of GNA, although the plateau occurs earlier for GNA than for ConA. Already with the addition of 10 μM GNA the plateau is almost reached and the total fluorescence increase at 22 μM GNA is fivefold. The photo of **Man-TPE** and **Gal-TPE** with identical concentration mixed with GNA offers a specific fluorescence detection. (Fig. 2B) In this context, **Man-TPE** can be classified as a bio-probe for tetrameric Con A and GNA.

The dimeric PSA shows a different behavior where the fluorescence increases only slightly (Fig. 2 C) upon addition of the protein. TAt the highest protein concentration, fluorescence is increased only by a factor of 2. In addition, no turbidity is observed. Again, the negative control shows no increase in fluorescence. LCA showed no increase in fluorescence or turbidity for **Man-TPE** as well as **Gal-TPE**.

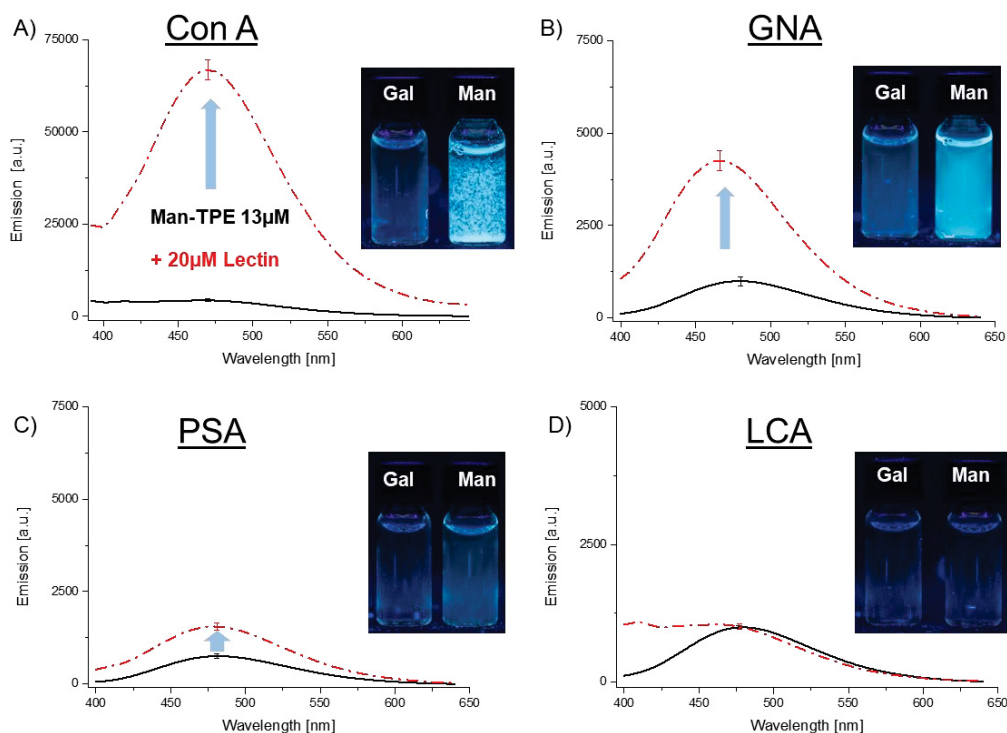


*Figure 2: The emission spectra of **Man-TPE** are shown with the starting curve of 13 μ M in LBB (black) and with titration of 22 μ M lectin in red for Con A (A), GNA (B), PSA (C) and LCA (D). The excitation wavelength is 340 nm and the entire emission spectra are plotted. In addition, photos of **Man-TPE** and **Gal-TPE** with added 22 μ M of respective lectin are illustrated.*

As the samples showing the highest AIE effect also showed formation of turbidity during the measurement, quantitative turbidity measurements were performed to investigate this effect further. For turbidity measurements, the ligand is titrated to the protein solution and turbidity is recorded using the transmission values at 420 nm, which is not in the absorption area of the TPE-luminophore. Turbidity is correlated to the formation of ligand-protein clusters and often used as a measure for multivalency.^[18]

In the turbidity assay of **Man-TPE**, Con A shows the occurrence of turbidity, with the transmission signal being reduced by 50% already at a ligand concentration of 3.5 μ M ($c_{1/2}$ Tmax: 3.5 μ M, Fig 3). It is well known that tetrameric ConA is prone to cluster formation with multivalent glycoligands. Importantly, Gal-TPE showed no cluster formation, indicating that the observed effect is specific for the glycan-protein interaction.

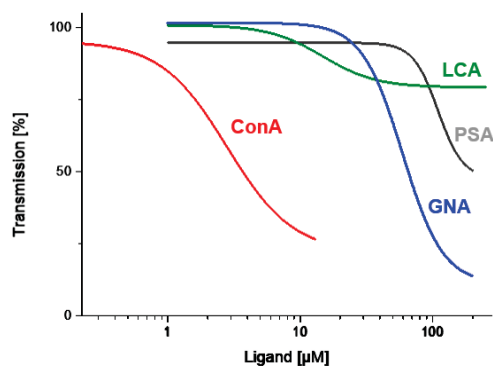


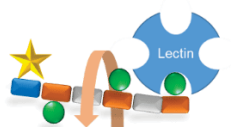
Figure 3: Hill plots of UV-Vis Turbidity assays [Transmission at 420 nm, lectins conc. 100μM] of Con A (red), GNA (blue), PSA (gray), LCA (green) with titration of the ligand **Man-TPE** in LBB (All measuring points and the **Gal-TPE** results see SI) .

In comparison to Con A, the tetramer GNA shows turbidity at higher **Man-TPE** concentration ($c_{1/2Tmax}$: 65 μM). This can be correlated with the lower affinity of GNA for Mannose. Again Gal-TPE showed no turbidity and thus no binding.

When looking at dimeric lectins PSA and LCA, PSA shows a weak clustering effect, reaching the half maximum transmission at a concentration of 200 μM. This observation is in line with both, the lower affinity of PSA for Mannose as well as the reduced valency of the receptor, leading to less efficient cluster formation. LCA shows even further reduced interaction with **Man-TPE** and almost no turbidity is observed.

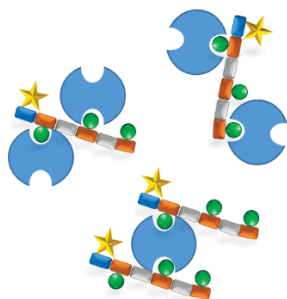
Overall turbidity measurements are well in line with fluorescence measurements and confirm that cluster formation seems to be necessary for efficient AIE effects. In our model, binding of a single ligand to a lectin still allows the AIE luminophore at the chain end to move freely and does not induce emission. Only when several ligands and proteins form a cluster, does the luminophore experience strong enough restrictions in its rotation and/or vibration to induce AIE (Figure 4). Clusters formed by lectins with two instead of four receptor sites potentially lead to less dense clusters and thus restrictions and accordingly AIE effects are less pronounced.

Single binding
(tetravalent or divalent lectin)



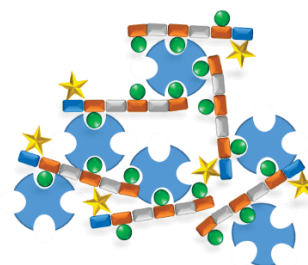
still free AIE motion

Cluster formation
(divalent lectin)



vs.

Cluster formation
(tetravalent lectin)



vs.

full restricted rotation & vibration

*Figure 4: Schematically, the differences of a simple binding of the **Man-TPE** to a lectin vs. a cluster formation with a divalent lectin and a tetravalent lectin are shown. In the case of a simple binding, the AIE is still free to move, whereas in the case of a cluster formation with a divalent lectin, the AIEs are already restricted in their rotation or vibration, resulting in an AIE effect. In the case of the tetravalent lectin, the system are constrained with respect to its rotational or vibrational capabilities, resulting in a particularly strong AIE effect.*

Conclusion

In conclusion, two glycooligomers with AIE luminophores were synthesized using solid phase polymer synthesis. While the carbohydrate ligands mediate interaction with lectins, the AIE luminophore allows for direct visualization and read-out of the binding. On the one hand the AIE effect is determined by the affinity of the lectin for carbohydrate presented on the glycooligomer, where all Gal glycooligomers showed no binding and no fluorescence for the Man recognizing lectins applied in this study. On the other hand, cluster formation of multivalent ligands and multivalent receptors is required to lead to AIE through restriction of the luminophores rotation/vibration. Accordingly, lectins with higher tendency to form clusters, based on their higher valency (tetrameric vs. dimeric) and higher affinity for the carbohydrate ligands, show higher AIE effects. Future studies will focus on developing glycooligomer-AIE conjugates as sensors of cluster formation events, not only in solution but also on membranes or cells.

Acknowledgements

We would like to thank Tobias Wilcke for the photographs of our compounds.

References

- 1) H. Lis, N. Sharon, *Chem. Rev.*, **1998**, 98, 637; b) M. Mammen, S. K. Choi, G. M. Whitesides, *Angew. Chem., Int. Ed.*, **1998**, 37, 2755; c) R. Jelinek, S. Kolusheva, *Chem. Rev.*, **2004**, 104, 5987;

-
- d) M. Mammen, S.-K. Choi, G. M. Whitesides, *Angew. Chem.*, **1998**, *110*, 2908–2953; e) H. Lis, N. Sharon, *Chem. Rev.*, **1998**, *98*, 637–674; f) P. R. Crocker, T. Feizi, *Curr. Opin. Struct. Biol.*, **1996**, *6*, 679–691; g) R. J. Linhardt, T. Toida, *Acc. Chem. Res.*, **2004**, *37*, (7), 431–438; h) G. A. Rabinovich, L. G. Baum, N. Tinari, R. Paganelli, C. Natoli, F.-T. Liu, S. Iacobelli, *Trends Immunol.*, **2002**, *23*, (6), 313–320; F) X.-Q. Yu, M. R. Kanost, *Devel. Comp. Immunol.*, **2003**, *27*, (3), 189–196; i) T. B. H. Geijtenbeek, D. S. Kwon, R. Torensma, S. J. van Vliet, G. C. F. van Duynhoven, J. Middel, I. L. M. H. A. Cornelissen, H. S. L. M. Nottet, V. N. Kewal Ramani, D. R. Littman, C. G. Figdor, Y. van Kooyk, *Cell*, **2000**, *100*, (5), 587–597.
- 2) a) B. J. Appelmelk, I. van Die, S. J. van Vliet, C. M. J. E. Vandenbroucke-Grauls, T. B. H. Geijtenbeek, Y. van Kooyk, *J. Immunol.*, **2003**, *170*, (4), 1635–1639; b) S. Cecioni, A. Imberty, S. Vidal, *Chem. Rev.*, **2015**, *115*, 525; c) V. Vázquez-Dorbatt, J. Lee, E.-W. Lin, H. D. Maynard, *ChemBioChem*, **2012**, *13*, 2478; d) F. Shamout, A.; Monaco, G. Yilmaz, C. R. Becer, L. Hartmann, *Macromol. Rapid Commun.*, **2020**, *41*, 1900459; e) C. Gerke, M. F. Ebbesen, D. Jansen, S. Boden, T. Freichel, L. Hartmann, *Biomacromolecules*, **2017**, *18*, 787; f) D. Ponader, F. Wojcik, F. Beceren-Braun, J. Dervede, L. Hartmann, *Biomacromolecules*, **2012**, *13*, 1845; g) J. J. Lundquist, E. J. Toone, *Chem. Rev.*, **2002**, *102*, (2), 555–578; h) J. E. Gestwicki, C. W. Cairo, L. E. Strong, K. A. Oetjen, L. L. Kiessling, *J. Am. Chem. Soc.*, **2002**, *124*, (50), 14922–14933; i) E. M. Munoz, J. Correa, E. Fernandez-Megia, R. Riguera, *J. Am. Chem. Soc.*, **2009**, *131*, (49), 17765–17767.
- 3) a) M. Wang, G. Zhang, D. Zhang, D. Zhu, B. Tang, *J. Mater. Chem.*, **2010**, *20*, 1858; b) H. Tong, Y. Hong, Y. Dong, M. Haussler, J. W. Y. Lam, Z. Li, Z. Guo, Z. Guo, B. Z. Tang, *Chem. Commun.*, **2006**, 3705; c) T. Sanji, K. Shiraishi, M. Tanaka, *ACS Appl. Mater. Interfaces*, **2009**, *1*, 270.
- 4) a) J. Luo, Z. Xie, J. W. Y. Lam, L. Cheng, H. Chen, C. Qiu, H. S. Kwok, X. Zhan, Y. Liu, D. Zhu, B. Z. Tang, *Chem. Commun.*, **2001**, *18*, 1740–1741; b) Q. Chen, N. Bian, C. Cao, X.-L. Qiu, A.D. Qi, B.-H. Han, *Chem. Commun.*, **2010**, *46*, 4067; c) R. T. K. Kwok, C. W. T. Leung, J. W. Y. Lam, B. Z. Tang, *Chem. Soc. Rev.*, **2015**, *44*, 4228–4238; d) B. Schmidt, S. Sankaran, L. Stegemann, C. A. Strassert, P. Jonkheijm, J. Voskuhl, *J. Mater. Chem. B*, **2016**, *4*, 4732–4738.
- 5) M. Gao, B. Z. Tang, *ACS Sens.*, **2017**, *2*, 1382–1399.
- 6) A. Qin, J. W. Y. Lam, L. Tang, C. K. W. Jim, H. Zhao, J. Sun, B. Z. Tang, *Macromolecules*, **2009**, *42*, 1421.
- 7) Y. Dong, J. W. Y. Lam, A. Qin, J. Liu, Z. Li, B. Z. Tang, J. Sun, H. S. Kwok, *Appl. Phys. Lett.*, **2007**, *91*, 11111.
- 8) L. Liu, G. Zhang, J. Xiang, D. Zhang, D. Zhu, *Org. Lett.*, **2008**, *10*, 4581.
- 9) a) H. Tong, Y. N. Hong, Y. Q. Dong, M. Haussler, Z. Li, J. W. Y. Lam, Y. P. Dong, H. H. Y. Sung, I. D. Williams, B. Z. Tang, *J. Phys. Chem. B*, **2007**, *111*, 11817; b) Y. Hong, M. Haussler, J. W. Y.

-
- Lam, Z. Li, K. K. Sin, Y. Dong, H. Tong, J. Liu, A. Qin, R. Renneberg, B. Z. Tang, *Chem.–Eur. J.*, **2008**, *14*, 6428; c) M. Wang, X. Gu, G. Zhang, D. Zhang, D. Zhu, *Anal. Chem.*, **2009**, *81*, 4444; d) L. Peng, G. Zhang, D. Zhang, J. Xiang, R. Zhao, Y. Wang, D. Zhu, *Org. Lett.*, **2009**, *11*, 4014; e) Q. Chen, N. Bian, C. Cao, X.-L. Qiu, A.-D. Qi, B.-H. Han, *Chem. Commun.*, **2010**, *46*, 4067.
- 10) a) A. Qin, J. W. Y. Lam, L. Tang, C. K. W. Jim, H. Zhao, J. Sun, B. Z. Tang, *Macromolecules*, **2009**, *42*, 1421; b) S. Umar, A. K. Jha, D. Purohit, A. Goel, *J. Org. Chem.*, **2017**, *82*, 4766–4773; c) W. Guan, W. Zhou, C. Lu, B. Z. Tang, *Angew. Chem. Int. Ed.*, **2015**, *54*, 15160–15164.
- 11) J. X. Wang, Q. Chen, N. Bian, F. Yang, J. Sun, A. D. Qi, C. G. Yan, B. H. Han, *Org. Biomol. Chem.*, **2011**, *9*, 2219–2226.
- 12) T. Sanji, K. Shiraishi, M. Nakamura, M. Tanaka, *Chem. Asian J.* **2010**, *5*, 817-824.
- 13) a) R. B. Merrifield, *Angew. Chem. Int. Ed.*, **1985**, *24*, (10), 799-810; b) S. A. Hill, C. Gerke, L. Hartmann, *Chem. - Asian J.*, **2018**, *13*, 3611.
- 14) a) D. Ponader, S. Igde, M. Wehle, K. Märker, M. Santer, D. Bléger, L. Hartmann, *Beilstein J. Org. Chem.* **2014**, *10*, 1603-1612; b) C. Gerke, M. F. Ebbesen, D. Jansen, S. Boden, T. Freichel, L. Hartmann, *Biomacromolecules* **2017**, *18*, (3), 787-796; c) D. Ponader, F. Wojcik, F. Beceren-Braun, J. Dervede, L. Hartmann, *Biomacromolecules* **2012**, *13*, (6), 1845-1852.
- 15) a) M. Baier, M. Giesler, L. Hartmann, *Chem. Eur. J.* **2018**, *24*, (7), 1619-1630; b) F. Shamout, A. Monaco, G. Yilmaz, C. R. Becer, L. Hartmann, *Macromol. Rapid Commun.* **2019**, 1900459.
- 16) F. Shamout, L. Fischer, N. L. Snyder, L. Hartmann. *Macromol. Rapid Commun.* **2019**, 1900473.
- 17) a) F. P. Schwarz, K. D. Puri, R. G. Bhat, A. Surolia, *J. Biol. Chem.*, **1993**, *268*, 7668-7677; b) E. J. M. V. Damme, A. K. Allen, W. J. Peumans, *FEBS Lett.*, **1987**, *215*, 1873-3468; c) K. H. Schlick, R. A. Udelhoven, G. C. Strohmeyer, M. Cloninger, *J. Mol. Pharm.*, **2005**, *2*, (4), 295-301.
- 18) J. E. Gestwicki, C. W. Cairo, L. E. Strong, K. A. Oetjen, L. L. Kiessling, *J. Am. Chem. Soc.* **2002**, *124* (50), 14922–14933.

Supporting Information

Sequence-defined glycomacromolecules using AIE for direct read-out of lectin binding

Peter Pasch¹, Jens Voskuhl², Laura Hartmann*¹

Address: ¹Department for Organic Chemistry and Macromolecular Chemistry Heinrich Heine University Düsseldorf, Universitätsstraße 1, Düsseldorf 40225, Germany and ²Department, Institute of Organic Chemistry, University of Duisburg-Essen, Universitätsstraße 7, 45141 Essen, Germany.

Email: Laura.Hartmann@hhu.de

* Corresponding author

Materials:

Diethyl ether (with BHT as inhibitor, $\geq 99.8\%$), triisopropylsilane (TIPS) (98%), 1-Ethynyl-4-(1,2,2-triphenylethenyl) benzene (TPE-luminophore) and formic acid (pa) were purchased from Sigma Aldrich. N, N-diisopropylethylamine (DIPEA) ($\geq 99\%$) was purchased from Carl Roth. N, N-dimethylformamide (DMF) (99.8%, for peptide synthesis), piperidine (99%) were obtained from Acros Organics. Dichloromethane (DCM) (99.99%), (analytical reagent grade) was purchased from Fisher Scientific. Acetonitrile was purchased from AppliChem. Trifluoroacetic acid (TFA) (99%), (benzotriazol-1-yl-oxytripyrrolidinophosphonium hexafluorophosphate (PyBOP), and triethylsilane (analytical reagent grade) were purchased from Fluorochem. TentaGel® S RAM resin (Rink Amide, loading: 0.23 mmol/g) was purchased from RAPP Polymer.

Analytic Methods:

Purification (Preparative RP-HPLC)

An Agilent 1260 Infinity device was used to purify the oligo(amidoamines), which is coupled to a variable wavelength detector (VWD) (set to 214 nm) and an automated fraction collector. The RP-HPLC column, CAPCELL PAK C18 (20 x 250 mm, 5 μ m), was used. The mobile phases A and B were H₂O and acetonitrile, each containing 0.1 vol% formic acid. The flow rate was set at 15 ml/min.

Reversed Phase- High Pressure Liquid Chromatography- Mass Spectrometry (RP- HPLC-MS)/Electron Spray Ionization- Mass Spectrometry (ESI-MS)

RP-HPLC-MS was carried out on an Agilent 1260 Infinity instrument coupled to a variable wavelength detector (VWD) (set to 214 nm) and a 6120 Quadrupole LC/MS containing an Electrospray Ionization (ESI) source (operation mode positive, m/z range from 200 to 2000). A MZ-AquaPerfect C18 (3.0 × 50 mm, 3 μ m) RP column from Mz-Analysentechnik was used. As eluent system water/acetonitrile containing 0.1 vol% formic acid was applied. The mobile phases A and B were: System A) H₂O/acetonitrile (95/5, v/v); System B) H₂O / acetonitrile (5/95, v/v). The samples were analyzed at a flow rate of 0.4 ml/min using a linear gradient, starting with 100% of system A) and reaching 100% system B) within 30 min. The temperature of the column room was set to 40 °C. All purities were determined using the OpenLab ChemStation software for LC/MS from Agilent Technologies.

ESI-MS measurements were performed with the above mentioned ESI source and quadrupole detector.

Ultra High Resolution - Mass Spectrometry (UHR-MS)

UHR-MS measurements were performed with a Bruker UHR-QTOF maXis 4G instrument with a direct inlet via syringe pump, an ESI source and a quadrupole followed by a Time of Flight (QTOF) mass analyzer.

Nuclear Magnetic Resonance Spectroscopy (NMR)

The ¹H-NMR spectra were recorded on a Bruker Avance III 600 (600 MHz). These spectra were evaluated according to the following scheme: (frequency in MHz, deuterated solvent), chemical shift in ppm (multiplicity, coupling constant, integral, signal assignment). The chemical shift is given in relation to the ¹H signals of the deuterated solvents used (D₂O: 4.79 ppm). The multiplicities of the signals were abbreviated as follows: s (singlet), d (doublet), t (triplet), m (multiplet).

Freeze dryer

The final oligomers were lyophilized with an Alpha 1-4 LD plus instrument from Martin Christ Freeze Dryers GmbH. The drying method was set to -40 °C and 0.1 mbar.

Fluorescence

The fluorescence spectra were recorded on a RF-6000 from the company Shimadzu Corporation in Japan.

UV-Vis Turbidity assays

Turbidity measurements were performed with a SPECORD 210 PLUS UV-Vis photometer from Analytik Jena AG. The instrument was operated using Win ASPECT PLUS software. All measurements were performed in 0.1 mL precision quartz glass cuvettes from Carl Roth GmbH + Co. KG. The Transmission signal at 420 nm was detected.

Oligo(amidoamines) Synthesis:

General:

The oligo(amidoamines) synthesis were carried out manually in 10 ml polypropylene syringe reactors with a polyethylene frit and a Luer stopper from MultisynTech GmbH. Both oligo(amidoamines) were synthesized on the TentaGel® S RAM (Rink Amide) with capacity of 0.23 mmol/g. Batch size of both oligo (amido)amines were 0.15 mMolar.

Fmoc cleavage

The resin was swollen in DCM for 30 min and subsequently washed three times with DMF. Secondly the Fmoc protecting group of the resin as well as from the coupled building blocks or amino acids was cleaved by means of a 25% solution of piperidine in DMF achieving an amine end group. The deprotection was carried out twice with the mentioned cleavage solution for 20 min and 7 ml. Afterwards the resin was washed 10 times with DMF.

Coupling protocol

First the resin was swollen in DCM for 30 min and then washed three times with DMF. The Fmoc protecting group had to be removed before further couplings!

For the building block coupling 5 eq., 5 eq. PyBOP and 10 eq. DIPEA were dissolved in 5 mL DMF, drawn into the reactor syringe and shaken for 90 min, followed by washing ten times with DMF.

CuAAC protocol of pyranoside

To the oligomeric structure loaded on the resin 2 eq of acetyl protected 2-azidoethyl pyranoside (α-Mannose/β-Galactose) per alkyne group dissolved in 3 mL DMF were added. Secondly 20 mol% sodium ascorbate per alkyne group and 20 mol% CuSO₄ per alkyne group were dissolved each in 1 mL water and also added to the resin. The reaction time was 24 h and subsequently washed with a 23 mM solution of sodium diethyldithiocarbamate in DMF and water (50/50, v/v) and alternating with DMF and DCM until no further color change occur.

CuAAC protocol of 1-Ethynyl-4-(1,2,2-triphenylethenyl) benzene

To the oligomeric structure loaded on the resin 2 eq of 1-Ethynyl-4-(1,2,2-triphenylethenyl) benzene per azido group dissolved in 3 mL DMF were added. Further implementations are identical to the CuAAC protocol of pyranoside.

Acetyl deprotection

The acetyl protection groups of the 2-azidoethylpyranoside are cleaved off using 10 ml of a 0.2 M solution of sodium methoxide in methanol. The reaction time is 1 hour and subsequently resin was washed 5 times alternating with 10 ml of DMF and DCM.

Cleavage from solid phase

The oligo(amidoamines) were cleaved from the TentaGel® S RAM resin by drawing up a solution of 5 vol% triisopropylsilane (TIPS) and 95 vol% TFA into the syringe and shaking for 1.5 hours.

Afterwards the solution was placed in ice cooled diethyl ether. The resulting precipitate was centrifuged off and the supernatant was decanted off. The pellet was washed 3 times with diethyl ether.

The product was dried and dissolved in Millipore water. The entire solution was collected in a falcon and freeze-dried to isolate the product. Subsequently, the products **Man-TPE** & **Gal-TPE** were purified by means of preparative HPLC.

Analytical data of oligomers Man-TPE & Gal-TPE:

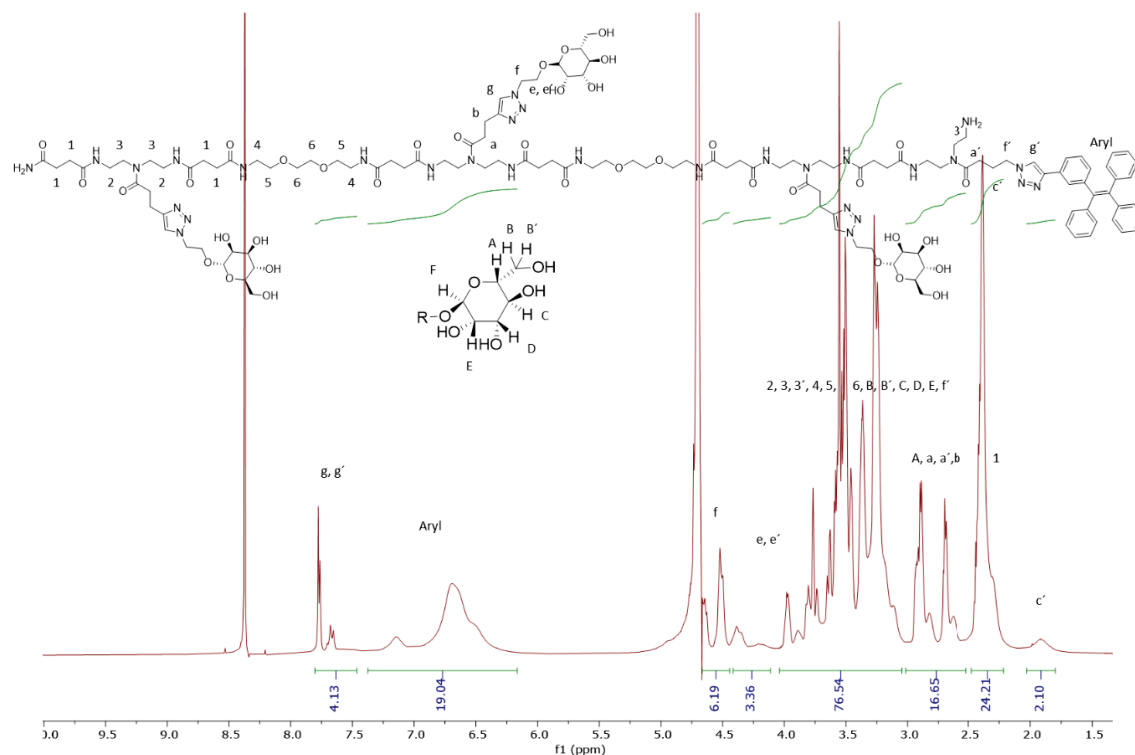


Figure S 1: 600 MHz ^1H NMR spectrum of **Man-TPE** in D_2O at 25°C.

^1H -NMR (600 MHz, D_2O): δ (ppm) = In the range from 8.25 to 8.70 amide functionalities occur, 7.84-7.47 (m, 4H, Hg, Hg'), 7.40-6.19 (m, 19H, HAryl), 4.68-4.44 (m, 6H, Hf), 4.42-4.09 (m, 3H, He), 4.05-3.04 (m, 76H, H2-H6, H3', HB-HE, HB', He', Hf'), 2.99-2.53 (m, 16H, HA, Ha, Ha', Hb), 2.48-2.21 (m, 24H, H1), 2.07-1.90 (m, 2H, Hc').

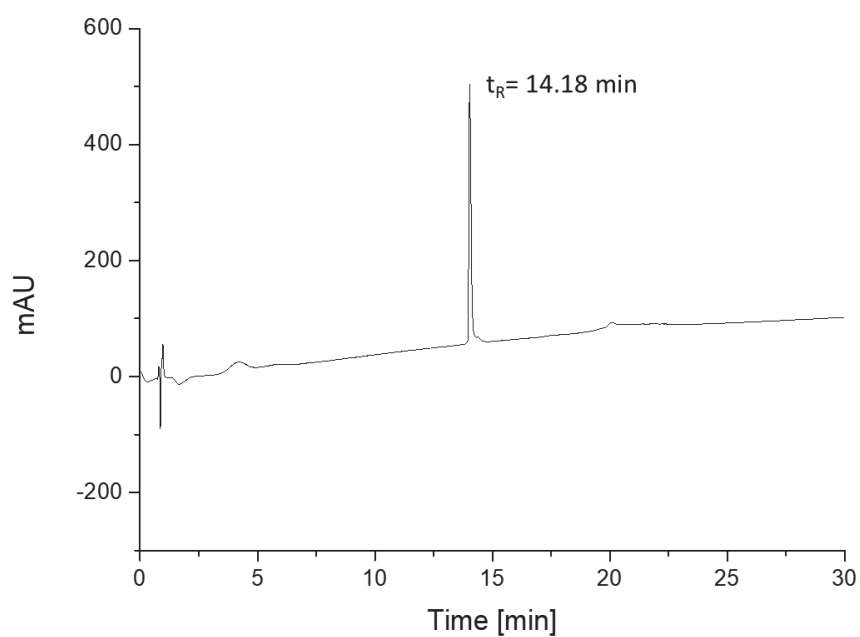


Figure S 2: **Man-TPE** detected by RP-HPLC analysis (linear gradient from 5 – 95 vol% eluent H₂O/acetonitrile) in 30 min at 40 °C.

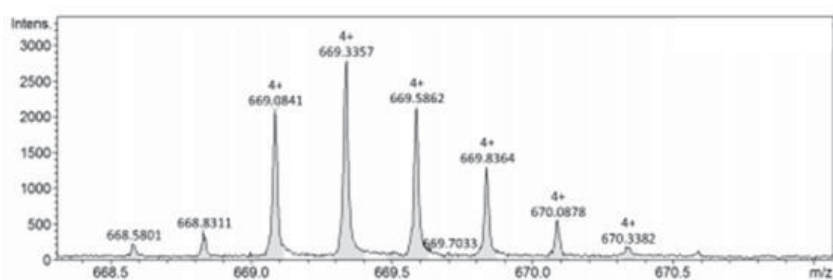


Figure S 3: HR-ESI-MS of **Man-TPE**.

HR-ESI-MS: for C₁₂₃H₁₈₅N₂₉O₃₈ m/z [M+4H]⁴⁺ calcd: 669.0853 , found: 669.0841

mass accuracy +1.9 ppm.

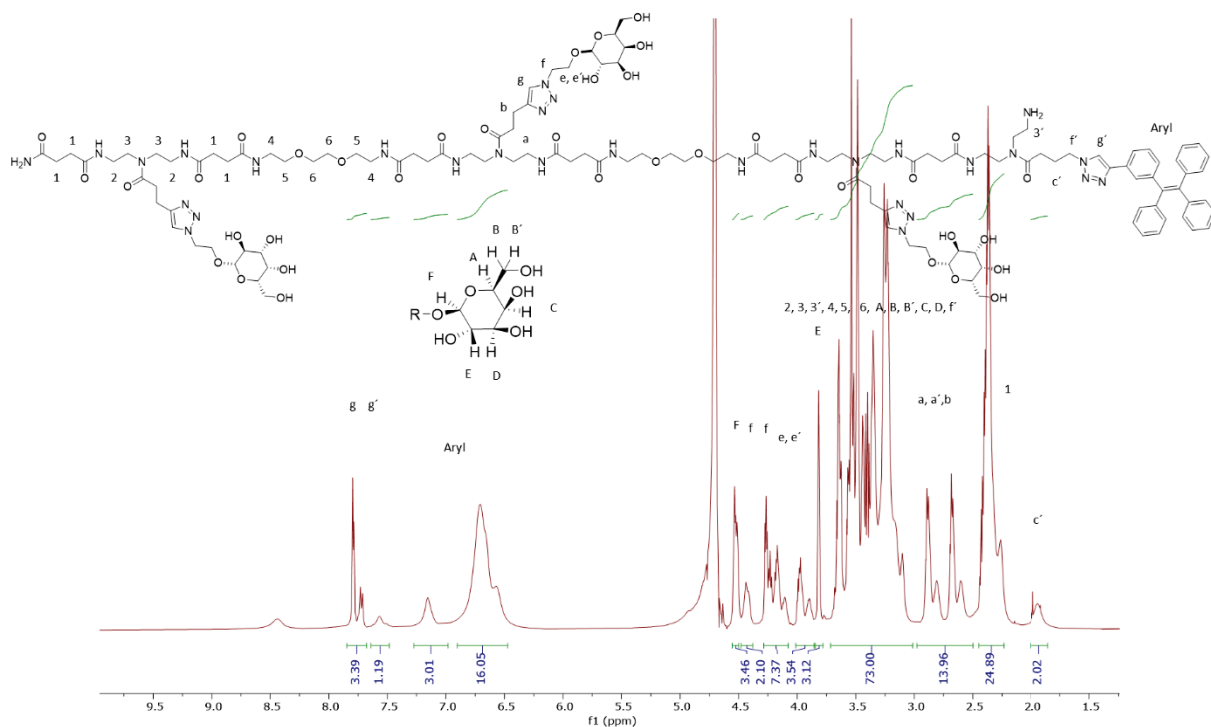


Figure S 4: 600 MHz ^1H NMR spectrum of **Gal-TPE** in D_2O at 25°C .

^1H -NMR (600 MHz, D_2O): δ (ppm) = In the range from 8.25 to 8.70 amide functionalities occur, 7.83-7.69 (m, 3H, Hg), 7.66-7.47 (m, 1H, Hg'), 7.27-6.95 (m, 3H, HAryl), 7.89-6.47 (m, 16H, HAryl), 4.58-4.50 (m, 3H, HF), 4.48-4.38 (m, 2H, Hf), 4.29-4.09 (m, 7H, Hf, He), 4.04-3.83 (m, 3H, He'), 3.80-3.76 (m, 3H, HE), 3.70-3.05 (m, 73H, H2-H6, H3', HA-D, HB', Hf'), 2.96-2.50 (m, 14H, Ha, Ha', Hb), 2.46-2.23 (m, 24H, H1), 2.02-1.79 (m, 2H, Hc').

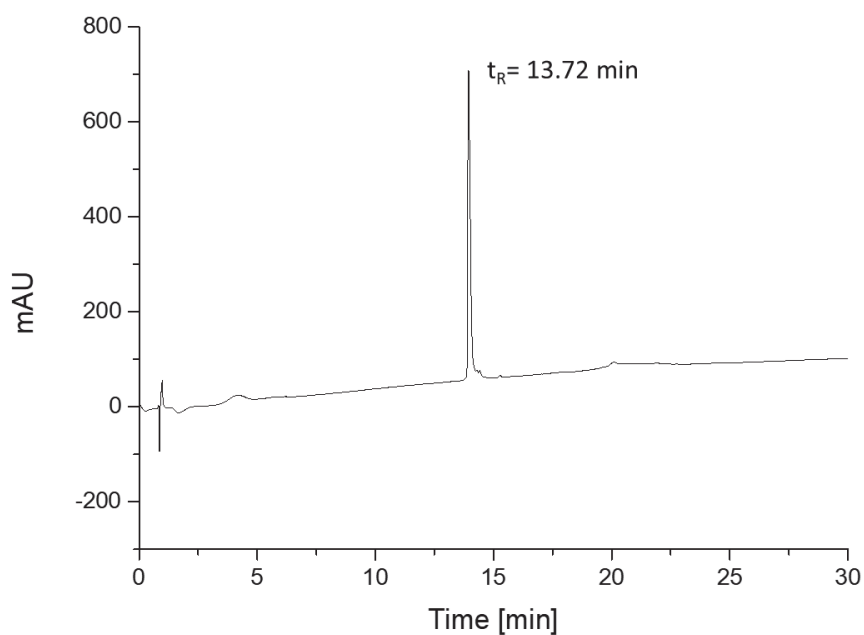


Figure S 5: **Gal-TPE** detected by RP-HPLC analysis (linear gradient from 5 – 95 vol% eluent H₂O/acetonitrile) in 30 min at 40 °C

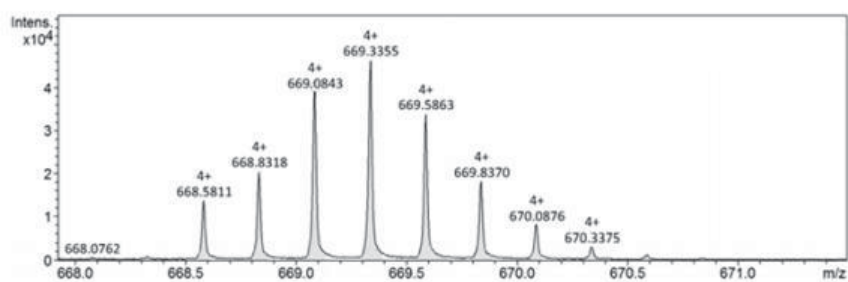


Figure S 6: HR-ESI-MS of **Gal-TPE**.

HR-ESI-MS: for C₁₂₃H₁₈₅N₂₉O₃₈ m/z [M+4H]⁴⁺ calcd: 669.0853, found: 669.0843
mass accuracy +1.5 ppm.

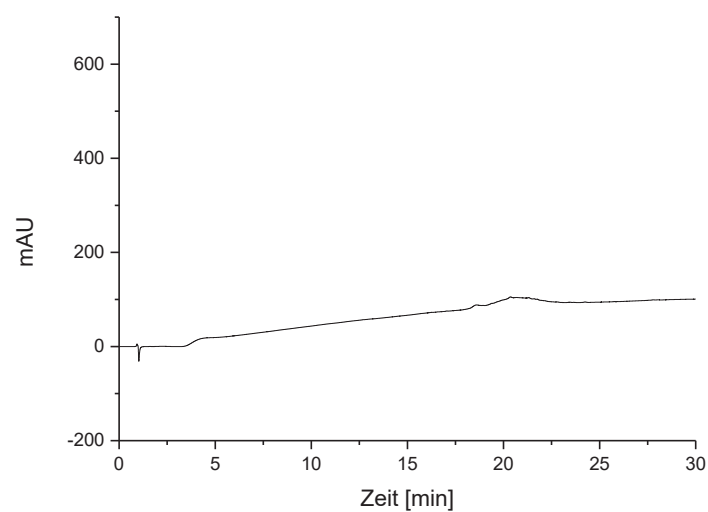


Figure S 7: Blank detected by RP-HPLC analysis (linear gradient from 5 – 95 vol% eluent H₂O/acetonitrile) in 30 min at 40 °C.

Further Fluorescence analytical data of oligomers:

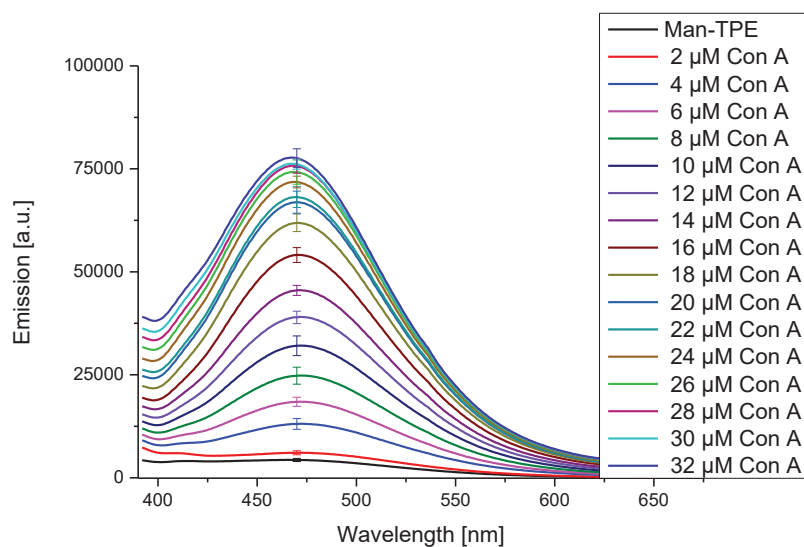


Figure S 8: **Man-TPE** emission signal (exci: 340 nm) in the presence of increasing Con A titration in LBB (triplicate with measurement error, concentration from the bottom curve to the top curve: 0 to 32 μM Con A).

Concentration of **Man-TPE** is 13 μM in LBB.

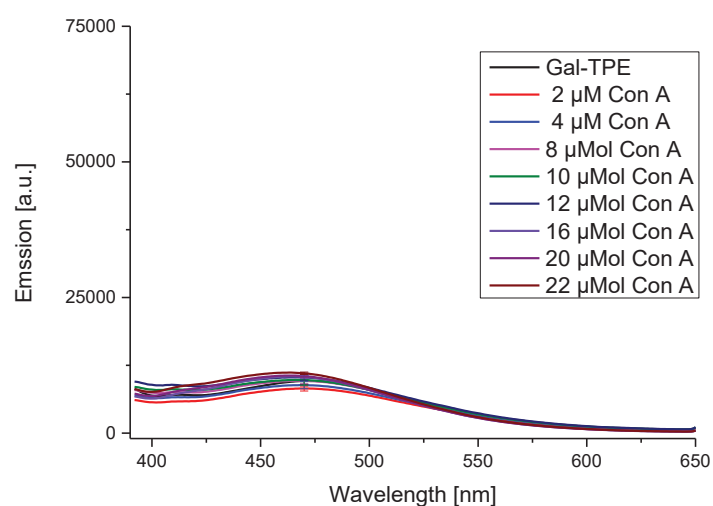


Figure S 9: **Gal-TPE** emission signal (exci: 340 nm) in the presence of increasing Con A titration in LBB (triplicate with measurement error, concentration from the bottom curve to the top curve: 0 to 32 μM Con A).

Concentration of **Gal-TPE** is 13 μM in LBB.

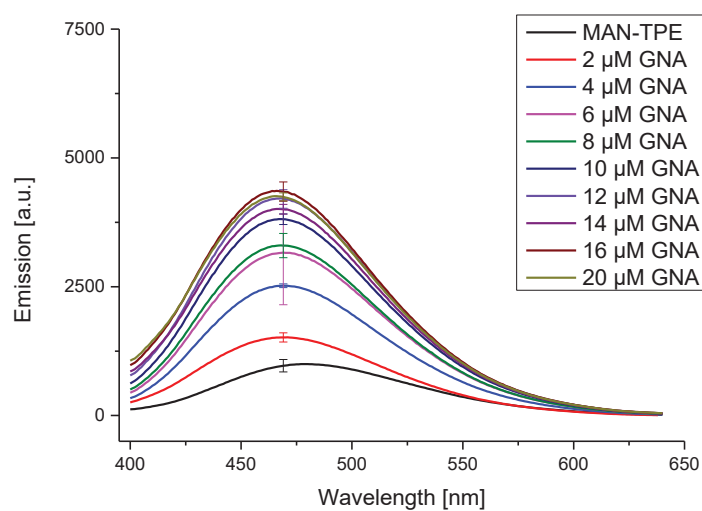


Figure S 10: **Man-TPE** emission signal (exci: 340 nm) in the presence of increasing GNA titration in LBB (triplicate with measurement error, concentration from the bottom curve to the top curve: 0 to 20 μM GNA).

Concentration of **Man-TPE** is 13 μM in LBB.

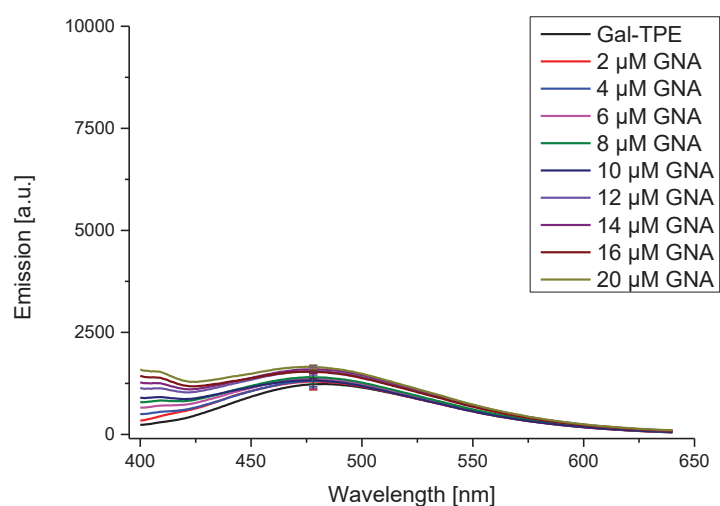


Figure S 11: **Gal-TPE** emission signal (exci: 340 nm) in the presence of increasing GNA titration in LBB (triplicate with measurement error, concentration from the bottom curve to the top curve: 0 to 20 μM GNA).

Concentration of **Gal-TPE** is 13 μM in LBB.

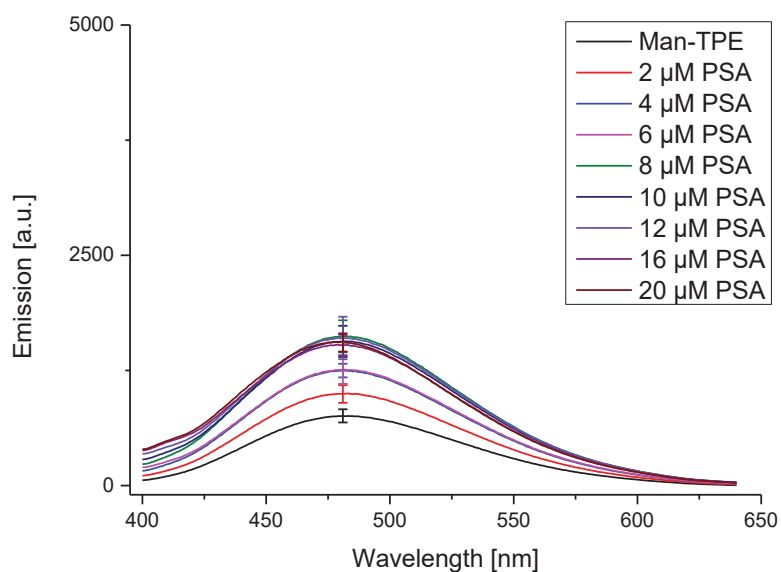


Figure S 12: **Man-TPE** emission signal (exci: 340 nm) in the presence of increasing PSA titration in LBB (triplicate with measurement error, concentration from the bottom curve to the top curve: 0 to 20 μM PSA). Concentration of **Man-TPE** is 13 μM in LBB.

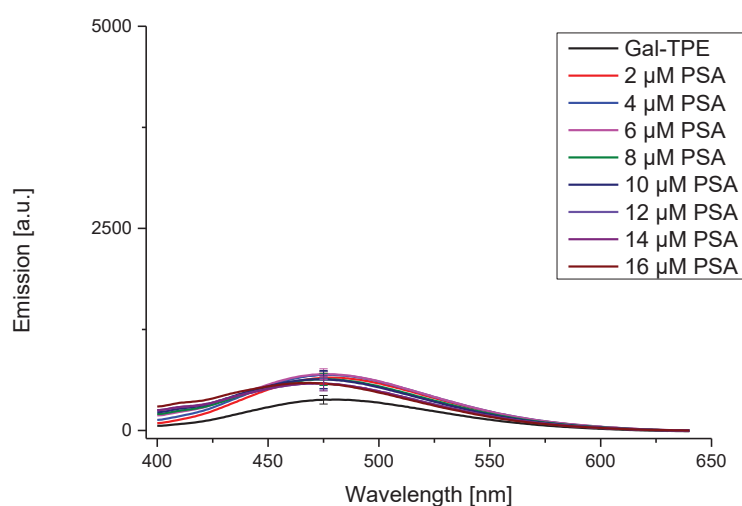


Figure S 13: **Gal-TPE** emission signal (exci: 340 nm) in the presence of increasing PSA titration in LBB (triplicate with measurement error, concentration from the bottom curve to the top curve: 0 to 20 μM PSA). Concentration of **Gal-TPE** is 13 μM in LBB.

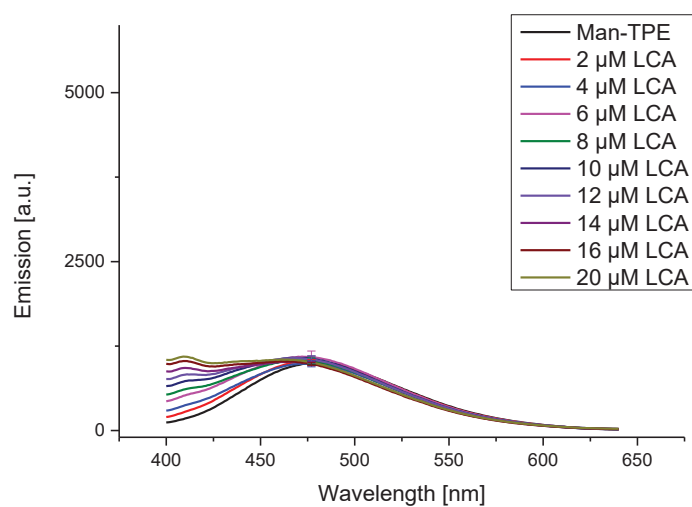


Figure S 14: **Man-TPE** emission signal (exci: 340 nm) in the presence of increasing LCA titration in LBB (triplicate with measurement error, concentration from the bottom curve to the top curve: 0 to 20 μM LCA). Concentration of **Man-TPE** is 13 μM in LBB.

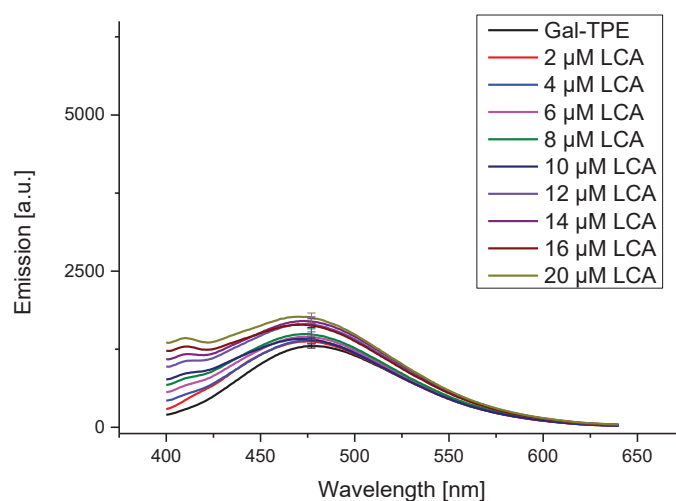


Figure S 15: **Gal-TPE** emission signal (exci: 340 nm) in the presence of increasing LCA titration in LBB (triplicate with measurement error, concentration from the bottom curve to the top curve: 0 to 20 μM LCA). Concentration of **Gal-TPE** is 13 μM in LBB.

Further Turbidity analytical data of oligomers:

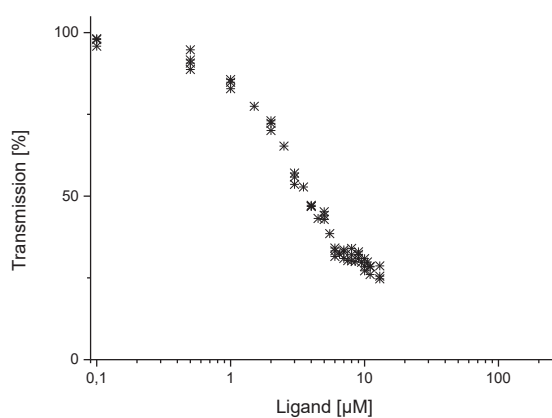


Figure S 16: Turbidity assays [Transmission at 420 nm, lectins conc. Con A 100 μM , triplicate] with titration of **Man-TPE** in LBB.

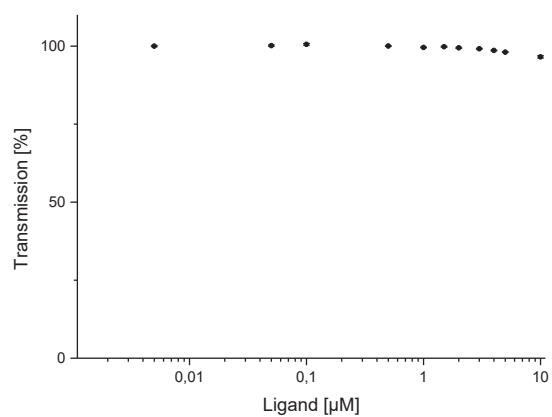


Figure S 17: Turbidity assays [Transmission at 420 nm, lectins conc. Con A 100μM] with titration of **Gal-TPE** in LBB.

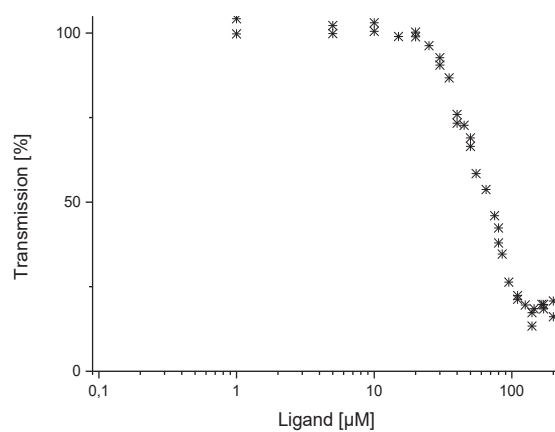
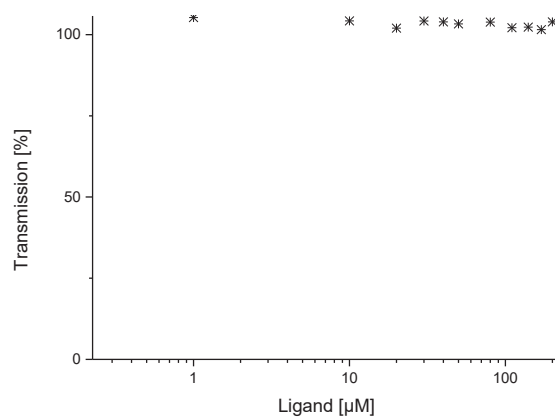


Figure S 18: Turbidity assays [Transmission at 420 nm, lectins conc. GNA 100μM, triplicate] with titration of **Man-TPE** in LBB.



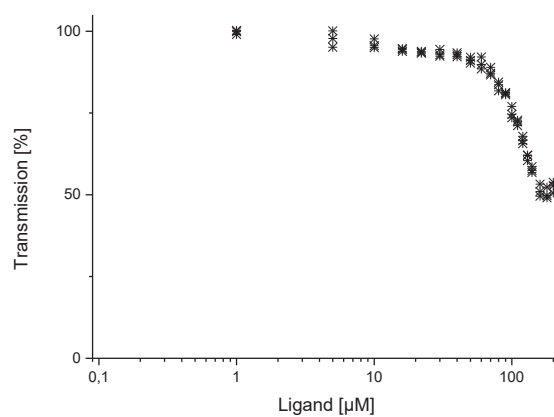


Figure S 20: Turbidity assays [Transmission at 420 nm, lectins conc. PSA 100μM, triplicate] with titration of **Man-TPE** in LBB

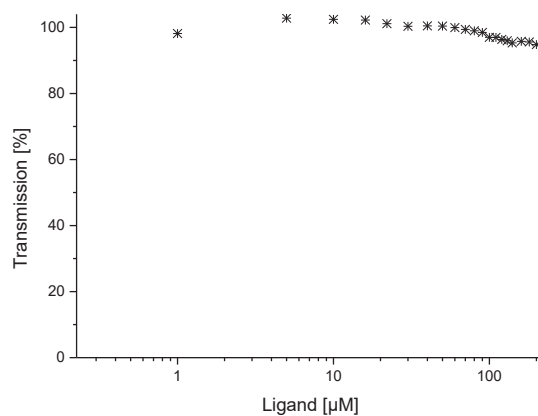


Figure S 21: Turbidity assays [Transmission at 420 nm, lectins conc. PSA 100μM] with titration of **Gal-TPE** in LBB.

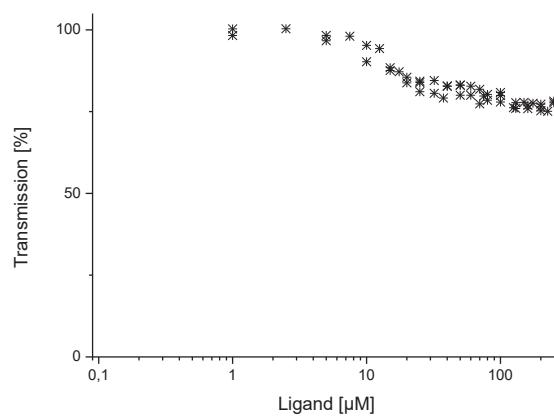


Figure S 22: Turbidity assays [Transmission at 420 nm, lectins conc. LCA 100μM, triplicate] with titration of **Man-TPE** in LBB.

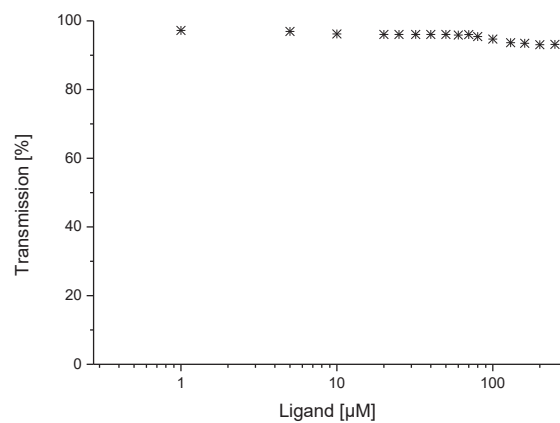


Figure S 23: Turbidity assays [Transmission at 420 nm, lectins conc. LCA 100μM] with titration of **Gal-TPE** in LBB.

5.4 Amphiphilic glyco(oligoamidoamines) with AIE luminophores to visualize cluster formation in self-assembled systems

In the previous chapter, glycooligomers equipped with AIE luminophores showed AIE effects with different lectins, but with clustering effects. Cluster formation is indeed an important phenomenon in multivalent binding and directly related to many biological functions, e.g. the clustering of receptors in a membrane upon binding to a multivalent ligand (Figure 1).^[1] However, detection of such clustering events in membranes is not trivial and usually requires complex methods such as the use of fluorescence resonance energy transfer (FRET) or fluorescence correlation spectroscopy (FCS).^[2-4] Alternatively, the use of AIE luminophores could offer new possibilities for the detection of clustering events. By monitoring the emission intensity, conclusions could be drawn about clustering behaviour of the system. Many clusters with many AIE interactions would cause a strong emission intensity, while individual AIEs would give only a small or even no emission signal.

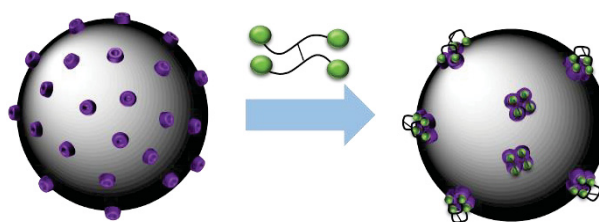


Figure 1: Modulation of in-membrane receptor clustering (purple dots) upon binding of tetraivalent ligands.^[1]

Based on this idea, the first goal was to synthesize amphiphilic glycooligomers that can assemble into micelles, as was recently demonstrated by Banger et al.^[5], and equip them with an AIE luminophore. Additionally, amphiphilic glycooligomers without luminophore as well as glycooligomers with either binding (Mannose) or non-binding (Galactose) carbohydrates were targeted (Figure 2).

In total, three AIE-modified glycooligomers (Mannose-TPE oligomer (**MTO**), Galactose-TPE oligomer (**GTO**), and Mannose-CATE oligomer (**MCO**)) were synthesized, two TPE derivatives, each with mannose or galactose as a binding motif, and an aromatic thioether luminophore (ATE) AIE^[6] derivative with mannose. All oligomers were synthesized using previously established solid phase polymer synthesis protocols and tailor-made building blocks, specifically two functional building blocks introducing an alkyne (TDS)^[7] or an azide side chain (ADS)^[8], azido-functionalized acetylated α -D-mannose (Man) and β -galactose (Gal)^[7], carboxylated aromatic thioether luminophores (CATE)^[9] and the commercially available alkyne functional TPE luminophores.

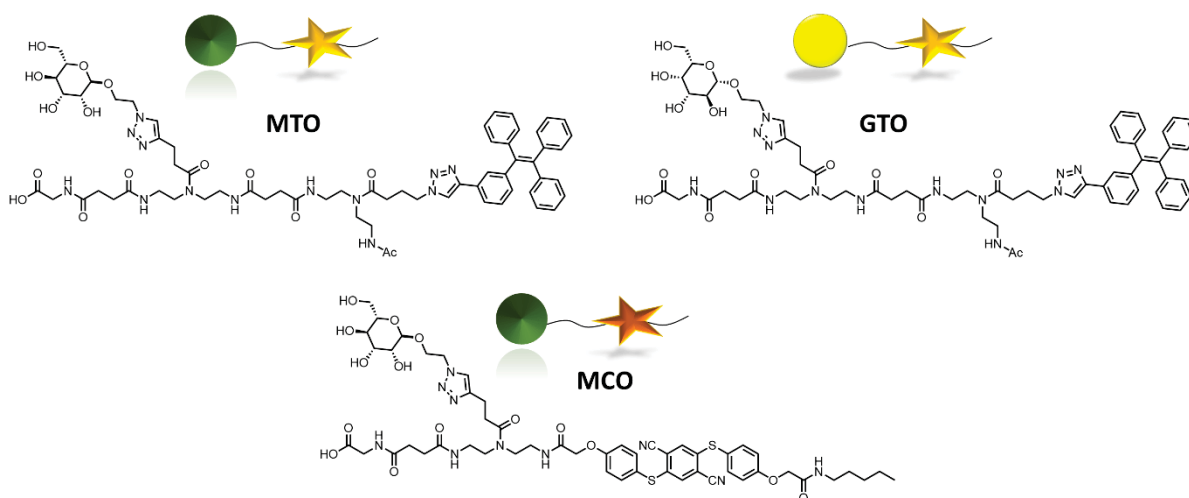


Figure 2: An overview of the three synthesized structures with schematic illustration as surfactant. Man-derivatives have a green and Gal- derivatives a yellow head group. TPE is shown as a yellow and CATE as a bronze star.

In short, glycooligomers were assembled as previously described in this work (Chapter 5.3). In order to couple the AIE luminophore, terminal Fmoc protecting group was released and CATE luminophore for **MCO** was incorporated via the carboxylate, requiring double coupling in tenfold excess to prevent dimerization at CATE. After CATE coupling, the second free acid on **MCO** was capped with pentylamine in order to form the hydrophobic component of the amphiphilic glycooligomers. For **MTO** and **GTO**, after assembly of the glycooligomer, an additional ADS building block was introduced, which allows a secondary CuAAC reaction to couple alkyne-functionalized TPE. After TPE conjugation, the Fmoc group was cleaved and the free amine was acetylated. For all glycooligomers, carbohydrates were deprotected on resin, oligomers cleaved from the resin and isolated by precipitation from diethylether and freeze drying.

All glycooligomers were further purified by either dialysis (**MTO**, **GTO**) or preparative HPLC (**MCO**) giving the final products in relative purities of >95% (LC analysis). All structures were confirmed by ^1H NMR and UHR-MS analyses (see exemplary ^1H NMR spectrum of **MCO** in Figure 3) (see SI for detailed analytical data). Aryl protons (δ (ppm) 8.41-7.26) of the incorporated CATE luminophore as well as the alkyl protons of the amylamine (δ (ppm) = 2.90-1.32, 1.26-0.90) can be clearly assigned.

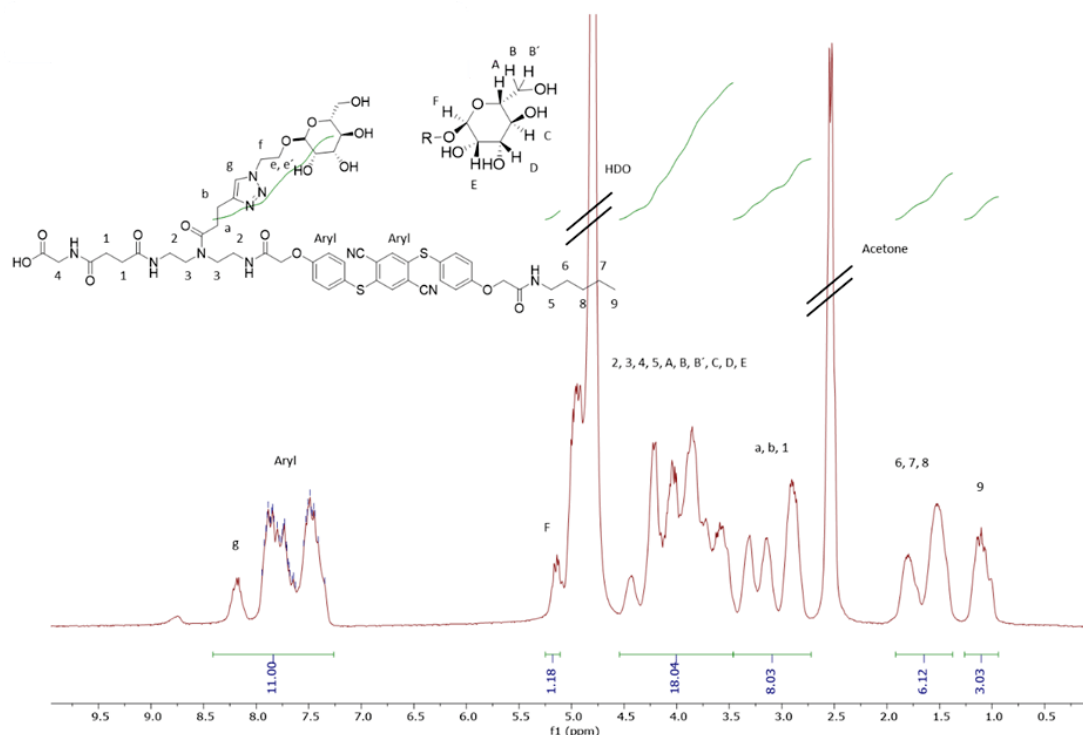


Figure 3: 600 MHz ^1H NMR spectrum of MCO in D_2O and Aceton- D_6 at 45°C .

With these molecules in hand, the use of AIE dye-containing amphiphilic glycooligomers as fluorescent sensors of cluster formation was investigated. First, AIE behavior of the free oligomers was tested with different fractions of acetonitrile and water. The AIE behavior is usually observed when a certain ratio of the poor solvent, in this case water, is reached and small aggregates are formed. This is due to rotational limitations of the groups in the luminophores, as shown by Tan et al.^[10] The amphiphilic nature of the oligomers is the reason why a water concentration of 100% can be achieved through self assembly into micelles without solid aggregation and precipitation, but with a high emission intensity. As an example, Figure 4A shows the increase in normalized fluorescence intensity of $300\ \mu\text{M}$ **GTO** as a function of $\text{H}_2\text{O}/\text{ACN}$ ratio (triplicates, $\lambda_{\text{ex}} = 340\ \text{nm}$, $\lambda_{\text{em}} = 457\ \text{nm}$) with photo series and measurement points. With an environmental change adding acetonitrile, the micelles were dissolved so that only single oligomers were present in solution and no AIE effect is observed (Fig.4B).

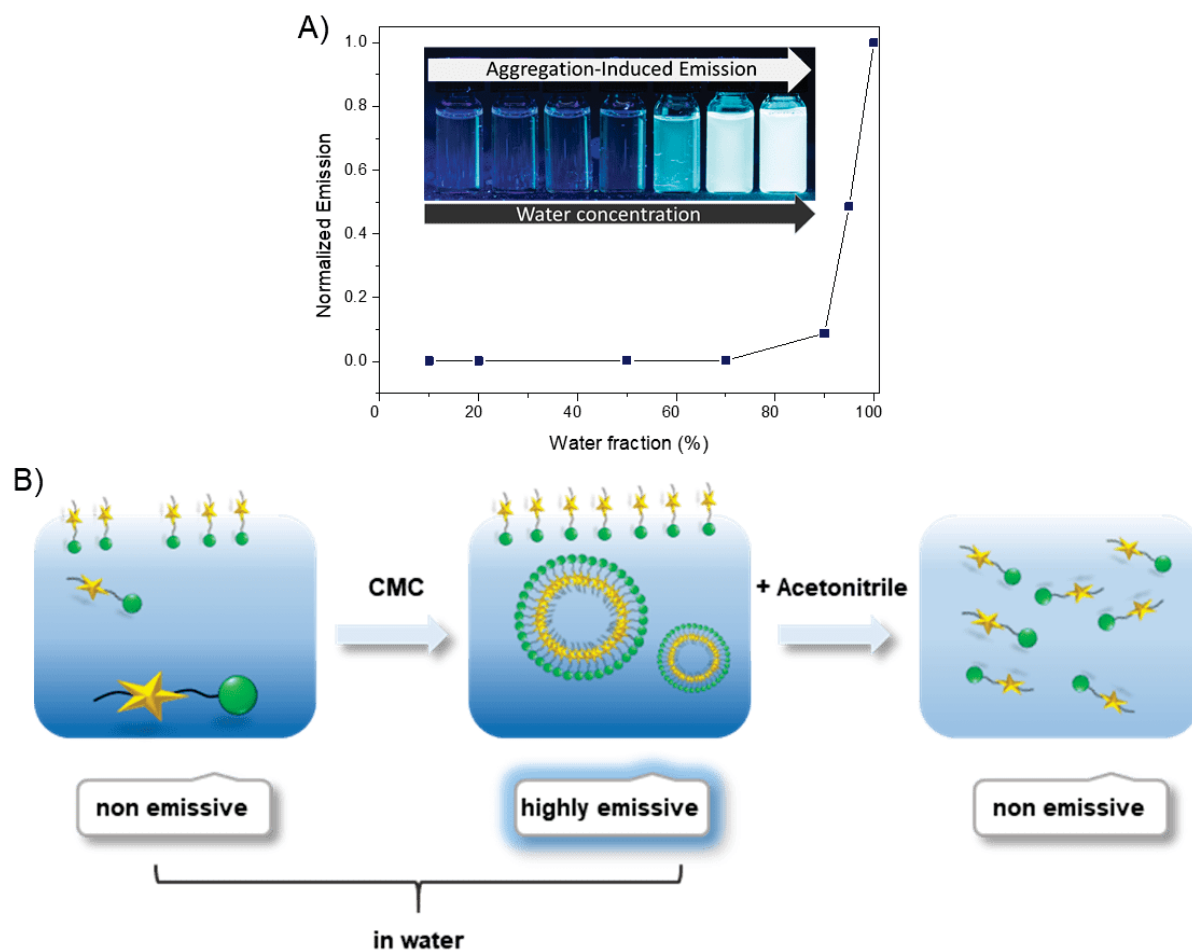


Figure 4: A) Rise of the normalized fluorescence intensity of 300 μM **GTO** in dependency of the $\text{H}_2\text{O}/\text{ACN}$ ratio (triplicates, $\lambda_{\text{ex}} = 340 \text{ nm}$, $\lambda_{\text{em}} = 457 \text{ nm}$) with photo series of the measuring points. B) Schematic illustration of the free AIE ligand below its CMC in water (no emission), above its CMC as aggregation in micelles with emission and with addition of the poor solvent acetonitrile, causing micelles to dissolve and emission to decrease.

Since AIE behavior is closely linked to the self-assembly of amphiphilic glycooligomers into micelles, in the next step critical micelle concentration (CMC, see Figure 5) was determined. For this purpose, concentration series were measured (0.004 to 1 mM) and fluorescence was detected based on the emission characteristics of the luminophore ($\lambda_{\text{ex}} = 340 \text{ nm}$, $\lambda_{\text{em}} = 457 \text{ nm}$).

The CMCs of the two TPE derivatives (**MTO** and **GTO**) are very similar with values of 77 μM and 74 μM , respectively. This is in agreement with previous studies that showed only little effects of Mannose vs. Galactose in the micelle formation of amphiphilic glycooligomers.^[11] The **MCO** derivative, on the other hand, has a clearly higher CMC value of 135 μM . The CMC difference can be attributed to the low flexibility of the TPE compared to the CATE-AIE. Similarly, weaker intramolecular interactions of the CATE units compared to TPE may cause the lower CMC value.

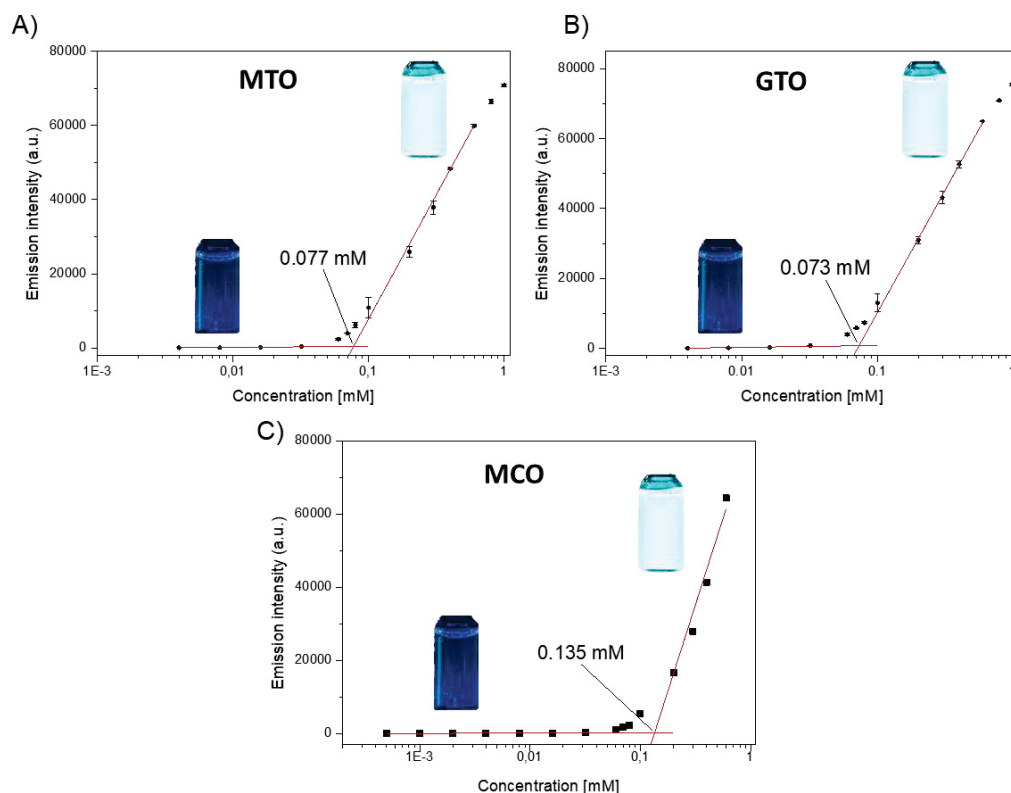


Figure 5: Determination of the critical micelle concentration (CMC) for A) **MTO** B) **GTO** and C) **MCO** by emission intensity of the AIE-surfactants in the concentration range from 0.004 to 1 mM in water (triplicates, $\lambda_{ex} = 340$ nm, $\lambda_{em} = 457$ nm).

Since the glycooligomers should be used to detect clustering, first an assembly with no clustering needs to be realized. Therefore, mixing experiments were performed with a non-fluorescent, non-carbohydrate surfactant and **MTO**. Sodium dodecyl sulfate, a well-established surfactant was used. Figure 5 shows the fluorescence reduction of **MTO** as a function of the concentration of SDS. SDS was found to be potent in terms of fluorescence reduction. With SDS, a fluorescence reduction of more than 90% was already achieved at 1.5 mM and at 3.5 mM the emission reduction was 97%. This effect can be explained by lower interactions within the mixed micelle systems, such as stacking of the luminophores, which reduces the rotational constraint of the luminophores, resulting in lower emission (see Fig. 6A). Similar reduction results could also be obtained with **MCO** and SDS (Fig. S11).

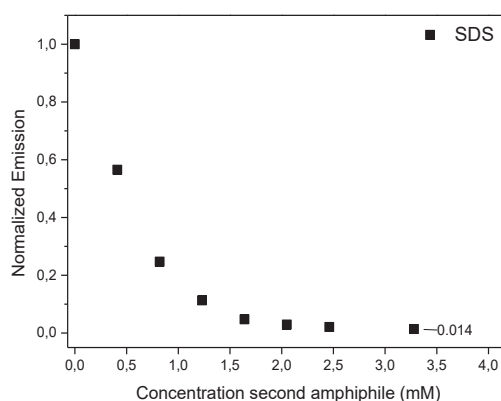


Figure 5: Fluorescence reduction of 300 μM **MTO** by addition of SDS in water (triplicates, $\lambda_{\text{ex}} = 340 \text{ nm}$, $\lambda_{\text{em}} = 457 \text{ nm}$).

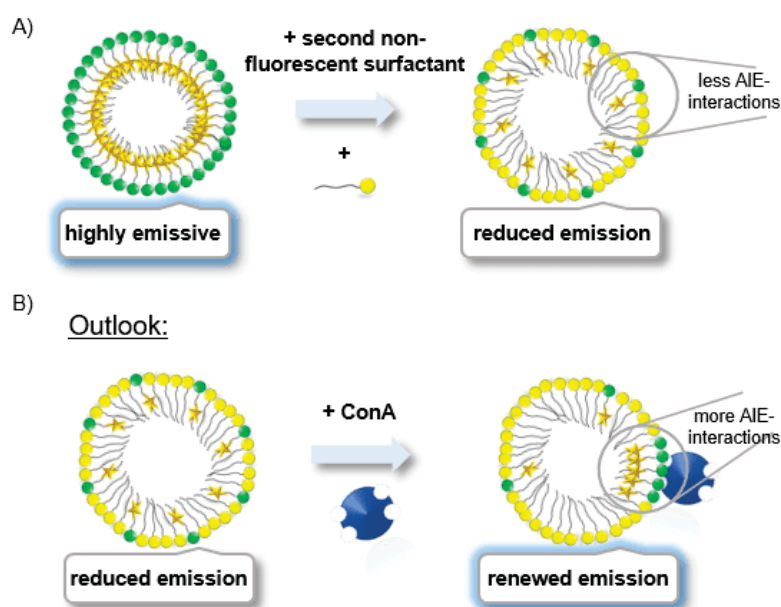


Figure 6: Schematically shown in A) is the addition of a second non-fluorescent surfactant, which leads to mixed micelles, resulting in fewer AIE interactions and a decrease in emission intensity. In B) our mid-term goal of the project is shown: After successful reduction of the emission intensity with mixed micelles, clustering of the AIE surfactants through interactions with lectins such as ConA will be investigated in the future. This could lead to more AIE interactions within the micelles, which would increase the emission intensity again.

In general, these experiments show that the initial emission intensity of luminophore-containing micelles can be selectively reduced by the addition of a non-fluorescent second surfactant and now open up the possibility to add multivalent receptors, e.g. ConA as was used in the previous chapter, and study whether clustering can be induced and observed by a potential increase in fluorescence from the AIE luminophore (Fig.6B). Due to time constraints, this next part of the project was performed by Alexaner Banger.

Supporting Information

Synthesis part:

Synthesis EDS, TDS, α -D Mannose and β -Galaactose

(4-((2-(2-(2-aminoethoxy)ethoxy)ethyl)-amino)-4-oxobutanoic), tripple-bond diethylene-triamine succinamide as well as acetylated α -D Mannose or β -Galcatoose were synthesized according to literature procedures.^[7]

General:

The oligo(amidoamines) synthesis were carried out manually in 10 ml polypropylene syringe reactors with a polyethylene frit and a Luer stopper from Multisynthetech GmbH. Oligo(amidoamines) were synthesized on the a Fmoc Gly TentaGel® S Trt resin (with capacity of 0.21 mmol/g. Batch size of oligo (amido)amines were 0.15 mMolar.

Fmoc cleavage

The resin was swollen in DCM for 30 min and subsequently washed three times with DMF. Secondly the Fmoc protecting group of the resin as well as from the coupled building blocks or amino acids was cleaved by means of a 25% solution of piperidine in DMF achieving an amine end group. The deprotection was carried out twice for 20 min and 7 ml. Afterwards the resin was washed 10 times with DMF.

Coupling protocol

First the resin was swollen in DCM for 30 min and then washed three times with DMF. The Fmoc protecting group had to be removed before further couplings!

For the building block coupling 5 eq., 5 eq. PyBOP and 10 eq. DIPEA were dissolved in 5 mL DMF, drawn into the reactor syringe and shaken for 90 min, followed by washing ten times with DMF. The same procedure was followed for the coupling of amylamine. For CATE coupling, the duplicate quantities of building block (CATE), PyBOP and DIPEA were used.

CuAAC protocol of pyranoside

To the oligomeric structure loaded on the resin 2 eq of acetyl protected 2-azidoethyl pyranoside (α -Mannose/ β -Galactose) per alkyne group dissolved in 3 mL DMF were added. Secondly 20 mol% sodium ascorbate per alkyne group and 20 mol% CuSO₄ per alkyne group were dissolved each in 1 mL

water and also added to the resin. The reaction time was 24 h and subsequently washed with a 23 mM solution of sodium diethyldithiocarbamate in DMF and water (50/50, v/v) and alternating with DMF and DCM until no further color change occur.

CuAAC protocol of 1-Ethynyl-4-(1,2,2-triphenylethenyl) benzene

To the oligomeric structure loaded on the resin 2 eq of 1-Ethynyl-4-(1,2,2-triphenylethenyl) benzene per azido group dissolved in 3 mL DMF were added. Further implementations are identical to the CuAAC protocol of pyranoside.

Acetyl deprotection and cleavage from solid phase

For the glycine loaded resin the sugar moiety was deprotected and at the same time the oligomer was cleaved off the resin using 0.05 M NaOH in methanol and water (vol% 99:1) for 90 min. The cleavage solution was precipitated in ether, centrifuged, dried and dialysed.

Analytical data for macromolecules:

Macromolecule *MTO*

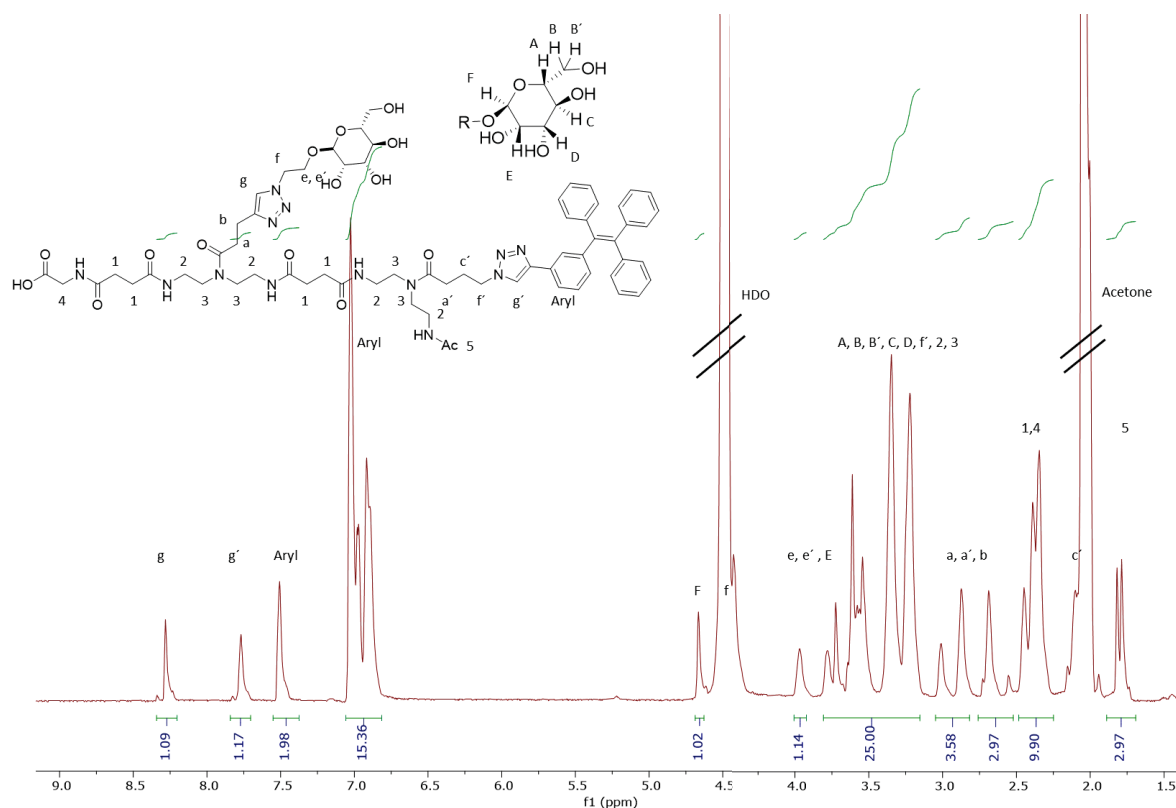


Figure S 24: 600 MHz ^1H NMR spectrum of *MTO* in D_2O and Acetone- D_6 at 45°C .

¹H-NMR (600 MHz, D₂O+ Acetone-D₆, ratio 3:1, 45°C): δ (ppm) = 8.71-8.63 (m, 1H, Hg), 8.19-7.77 (m, 3H, Hg', HAryl), 7.52-7.42 (m, 2H, HAryl), 7.18-6.76 (m, 15H, HAryl), 4.68 (s, HF), 3.98 (m, 1H, He), 3.79-3.15 (m, 25H, H2-H4, HA-E, HB', Hf', He'), 3.10-3.2.81 (m, 4H, Ha, Hb), 2.76-2.58 (m, 10H, H1, H4), 2.28-2.18 (m, Hc'), 1.91-1.73 (m, 3H, H5).

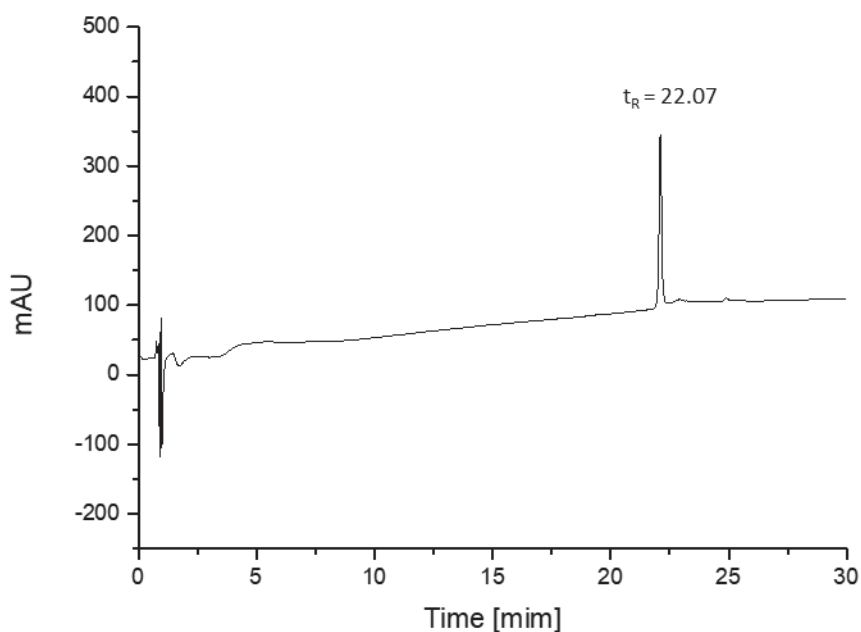


Figure S 25: **MTO** detected with relative purities >95% by RP-HPLC analysis (linear gradient from 25 – 75 vol% eluent H₂O/acetonitrile) in 30 min at 40 °C.

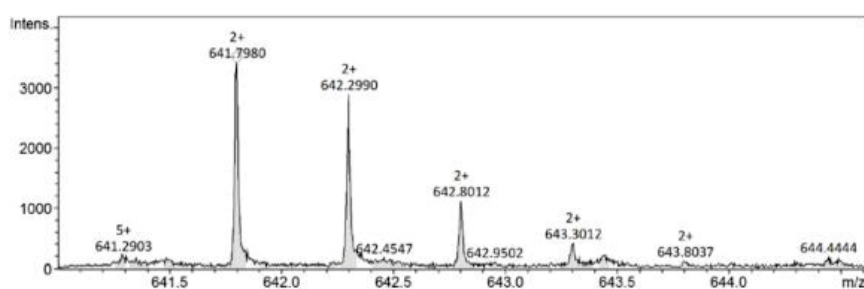


Figure S 26: HR-ESI-MS of **MTO**.

HR-ESI-MS: for C₆₅H₈₁N₁₃O₁₅ m/z [M+2H]²⁺ calcd.: 641.7982, found: 641.7980
mass accuracy +0.3 ppm.

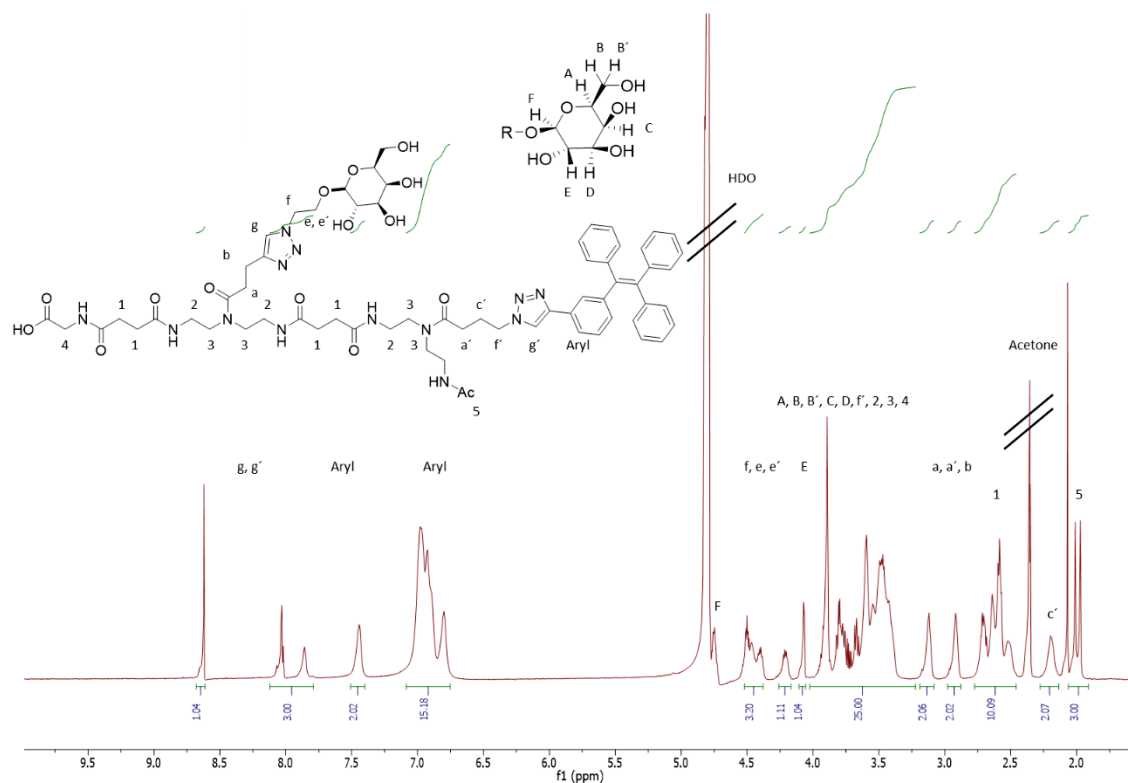


Figure S 27: 600 MHz ^1H NMR spectrum of **GTO** in D_2O and Aceton- D_6 at 35°C .

^1H -NMR (600 MHz, D_2O + Aceton- D_6 , ratio 3:1, 35°C): δ (ppm) = 8.71-8.63 (m, 1H, Hg), 8.19-7.77 (m, 3H, Hg', HAryl), 7.52-7.42 (m, 2H, HAryl), 7.18-6.76 (m, 15H, HAryl), 4.77-4.74 (m, HF), 4.54-4.39 (m, 3H, He, Hf), 4.26-4.20 (m, 1H, He'), 4.17 (s, 1H, HE), 4.04-3.25 (m, 25H, H2-H4, HA-D, HB', Hf'), 3.16 (s, 2H, Ha), 2.93 (s, 2H, Ha'), 2.76-2.48 (m, 10H, H1, Hb), 2.22 (s, 2H, Hc'), 2.12-1.90 (m, 3H, H5).

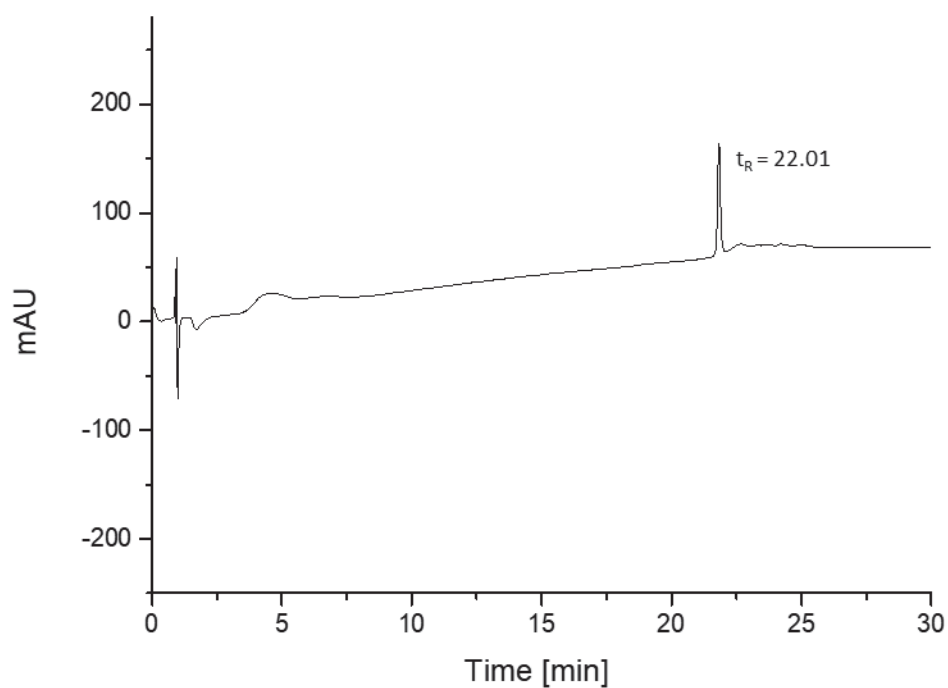


Figure S 28: **GTO** detected with relative purities >95% by RP-HPLC analysis (linear gradient from 25 – 75 vol% eluent H₂O/acetonitrile) in 30 min at 40 °C.

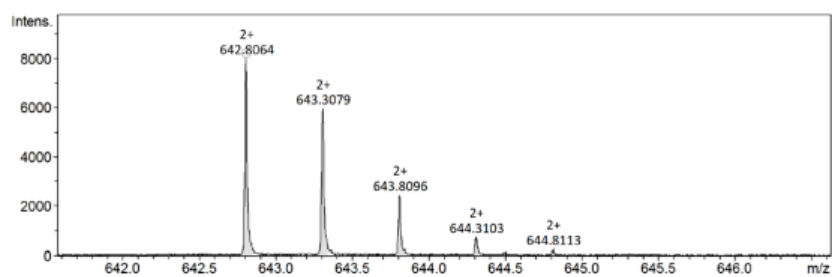


Figure S 29: HR-ESI-MS of **GTO**.

HR-ESI-MS: for C₆₅H₈₁N₁₃O₁₅ m/z [M+2H]²⁺ calcd.: 642.8060, found: 642.8064
mass accuracy -0.5 ppm.

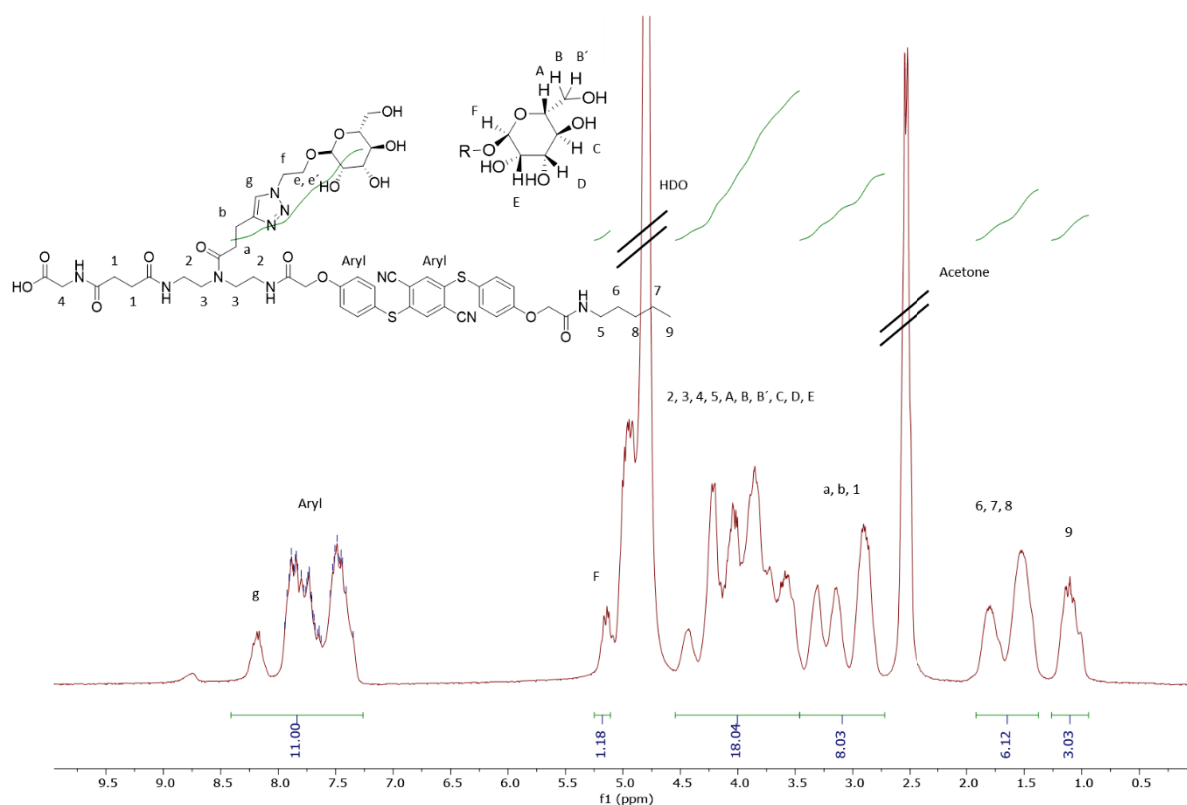


Figure S 30: 600 MHz ^1H NMR spectrum of **MCO** in D_2O and Aceton- D_6 at 45°C .

^1H -NMR (600 MHz, D_2O + Aceton- D_6 , ratio 1:1, 45°C): δ (ppm) = In the range from 8.50 to 8.70 amide functionalities occur, 8.41-7.26 (m, 11H, Hg, HAryl), 5.26-5.08 (m, 1H, HF), 4.55-3.48 (m, 18H, H2-H5, HA-HE, HB'), 3.47-2.73 (m, 8H, H1, Ha, Hb), 1.90-1.32 (m, 6H, H6-H8), 1.26-0.90 (m, 3H, H9).

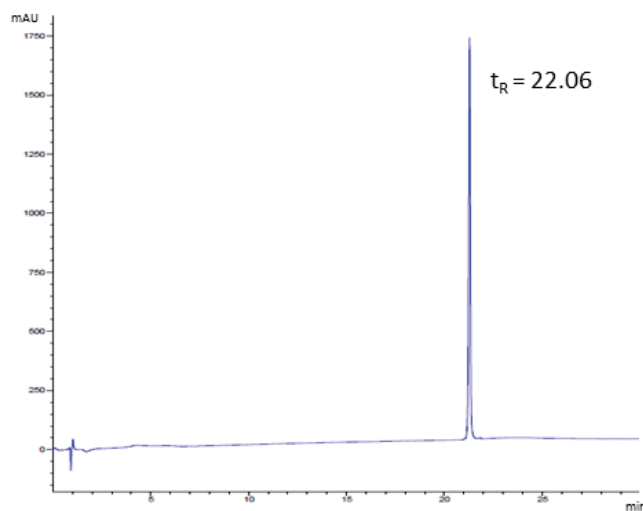


Figure S 31: **MCO** detected with relative purities >95% by RP-HPLC analysis (linear gradient from 25 – 75 vol% eluent H_2O /acetonitrile) in 30 min at 40°C .

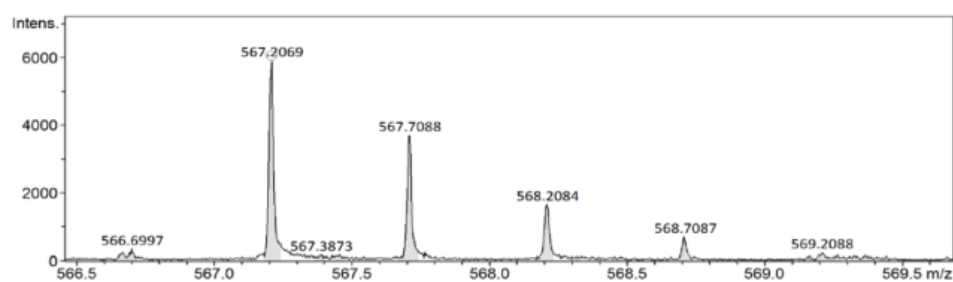


Figure S 32: HR-ESI-MS of **MCO**.

HR-ESI-MS: for $C_{52}H_{64}N_{10}O_{15}S_2$ m/z $[M+2H]^{2+}$ calcd. : 567.2070 found: 567.2069

mass accuracy +0.1 ppm.

Fluorescence-data

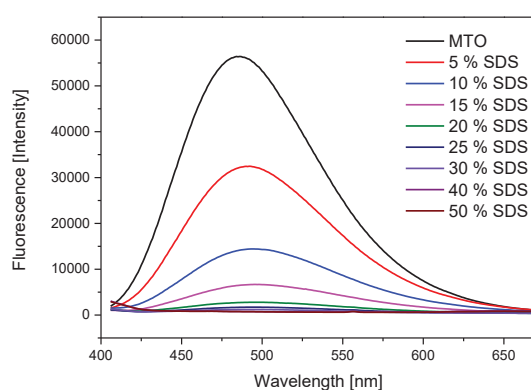


Figure S 33: Fluorescence reduction of 300 μM **MTO** by addition of SDS (percent of the SDS CMC value 8.200 μM , (λ_{ex} = 340 nm).

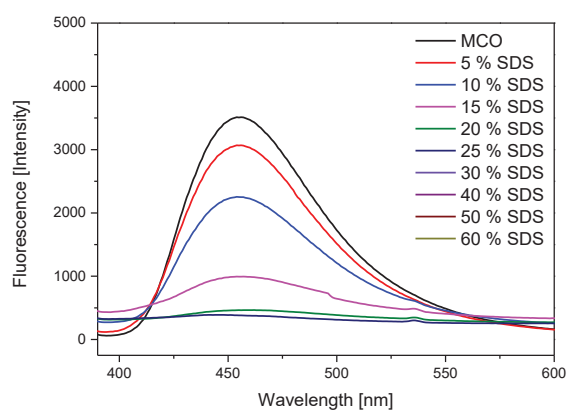


Figure S 34: Fluorescence reduction of 300 μM **MCO** by addition of SDS (percent of the SDS CMC value 8.200 μM (λ_{ex} = 380 nm).

References

1. A. Grochmal, E. Ferrero, L. Milanesi, S. Tomas, *Am. Chem. Soc.* **2013**, *135*, 10172–10177.
2. L. Wawrezinieck, H. Rigneault, D. Marguet, P.F. Lenne, *Biophys. J.* 2005, *89* (6), 4029-4042.
3. I. Mikhalyov, N. Gretskaya, L.B.A. Johansson, *Chem. Phys. Lipids* 2009, *159* (1), 38-44.
4. R. Šachl, M. Amaro, G. Aydogan, A. Koukalová, I. I. Mikhalyov, I. A. Boldyrev, J. Humpolíčková, M. Hof, *Biochim Biophys Acta Biomembr* **2015**, *1853* (4), 850-857.
5. A. Banger, J. Sindram, M. Otten, J. Kania, D. Wilms, A. Strzelczyk, S. Mileticcd, T. C. Marlovitscd, M. Karg, L. Hartmann, *Polym. Chem.* **2021**, DOI: 10.1039/D1PY00422K.
6. a) J. Stelzer, C. Vallet, A. Sowa, D. Gonzalez-Abradelo, S. Riebe, C. G. Daniliuc, M. Ehlers, C. A. Strassert, S. K. Knauer, J. Voskuhl, *ChemistrySelect* **2018**, *3*, 985-991; b) S. Riebe, C. Wölper, J. Balszuwei, M. Hayduk, M. E. Gutierrez Suburu, C.A. Strassert, N. L. Doltsinis, J. Voskuhl, *ChemPhotoChem* **2020**, *4*, 383-384.
7. a) D. Ponader, S. Igde, M. Wehle, K. Märker, M. Santer, D. Bléger, L. Hartmann, *Beilstein J. Org. Chem.* **2014**, *10*, 1603-1612; b) C. Gerke, M. F. Ebbesen, D. Jansen, S. Boden, T. Freichel, L. Hartmann, *Biomacromolecules* **2017**, *18* (3), 787-796; c) D. Ponader, F. Wojcik, F. Beceren-Braun, J. Dervede, L. Hartmann, *Biomacromolecules* **2012**, *13* (6), 1845-1852.; d) M. F. Ebbesen, C. Gerke, P. Hartwig, L. Hartmann, *Polym. Chem.* **2016**, *7* (46), 7086-7093.
8. F. Shamout, L. Fischer, N. L. Snyder, L. Hartmann. *Macromol. Rapid Commun.* **2019**, 1900473.
9. M. Externbrink, S. Riebe, C. Schmuck, J. Voskuhl, *Soft Matter* **2018**, *14*, 6166-6170.
10. a) J. Li, J. Wang, H. Li, N. Song, D. Wang, B. Z. Tang, *Chem. Soc. Rev.* **2020**, *49*, 1144-1172; b) R. Hu, N. L. C. Leung, B. Z. Tang, *Chem. Soc. Rev.* **2014**, *43*, 4494; c) J. Mei, Y. Hong, J. W. Y. Lam. A. Qin, Y. Tang, B. Z. Tang, *Adv. Mater.* **2014**, *6*, 5429-5479; d) R. Hu, A. Qin, B. Z. Tang, *Prog. Polym. Sci.* **2020**, *100*, 101176; e) Y. Yu, A. Qin, C. Feng, P. Lu, K. M. Ng, K. Q. Luo, B. Z. Tang, *Analyst* **2012**, *137*, 5592-5596.
11. S. Matsumura, Y. Kawamura, S. Yoshikawa, K. Kawada, T. Uchibori, *J. Am. Oil Chem. Soc.* **1993**, *70* (1), 17-22.

6. Summary & Conclusion

The overall aim of this work was to make new hybrid macromolecules accessible that combine natural and non-natural building blocks and to investigate their potential for applications as biological ligands, sensors or inhibitors. The approach of combining natural and non-natural building blocks into macromolecules offers access to biofunctional materials with tailor-made properties. A classic example of this is the PEGylation of proteins to increase protein stability to heat, organic solvents and enzymatic degradation.^[117,118] While a PEGylated protein is a conjugate of two components, protein and polymer, much more complex hybrid structures are also possible today, e.g. by replacing individual amino acids with non-natural building blocks in a protein. From a synthetic point of view, solid phase synthesis offers an ideal platform for creating such hybrid structures. Since the 1960s and through the pioneering work of Merrifield, solid phase synthesis has been used as a standard synthetic method for the generation of peptides and proteins in the laboratory.^[22] Today, other bio- but also synthetic macromolecules are accessible by means of solid phase synthesis. In Laura Hartmann's research group, the so-called solid-phase polymer synthesis (SPPoS) of oligo(amidoamines) in particular has been established.^[18,19,30-31] Here, synthetic building blocks are already successfully combined with natural building blocks such as amino acids and carbohydrates.

The aim of this work was now to supplement solid-phase polymer synthesis with further building blocks and thus expand the spectrum of accessible hybrid structures. Specifically, the non-natural binding motif guanidiniocarbonylpyrrole (GCP), an arginine mimetic, is to be used.^[81] The GCP, which was established by Schmuck in 1999 et al., has a high affinity for oxyanions, and could therefore already be used as a binding motif in biological ligands to inhibit or detect proteins.^[17,83,85,119] Secondly, aggregation-induced emission luminophores (AIE) will be conjugated to oligo(amidoamines) for the first time. The AIE phenomenon allows bioassays to be performed at low concentrations and provides information on binding events and clustering by fluorescence spectroscopy. To demonstrate that the combination of these building blocks with the solid-phase polymer synthesis platform can provide access to new bioactive hybrid structures, four different classes of macromolecules with different applications were generated in this work.

In the first part of this dissertation, GCP-containing macromolecules were synthesised to be used for the development of new modulators of protein-protein interactions. The design of the synthesised macromolecules was based on multivalence concepts. Similar to the GCP-containing sequence-defined oligomers first synthesised by P. Reuter, homomultivalent mono- and trivalent GCP oligomers were synthesised.^[120] This approach was extended by heteromultivalent combinations with free lysines in the direct vicinity of the GCP, which was intended to increase the binding strength of the ligand, as

was already possible with other GCP structures with additional lysines.^[121] In addition, a steric shielding of the partner protein by the incorporation of PEG block was targeted (see Figure 10).^[122-125]

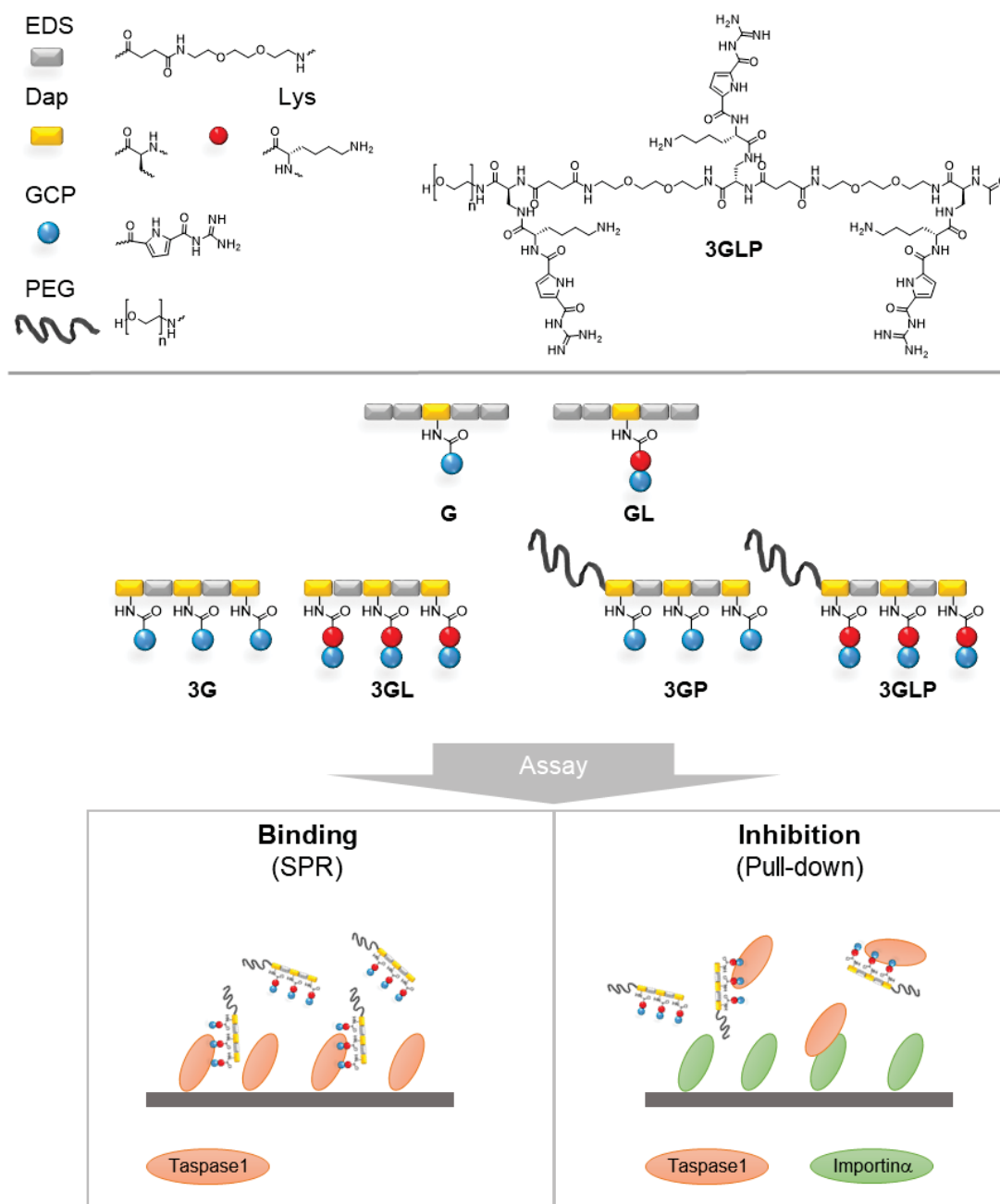


Figure 10: Final with GCP, lysine and PEG block, **G** (one GCP), **GL** (one GCP & lysine), **3G** (three GCP), **3GL** (three GCP & lysine), **3GP** (three GCP + PEG) and **3GLP** (three GCP & lysine + PEG). Due to purification by preparative HPLC, the compounds are present as formate salts. In addition, the two assays are schematically illustrated with regard to the binding of the ligands (SPR) and the inhibitory properties (pull-down).

As a model system for demonstrating the biological potential of GCP-containing macromolecules the tumour-relevant Threoninaspertase 1 (Taspase1) was selected.^[126,127] Taspase1 is particularly suitable because it requires interaction with the import receptor Importin α for activation and because the

bipartite NLS (nuclear localisation sequence) of Taspase1 is flanked by several anionic amino acids such as aspartic acid and glutamic acid^[128], which can act as binding partners of the GCP ligands.

To ensure that the ligands can bind to the Taspase1 surface, surface plasmon resonance (SPR) assays with bound Taspase1 were performed by S. Ueclue. In this assay, the two monovalent GCP macromolecules showed no binding to Taspase1, which can be explained by the absence of multivalence and the resulting weaker binding strength. In contrast, dissociation constants in μM range could be detected for the trivalent macromolecules, with a significant increase in binding strength occurring for the trivalent lysine derivatives.

To evaluate the potential as inhibitors of the Taspase1 and Importin- α complex formation, in vitro pull-down assays with the trivalent ligands were subsequently performed by A. Höing. Interestingly, the ligands without the PEG-Stealth block failed to affect the formation of the Taspase1-Importin- α complex. This suggests that NLS cannot be adequately shielded without the PEG block. In contrast, a mechanism of inhibition could be demonstrated for the PEG derivatives. Whereby the PEG derivative with additional free lysines again enhances the inhibitory effect.

Overall, these results show that by multivalent presentation of a non-natural supramolecular binding motif along an oligomer, a ligand can be obtained that can firstly bind to Taspase1 and secondly inhibit Taspase1-Importin- α interactions. However, no precise statements can currently be made about the location of the binding of the ligands, e.g. which anionic amino acids on the surface of Taspase1 are precisely targeted and how exactly it comes to blocking the interaction with the partner Importin α . This must be clarified in more detail in the future. Nevertheless, these results already provide enough evidence to move on to cellular studies since, as already noted, the ligands showed no toxicity in the cell viability assay. In addition, it would be exciting to introduce cleavability between the blocks so that targeted binding processes could first be inhibited and afterwards even promoted. One approach to this could be the introduction of disulfide bridges, which has already been tested for other macromolecules derived from solid phase polymer synthesis.^[129,130]

For a second class of hybrid macromolecules, AIE luminophores and the previously used GCP binding motif were targeted. It could be rationalized that AIE properties are strongly influenced by the macromolecular scaffold itself, however, so far this had not been studied systematically. The aim of this part of the dissertation was therefore to systematically investigate how the position of the AIE within the overall construct affects its sensing properties. For the study, five different monovalent GCP-containing macromolecules with identical AIE luminophores were synthesised, with the position of the AIE varying from the immediate vicinity of the binding motif to the middle of the side or main chain to the end group (see Figure 11).

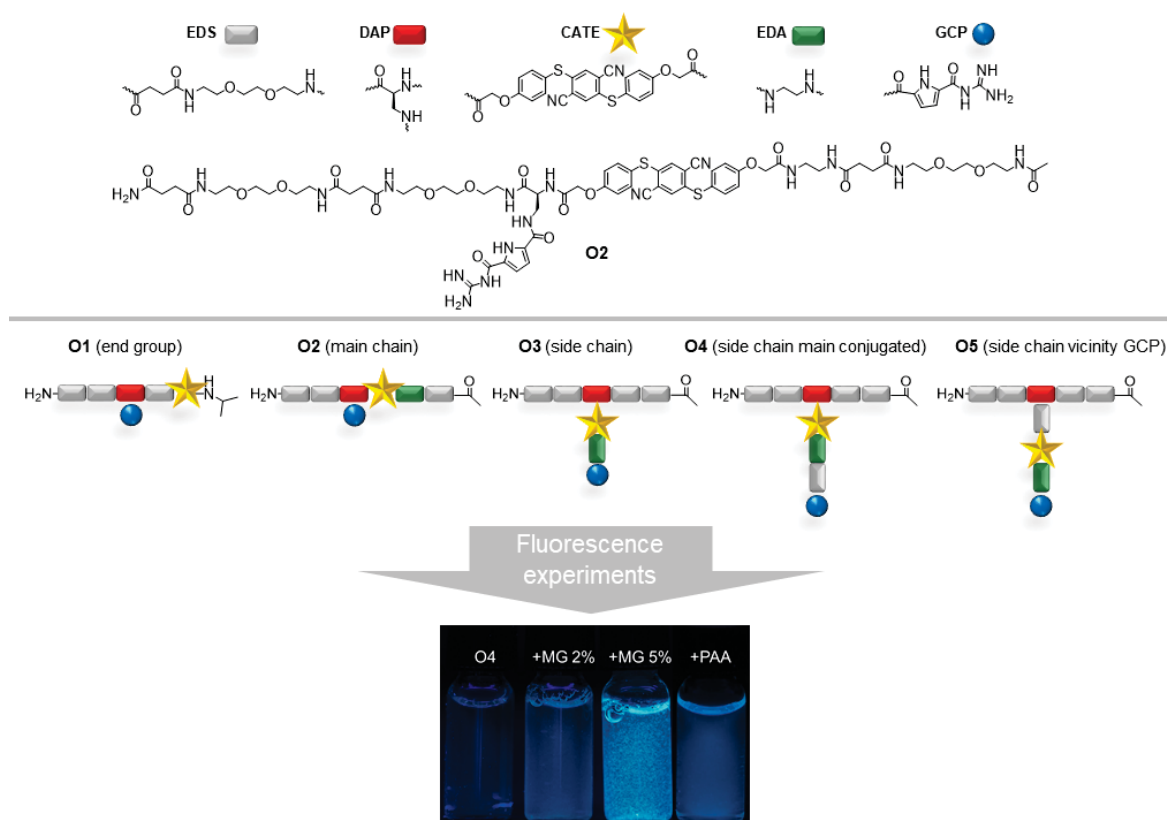


Figure 11: Final oligomers with AIE luminophore and GCP motif (**O1-O5**).

With the structures in hand, various fluorescence measurements were carried out. In the solid-state fluorescence experiments of the powders, there were no differences for the five derivatives, which was an ideal basis for the study. Subsequently, the AIE derivatives were observed in solution. In general, all structures in which the luminophore was incorporated into the side chain showed lower initial fluorescence intensity than the derivatives in which the luminophore was conjugated into the main chain. This suggests that the AIE in the side chains may be more advantageous for AIE behaviour in solution, as the luminophore is less restricted by the scaffold itself and is free to rotate. To evaluate the AIE behaviour of the compounds, fluorescence titrations were then performed with different potential binding partners. Surprisingly, only one of the five derivatives showed a significant increase in emission when interacting with anionic materials and biomolecules. Further, the trend showed that with a higher density of anionic groups on the target molecule, the emission intensity of the active compound became more pronounced. Within this framework, a first structure-activity correlation could then be established. The special feature of the active ligand (**O4**) with AIE in the side chain was probably the additional spacer building block, the diethylene glycol linker. This construction with an additional linker between the luminophore and the binding motif GCP leads to the AIE-active oligomer, which firstly has the necessary water solubility with weak initial fluorescence and secondly offers the

necessary flexibility for binding to the anionic material. At the same time, the GCP binding could then achieve rotational restriction or aggregation at the target molecule, resulting in the AIE effect.

In this part of the thesis, the aim was to systematically investigate the potential effects of positioning an AIE luminophore in flexible macromolecules with supramolecular binding motifs. And indeed, this novel study was able to show that the position of the AIE strongly influences the function, both for the ligand itself and when the ligand is applied for detection. While this study provides important insights into the structure-property relation of AIE-modified macromolecules, it has not been possible to obtain pronounced AIE effects by titrations with proteins.^[131] One explanation may be that a monovalent ligand cannot establish sufficient binding strength to the protein surface. This could also be due to the design of the scaffold, as the macromolecules in this study are quite flexible and thus a small restriction on the rotational ability of the AIE occurs. Therefore, in the future, multivalent GCP ligands could be constructed as in project 1, maintaining the position of the AIE as in **O4**. Equally, heteroevalent systems could also be considered, so that in both cases the binding strength increases. In the future, a change in emission intensity can also be targeted by varying the linker between the luminophore and binding motif, e.g. by introducing a more rigid or hydrophobic linker, which could increase the AIE effect.

In the third part, the non-natural GCP unit within the AIE-construct was exchanged towards a natural binding motif, a carbohydrate, deriving a macromolecular glycan mimetic. Over the past decades, a large number of glycan mimetics have been investigated for their interaction with lectins, in which multivalence has been shown to be a crucial factor in increasing affinity.^[29,132,133] Furthermore, when multivalent carbohydrate ligands bind to lectins, a pronounced clustering effect of the two binding partners was observed, leading to a partial aggregation of the system.^[63,134,135] As already addressed in project 2, aggregates also take on a crucial role in the AIE effect. Many other groups had synthesised AIE carbohydrate ligands in recent years and were able to target and detect diverse lectins, however, investigation of the correlation of the AIE effect and aggregate formation has received little consideration.

Therefore, one aim of this project was to first evaluate which lectins can be detected using a trivalent glyco-oligomer with AIE and also what influence the formation of aggregates and clusters has on the AIE effect. For this approach of correlation investigating, two trivalent sequence-defined glyco-oligomers with aggregation-induced emission luminophores. Both glyco-oligomers are identical in structure except that they carry different binding motifs. The ligand Man-TPE carries α -D-Mannose and Gal-TPE β -Galactose as motif (see Figure 12). Fluorescence and turbidity tests were carried out with the two ligands using different selective α -D-Mannose lectins. The lectins analysed were Con A (Concanavalin A), GNA (*Galanthus Nivalis*), PSA (*Pisum sativum*) and LCA (*Lens culinaris*), which are present as tetramers with four binding sites (Con A, GNA) or as dimers with two binding sites (PSA,

LCA) at the investigated pH.^[136-138] In addition to the confirmation differences, the lectins also show different binding affinities to α -D-Mannose. Among them, Con A shows the highest affinity, followed by GNA, PSA and LCA.^[136,138]

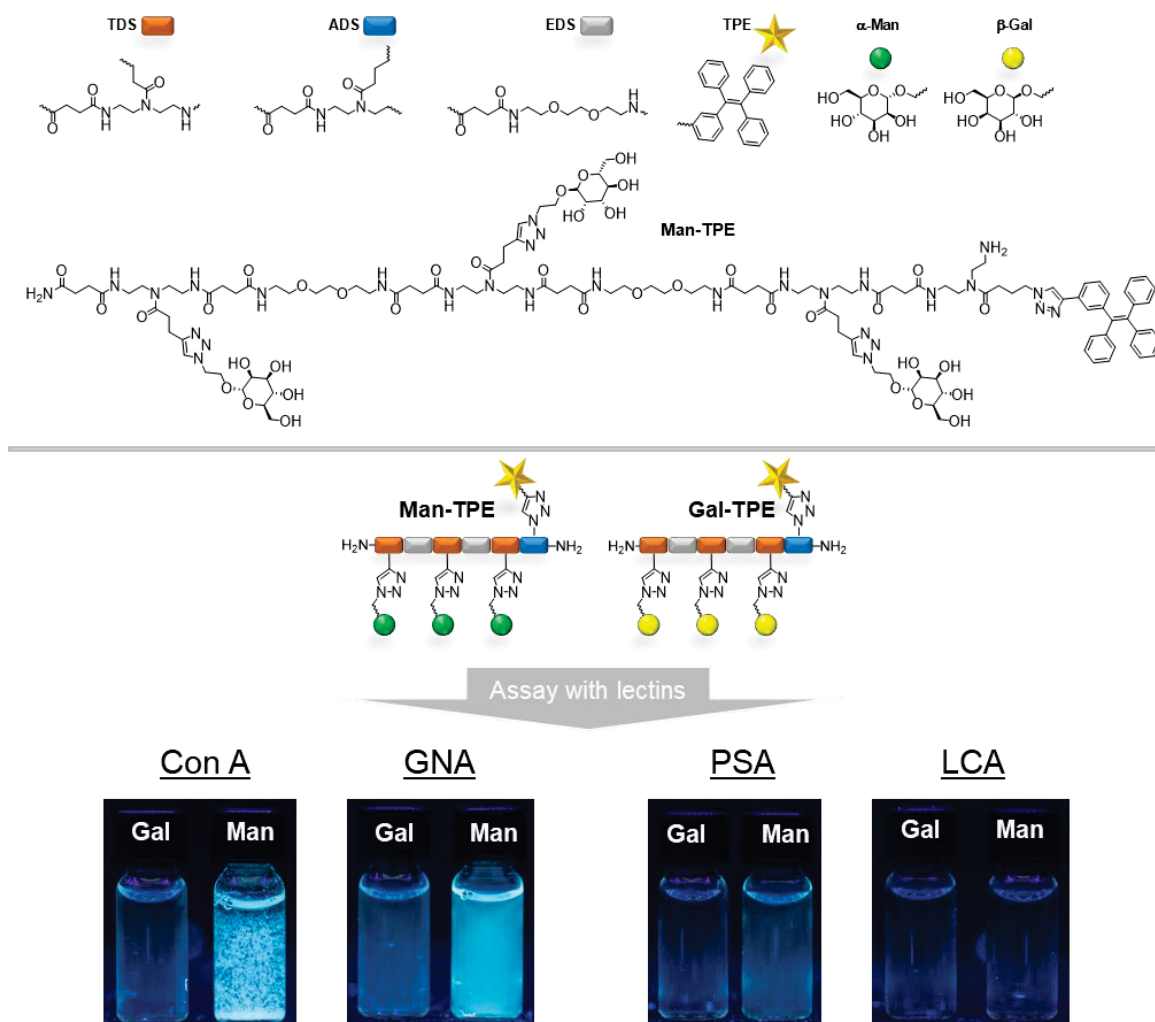


Figure 12: Final trivalent oligomers with α -D Mannose or β -Galactose and conjugated TPE luminophore. In addition, the photo series under UV light with different lectins (Con A, GNA, PSA, LCA), each vial with 13 μ M of the **Man-** or **Gal-TPE** with 22 μ M lectin in LBB.

In the fluorescence titrations with the tetrameric Con A and GNA to the Man-TPE solution, the addition of even small amounts of the lectins caused a marked increase in emission intensity, but the increase was particularly pronounced for the lectin Con A. Con A also showed the strongest affinity in the turbidity assays, halving the transmission signal at small amounts of the ligand. The tetramer Con A caused a strong cluster effect of the system, resulting in the strong turbidity. This change in aggregation state benefits the incorporated AIE luminophore. By restricting intramolecular rotation, the luminophore emits strongly and can be easily detected. Compared to Con A, the tetramer GNA shows a similar opacity effect, but only at a much higher Man-TPE concentration, which is consistent with the

lower emission increases for GNA. For the dimers PSA and LCA, the fluorescence and turbidity experiments with Man-TPE showed a different behaviour. The emission value of the Man-TPE solution increased only very slightly to not at all by the addition of the dimeric lectins. Likewise, slight turbidity could only be achieved at very high concentrations. Overall, this AIE study showed clear differences in the detection ability of tetrameric and dimeric lectins. The explanation for differences in AIE detectability could be the demonstrated necessity of clustering effects with restriction of intramolecular rotational ability and small aggregates.

However, it will be important to enable the detection of dimeric lectins in the future. One approach could be the development of higher-order multivalent structures that could promote the clustering of multiple dimeric lectins. In a first step, these could be precision macromolecules, but also polymer systems similar to those of Gerke et al. would be conceivable.^[72] In this case, each incorporated carbohydrate-containing macromolecule would carry carbohydrates and an AIE luminophore, which would increase the valence of the carbohydrates as well as the emission intensity due to the high number of conjugated luminophores. On the other hand, the AIE emission increases obtained in this work for the tetrameric lectins can be described as sensitive and meaningful compared to the literature, which in turn could open up new fields of application for the derivatives.^[139-142] For example, the structures could function as bioprobes for carbohydrate sensitive cell membrane due to their high sensitivity.

Clustering, as observed for the AIE-glycan mimetic compounds, is an important phenomenon in multivalent binding and is directly related to many biological functions, such as the clustering of receptors in a membrane after binding to a multivalent ligand.^[143] However, the detection of such clustering events in membranes is non-trivial and AIE luminophores could reveal new ways to detect clustering events. In theory, many clusters with many AIE interactions should thereby cause a strong emission intensity, while individual AIEs produce a low or no emission signal.

Based on this idea, the fourth part of this work aims to synthesise amphiphilic glycooligomers with an AIE luminophore that can assemble into micelles and specifically reduce as well as promote their clustering. A total of three AIE-modified glycooligomers (Mannose-TPE oligomer (**MTO**), Galactose-TPE oligomer (**GTO**) and Mannose-CATE oligomer (**MCO**)) were synthesised for this purpose, two TPE derivatives, each with Mannose or Galactose as binding motif, and an aromatic thioether luminophore (ATE) AIE derivative with Mannose (Figure 13).

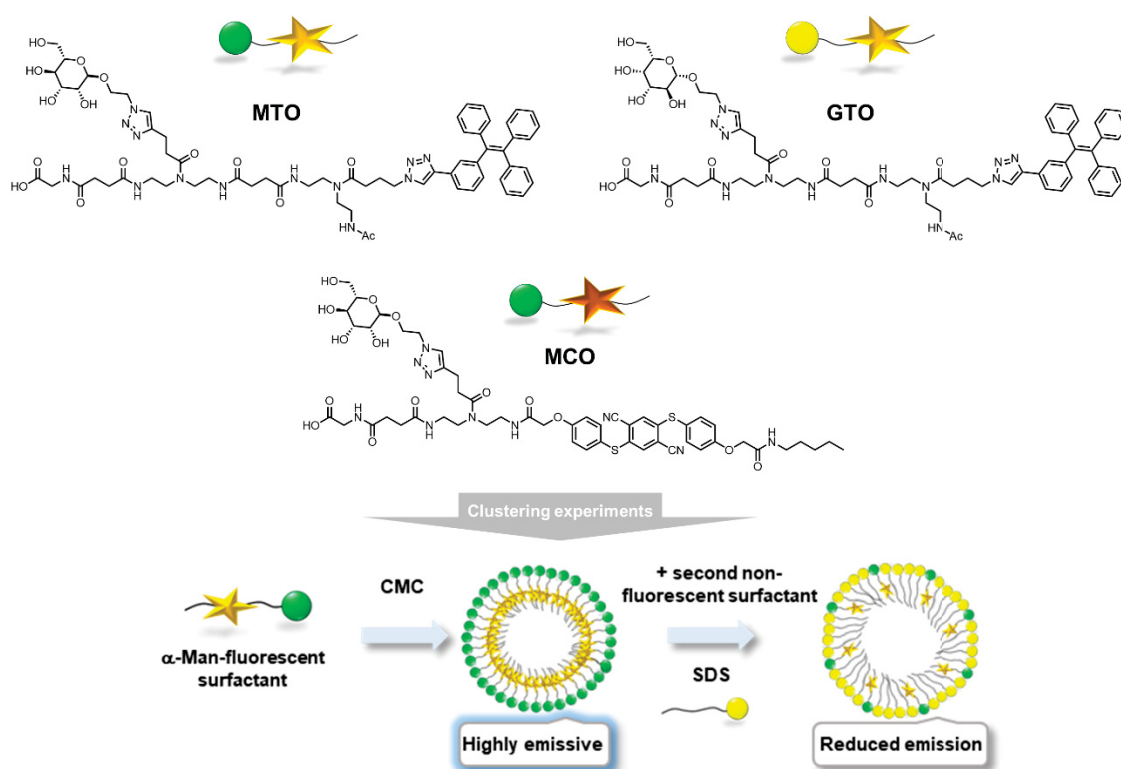


Figure 13: An overview of the three synthesized structures with schematic representation as surfactant. Man-derivatives have a green head group and Gal-derivatives have a yellow head group. TPE is shown with a yellow star and CATE with a bronze star. Schematically, the transition from a single AIE surfactant to a micelle is shown upon reaching the CMC, where the emission intensity increases due to increased luminophore interactions. Subsequently, the mixed micelles with fewer AIE-luminophore interactions are schematically obtained by adding the non-fluorescent second surfactant SDS, whereby the emission intensity decreases.

In fluorescence measurements in water, it was recognised that the derivatives assemble above their CMC (critical micelle concentration) by self-assembly to form micelles with a high emission intensity, whereby no solid aggregates or precipitation of the amphiphilic oligomers occurred. This behaviour is typical of AIE micelles and is reported in the literature.^[144] In the next step, the critical micelle concentrations were determined. The CMCs of the two TPE derivatives (**MTO** and **GTO**) are very similar, whereas the **MCO** derivative has a significantly higher CMC value. The CMC difference can be attributed to the lower flexibility of the TPE compared to the CATE-AIE. Likewise, the weaker intramolecular interactions of the CATE units compared to the TPE may cause the lower CMC value. Next, it is now exciting to specifically reduce the strong fluorescence of the micelles, which is caused by many AIE interactions. For this purpose, sodium dodecyl sulphate was added as a second non-fluorescent surfactant to the micelle system, resulting in mixed micelles. In fact, the fluorescence was reduced by up to 97 %. The strong reduction of fluorescence can be explained by significantly fewer interactions within the mixed micelle systems, such as the stacking of the luminophores, which reduces the rotational constraint of the luminophores.

In general, these experiments show that the initial emission intensity of luminophore-containing micelles can be selectively reduced by the addition of a non-fluorescent second surfactant and now open the possibility to now add multivalent receptors, e.g. Con A as used in the previous chapter, and to investigate whether clustering can be induced and observed by a potential increase in fluorescence of the AIE luminophore. If this becomes possible, the next step should be to transfer this approach to the detection of clustering of receptors in a membrane after binding to a multivalent ligand. This approach would immensely simplify monitoring by simple fluorescence spectroscopy and offers new opportunities maybe even to monitor clustering events in live cells.

Overall, this thesis successfully demonstrated the combination of solid phase polymer protocols, supramolecular building block GCP and AIE luminophores. With this synthetic platform available, new hybrid macromolecules became accessible, as was shown for four different classes of macromolecules combining natural and non-natural motifs. In all cases, macromolecules were studied as ligands or inhibitors of protein interactions and successfully served as model systems to investigate the effect of sequence-control of the macromolecules on their properties. Based on their promising activity and biocompatibility, future studies could now continue towards applications of these macromolecules, e.g. as Taspase inhibitors or for detection of glycan clustering.

7. References

- 1) J.-M. Lehn, *Science* **1985**, 227, (4689), 849-856.
- 2) R. A. Dwek, *Chem. Rev.* **1996**, 96, (2), 683–720.
- 3) A. Imberty, A. Varrot, *Curr. Opin. Struct. Biol.* **2008**, 18, (5), 567-576.
- 4) S. Cecioni, A. Imberty, S. Vidal, *Chem. Rev.* **2015**, 115, (1), 525–561.
- 5) D. H. Williams, M. S. Westwell, *Chem. Soc. Rev.* **1998**, 27, (1), 5764.
- 6) C. T. Walsh, S. L. Fisher, I. S. Park, M. Prahalad, Z. Wu, *Chemistry & Biology* **1996**, 3, (1), 21-28.
- 7) L. L. Kiessling, J. E. Gestwicki, L. E. Strong, *Curr. Opin. Chem. Biol.* **2000**, 4, (6), 696-703.
- 8) N. Jayaraman, *Chem. Soc. Rev.*, **2009**, 38, 3463-3483.
- 9) H. S. Bennett, *J. Histochem. Cytochem.* **1963**, 11, 14-23.
- 10) B. Ernst, J. L. Magnani, *Nat. Rev. Drug Discov.* **2009**, 8, 661-667.
- 11) C. P. Mandl, B. König, *J. Org. Chem.* **2005**, 70, (2), 670674.
- 12) L. A. Logsdon, C. L. Schardon, V. Ramalingam, S. K. Kwee, A. R. Urbach, *J. Am. Chem. Soc.* **2011**, 133, (42), 17087-17092.
- 13) F. Trusch, K. Kowski, K. Bravo-Rodriguez, C. Beuck, A. Sowislok, B. Wettig, A. Matena, E. Sanchez-Garcia, H. Meyer, T. Schrader, P. Bayer, *Chem. Commun.* **2016**, 52, 14141-14144.
- 14) J. Matic, F. Supljika, N. Tir, P. Piotrowski, C. Schmuck, M. Abramic, I. Piantanida, S. Tomic, *RSC Adv.* **2016**, 6, 83044.
- 15) M. Li, S. Schlesinger, S. K. Knauer, C. Schmuck, *Bio. Chem.* **2016**, 14, 8800.
- 16) Q.-Q. Jiang, W. Sicking, M. Ehlers, C. Schmuck, *Chem. Sci.* **2015**, 6, 1792.
- 17) P. Wich, C. Schmuck, *Angew. Chem. Int. Ed.* **2010**, 49, 4113-4116.
- 18) D. Ponader, S. Igde, M. Wehle, K. Märker, M. Santer, D. Bléger, L. Hartmann, *Beilstein J. Org. Chem.* **2014**, 10, 1603-1612.
- 19) C. Gerke, M. F. Ebbesen, D. Jansen, S. Boden, T. Freichel, L. Hartmann, *Biomacromolecules* **2017**, 18, (3), 787-796.
- 20) D. Ponader, F. Wojcik, F. Beceren-Braun, J. Dervedde, L. Hartmann, *Biomacromolecules* **2012**, 13, (6), 1845-1852.
- 21) F. Wojcik, S. Mosca, L. Hartmann, *J. Org. Chem.* **2012**, 77, 4226-4234.
- 22) R. B. Merrifield, *Am. Chem. Soc.* **1963**, 85, (14), 2149-2154.
- 23) W. Chan, P. White, *Fmoc Solid Phase Peptide Synthesis: A Practical Approach*. OUP Oxford: **2000**.
- 24) B. Castro, J.-R. Dormoy, B. Dourtoglou, G. Evin, C. Selve, J.-C. Ziegler, *Synthesis* **1976**, 11, 751-752.
- 25) C. A. G. N. Montalbetti, V. Falque, *Tetrahedron* **2005**, 61, (46), 10827-10852.

-
- 26) D. Orain, J. Ellard, M. Bradley, *J. Comb. Chem.* **2002**, 4, (1), 1-16.
- 27) S. Igde, S. Röblitz, A. Müller, K. Kolbe, S. Boden, C. Fessele, T. K. Lindhorst, M. Weber, L. Hartmann, *Biosci.* **2017**, 17, (12), 1700198.
- 28) S. Boden, K. G. Wagner, M. Karg, L. Hartmann, *Polymers* **2017**, 9, (12), 716.
- 29) D. Ponader, *Synthesis of Sequence-defined Glycooligomers for Studying Multivalent Interactions*. Freie Universität Berlin, **2014**.
- 30) T. Freichel, S. Eierhoff, N. L. Snyder, L. Hartmann, *J. Org. Chem.* **2017**, 82, 9400-9409.
- 31) F. Shamout, L. Fischer, N. L. Snyder, L. Hartmann. *Macromol. Rapid Commun.* **2019**, 1900473.
- 32) M. Baier, M. Giesler, L. Hartmann, *Chem. Eur. J.* **2018**, 24, (7), 1619-1630.
- 33) I. Coin, M. Beyermann, M. Bienert, *Nat. Protoc.* **2007**, 2, (12), 3247-3256.
- 34) T. Kimmerlin, D. Seebach, *J. Pept. Res.* **2005**, 65, (2), 229-260.
- 35) M. Stawikowski, G. B. Fields, *Curr. Protoc. Protein Sci.* **2012**, 69, (1), 18.1.1-18.1.13.
- 36) R. Huisgen, G. Szeimies, L. Möbius, *Chem. Ber.* **1967**, 100, (8), 2494-2507.
- 37) L. Liang, D. Astruc, *Coord. Chem. Rev.* **2011**, 255, (23), 2933-2945.
- 38) M. Baier, M. Giesler, L. Hartmann, *Chem. Eur. J.* **2018**, 24, (7), 1619-1630.
- 39) F. Shamout, A. Monaco, G. Yilmaz, C. R. Becer, L. Hartmann, *Macromol. Rapid Commun.* **2019**, 1900459.
- 40) M. Mammen, S.-K. Choi, G. M. Whitesides, *Angew. Chem.* **1998**, 37, (20), 2754-2794.
- 41) C. B. Carlson, P. Mowery, R. M. Owen, E. C. Dykhuizen, L. L. Kiessling, *Chem. Biol.* **2007**, 2, 119-127.
- 42) C. Fasting, C.A. Schalley, M. Weber, O. Seitz, S. Hecht, B. Koksche, J. Darnedde, C. Graf, E.-W. Knapp, R. Haag, *Angew. Chem. Int. Ed.* **2012**, 51, 10472-10498.
- 43) L. L. Kiessling, N. L. Pohl, *Chem. Biol.* **1996**, 3, 71-77.
- 44) R. Roy, *Curr. Opin. Struct. Biol.* **1996**, 6, 692-702.
- 45) C. Fasting, C. A. Schalley, M. Weber, O. Seitz, S. Hecht, B. Koksche, J. Darnedde, C. Graf, E. W. Knapp, R. Haag, *Angew. Chem.* **2012**, 51, 10472-10498.
- 46) S. M. Dimick, S. C. Powell, S. A. McMahon, D. N. Moothoo, J. H. Naismith, E. J. Toone, *J. Am. Chem. Soc.* **1999**, 121, 10286-10296.
- 47) J. J. Lundquist, E. J. Toone, *Chem. Rev.* **2002**, 102, 555-578.
- 48) W. P. Jencks, *PNAS* **1981**, 78, (7), 4046-4050.
- 49) E. T. Mack, P. W. Snyder, R. Perez- Castillejos, B. a. Bilgiçer, D. T. Moustakas, M. J. Butte, G. M. Whitesides, *J. Am. Chem.Soc.* **2011**, 134, 333-345.
- 50) P. I. Kitov, D. R. Bundle, *J. Am. Chem. Soc.* **2003**, 125, 16271-16284.
- 51) R. J. Pieters, *Org. Biomol. Chem.* **2009**, 7, 2013-2025.
- 52) Schwarzenbach, v. G. *Der chelateffekt*. **1952** Helvetica Chimica Acta 35, 2344-2359.

-
- 53) T. K. Dam, C. F. Brewer, *Biochemistry* **2008**, *47*, 8470-8476.
- 54) W. J. Lees, A. Spaltenstein, J. E. Kingery-Wood, G. M. Whitesides, *J. Med. Chem.* **1994**, *37*, 3419-3433.
- 55) G. B. Sigal, M. Mammen, G. Dahmann, G. M. Whitesides, *J. Am. Chem. Soc.* **1996**, *118*, 3789-3800.
- 56) T. W. Rademacher, R. B. Parekh, R. A. Dwek, *Annu. Rev. Biochem.* **1988**, *57*, (1), 785-838.
- 57) A. C. Weymouth-Wilson, *Nat. Prod. Rep.* **1997**, *14*, (2), 99-110.
- 58) M. Phillips, E. Nudelman, F. Gaeta, M. Perez, A. Singhal, S. Hakomori, J. Paulson, *Science* **1990**, *250*, (4984), 1130-1132.
- 59) R. J. Linhardt, T. Toida, *Chem. Res.* **2004**, *37*, (7), 431-438.
- 60) X.-Q. Yu, M. R. Kanost, *Devel. Comp. Immunol.* **2003**, *27*, (3), 189-196.
- 61) T. B. H. Geijtenbeek, D. S. Kwon, R. Torensma, S. J. van Vliet, G. C. F. van Duijnhoven, J. Middel, I. L. M. H. A. Cornelissen, H. S. L. M. Nottet, V. N. Kewal Ramani, D. R. Littman, C. G. Figdor, Y. van Kooyk, *Cell* **2000**, *100*, (5), 587-597.
- 62) H. Feinberg, D. A. Mitchell, K. Drickamer, W. I. Weis, *Science* **2001**, *294*, (5549), 2163-2166.
- 63) J. E. Gestwicki, C. W. Cairo, L. E. Strong, K. A. Oetjen, L. L. Kiessling, *J. Am. Chem. Soc.* **2002**, *124*, (50), 14922-14933.
- 64) C. R. Becer, *Macromol. Rapid Commun.* **2012**, *33*, (9), 742-752.
- 65) Y. Gou, J. Geng, S.-J. Richards, J. Burns, C. R. Becer, D. M. Haddleton, *J. Polym. Sci. A* **2013**, *51*, (12), 2588-2597.
- 66) S. André, R. J. Pieters, I. Vrasidas, H. Kaltner, I. Kuwabara, F. T. Liu, R. M. J. Liskamp, H. J. Gabius, *ChemBioChem* **2001**, *2*, (11), 822-830.
- 67) M. L. Wolfenden, M. J. Cloninger, *Bioconjugate Chem.* **2006**, *17*, (4), 958-966.
- 68) H. Xue, L. Peng, Y. Dong, Y. Zheng, Y. Luan, X. Hu, G. Chen, H. Chen, *RSC Adv.* **2017**, *7*, (14), 8484-8490.
- 69) M. Nagao, Y. Fujiwara, T. Matsubara, Y. Hoshino, T. Sato, Y. Miura, *Biomacromolecules* **2017**, *18*, (12), 4385-4392.
- 70) A. Fernández-Tejada, F., J. Cañada, J. Jiménez-Barbero, *Chem. Eur. J.* **2015**, *21*, (30), 10616-10628.
- 71) S. Bhatia, L. C. Camacho, R. Haag, *J. Am. Chem. Soc.* **2016**, *138*, (28), 8654-8666.
- 72) C. Gerke, *Sequence-Controlled Polymers via Thiol-ene Step-growth Polymerization of Precision Macromonomers*. Heinrich-Heine-Universität Düsseldorf, **2018**.
- 73) M. Baier, *Introducing selected variations in architecture, linker and ligand composition of glycooligo (amides) targeting non-enveloped viruses*. Heinrich-Heine-Universität Düsseldorf, **2019**.

-
- 74) T. Akasaka, K. Matsuura, K. Kobayashi, *Bioconjugate Chem.* **2001**, *12*, 5, 776–785.
- 75) A. Banger, J. Sindram, M. Otten, J. Kania, A. Strzelczyk, D. Wilms, S. Miletic, T. Marlovits, M. Karg, L. Hartmann, *Polym. Chem.* **2021**, *12*, 4795–4802.
- 76) S. S. Lee, T. Fyrner, F. Chen, Z. Álvarez, E. Sleep, D. S. Chun, J. A. Weiner, R. W. Cook, R. D. Freshman, M. S. Schallmo, K. M. Katchko, A. D. Schneider, J. T. Smith, C. Yun, G. Singh, S. Z. Hashmi, M. T. McClendon, Z. Yu, S. R. Stock, W. K. Hsu, E. L. Hsu, S. I. Stupp, *Nat. Nanotechnol.* **2017**, *12*, 821–829.
- 77) Trusch, K. Kowski, K. Bravo-Rodriguez, C. Beuck, A. Sowislok, B. Wettig, A. Matena, E. Sanchez-Garcia, H. Meyer, T. Schrader, P. Bayer, *Chem. Commun.* **2016**, *52*, 14141–14144.
- 78) D. Bier, R. Rose, K. Bravo-Rodriguez, M. Bartel, J. M. Ramirez-Anguila, S. Dutt, C. Wilch, F. Klärner, E. Sanchez-Garcia, T. Schrader, C. Ottmann, *Nat. Chem.* **2013**, *5*, 234–239.
- 79) C. P. Mandl, B. König, *J. Org. Chem.* **2005**, *70*, (2), 670674.
- 80) L. A. Logsdon, C. L. Schardon, V. Ramalingam, S. K. Kwee, A. R. Urbach, *J. Am. Chem. Soc.* **2011**, *133*, (42), 17087–17092.
- 81) C. Schmuck, W. Wienand, *J. Am. Chem. Soc.* **2003**, *125*, 452–459.
- 82) C. Schmuck, M. Schwegmann, *J. Am. Chem. Soc.* **2005**, *127*, 3373–3379.
- 83) D. Maity, A. Gigante, P. A. Sánchez-Murcia, E. Sijbesma, M. Li, D. Bier, S. Mosel, S. Knauer, C. Ottmann, C. Schmuck, *Org. Biomol. Chem.* **2019**, *17*, 4359–4363.
- 84) C. Schmuck, *Coord. Chem. Rev.* **2006**, *250*, 3053–3067.
- 85) C. Schmuck, M. Heil, *ChemBioChem.* **2003**, *4*, (11), 1232–1238.
- 86) T. Förster, K. Kasper, *Z. Phys. Chem.* **1954**, *1*, 275.
- 87) J. B. Birks, *Photophysics of Aromatic Molecules*, Wiley, London, **1970**.
- 88) S. W. Thomas III, G. D. Joly, T. M. Swager, *Chem. Rev.* **2007**, *107*, 1339.
- 89) M. Belletete, J. Bouchard, M. Leclerc, G. Durocher, *Macromolecules* **2005**, *38*, 880.
- 90) A. Menon, M. Galvin, K. A. Walz, L. Rothberg, *Synth. Met.* **2004**, *141*, 197.
- 91) W. H. Tan, K. M. Wang, T. J. Drake, *Curr. Opin. Chem. Biol.*, **2004**, *8*, 547.
- 92) K. E. Sapsford, L. Berti, I. L. Medintz, *Angew. Chem. Int. Ed.* **2006**, *45*, 4562.
- 93) S. M. Borisov, O. S. Wolfbeis, *Chem. Rev.* **2008**, *108*, 423.
- 94) M. Wang, G. Zhang, D. Zhang, D. Zhu, B. Tang, *J. Mater. Chem.* **2010**, *20*, 1858.
- 95) H. Tong, Y. Hong, Y. Dong, M. Haussler, J. W. Y. Lam, Z. Li, Z. Guo, Z. Guo, B. Z. Tang, *Chem. Commun.* **2006**, 3705.
- 96) T. Sanji, K. Shiraishi, M. Tanaka, *ACS Appl. Mater. Interfaces* **2009**, *1*, 270.
- 97) M. Gao, B. Z. Tang, *ACS Sens.* **2017**, *2*, 1382–1399.
- 98) J. Luo, Z. Xie, J. W. Y. Lam, L. Cheng, H. Chen, C. Qiu, H. S. Kwok, X. Zhan, Y. Liu, D. Zhu, B. Z. Tang, *Chem. Commun.* **2001**, 1740.

-
- 99) B. Z. Tang, X. Zhan, G. Yu, P. P. S. Lee, Y. Liu, D. Zhu, *J. Mater. Chem.* **2001**, *11*, 2974.
- 100) J. Liang, B. Z. Tang, B. Liu, *Chem. Soc. Rev.* **2015**, *44*, 2798-2811.
- 101) Y. Yu, A. Qin, C. Feng, P. Lu, K. M. Ng, K. Q. Luo, B. Z. Tang, *Analyst* **2012**, *137*, 5592-5596.
- 102) J. Mei, Y. Hong, J. W. Y. Lam, A. Qin, Y. Tang, B. Z. Tang, *Adv. Mater.* **2014**, *6*, 5429-5479.
- 103) R. Hu, A. Qin, B. Z. Tang, *Prog. Polym. Sci.* **2020**, *100*, 101176
- 104) S. Riebe, C. Vallet, F. van der Vight, D. Gonzalez-Abradelo, C. Wölper, C. A. Strassert, G. Jansen, S. Knauer, J. Voskuhl, *Chem. Eur. J.* **2017**, *23*, 13660-13668.
- 105) M. Hayduk, S. Riebe, K. Rudolph, S. Schwarze, F. van der Vight, C. G. Daniliuc, G. Jansen, J. Voskuhl, *Isr. J. Chem.* **2018**, *58*, 927-931.
- 106) B. Schmidt, S. Sankaran, L. Stegemann, C. A. Strassert, P. Jonkheijm, J. Voskuhl, *J. Mat. Chem. B* **2016**, *4*, 4732-4738.
- 107) M. Hayduk, S. Riebe, J. Voskuhl, *Chem. Eur. J.* **2018**, *24*, 12221-12230.
- 108) J. M. Berg, J. L. Tymoczko, G. J. Gatto Jr., L. Stryer, *Biochemistry*, W. H. Freeman, New York, **2015**.
- 109) F. Sanger, H. Tuppy, *Biochem. J.* **1951**, *49*, 481.
- 110) M. F. Perutz, *Nature* **1962**, *194*, 914.
- 111) J.-F. Lutz, *Macromol. Rapid Commun.* **2017**, 1700582.
- 112) N. Badia, J.-F. Lutz, *Chem. Soc. Rev.*, **2009**, *38*, 3383-3390.
- 113) J.-F. Lutz et al., *Science* **2013**, *341*, 1238149.
- 114) T. T. Trinh, C. Laure, J.-F. Lutz, *Macromol. Chem. Phys.* **2015**, *216*, 1498.
- 115) J.-F. Lutz, J.-M. Lehn, E. W. Meijer, K. Matyjaszewski, *Nat. Rev. Mater.* **2016**, *1*, 16024.
- 116) F. Shamout, A. Monaco, G. Yilmaz, C. R. Becer, L. Hartmann, *Macromol. Rapid Commun.* **2019**, 1900459.
- 117) M. J. Roberts, M. D. Bentley, J. M. Harris, *Adv. Drug Deliv. Rev.* **2002**, *54*, (4), 459-476.
- 118) J. Morgenstern, P. Baumann, C. Brunner, J. Hubbuch, *Int. J. Pharm.* **2017**, *519*, 408-417.
- 119) C. Schmuck, *ChemComm.* **1999**, *9*, 843-844.
- 120) P. Reuther, *Synthesis of precision macromolecules for the multivalent presentation of supramolecular ligands*. Heinrich-Heine-Universität Düsseldorf, **2017**.
- 121) J. Hatai, C. Schmuck, *Acc. Chem. Res.* **2019**, *52*, 6, 1709-1720.
- 122) S. Schöttler, G. Becker, S. Winzen, T. Steinbach, K. Mohr, K. Landfester, V. Mailänder and F. R. Wurm, *Nat. Nanotechnol.* **2016**, *11*, 372-377.
- 123) S. De Santis, R. Chiaraluce, V. Consalvi, F. Novelli, M. Petrosino, P. Punzi, F. Sciubba, C. Giordano, G. Masci, A. Scipioni, *ChemPlusChem.* **2017**, *82*, 241-250.
- 124) S. Akocak, M. R. Alam, A. M. Shabana, R. Kishore, K. Sanku, D. Vullo, H. Thompson, E. R. Swenson, C. T. Supuran, M. A. J. Ilies, *Med. Chem.* **2016**, *59*, 5077-5088.

-
- 125) K. Chitphet, S. M. Geary, C. H. F. Chan, A. L. Simons, G. J. Weiner, A. K. Salem, *Biomater. Sci. Eng.* **2020**, 6 (5), 2659–2667.
- 126) C. López-Otín, L. M. Matrisian, *Nat. Rev. Cancer* **2007**, 7, 800–808.
- 127) J. J.-D. Hsieh, E. H.-Y. Cheng, S. J. Korsmeyer, *Cell* **2003**, 115, 293–303.
- 128) D. Wünsch, A. Hahlbrock, S. Jung, T. Schirmeister, J. van den Boom, O. Schilling, S. K. Knauer, R. H. Stauber, *Oncogene* **2016**, 35, 3351–3364.
- 129) D. Giustarini et al. *Free Radical Biology and Medicine* **2015**, 89, 972–981,
- 130) G. Saito, J. A. Swanson, K.-D. Lee, *Adv. Drug Deliv. Rev.* **2003**, 55, 199–215.
- 131) G. R. Suman, M. Pandey, A. S. J. Chakravarthy, *Mater. Chem. Front.* **2021**, 5, 1541–1584.
- 132) S. Cecioni, A. Imberty, S. Vidal, *Chem. Rev.* **2015**, 115, 525.
- 133) V. Vázquez-Dorbatt, J. Lee, E.-W. Lin, H. D. Maynard, *ChemBioChem* **2012**, 13, 2478.
- 134) J. J. Lundquist, E. J. Toone, *Chem. Rev.* **2002**, 102, 555–578.
- 135) E. M. Munoz, J. Correa, E. Fernandez-Megia, R. Riguera, *J. Am. Chem. Soc.* **2009**, 131, (49), 17765–17767.
- 136) F. P. Schwarz, K. D. Puri, R. G. Bhat, A. Surolia, *J. Biol. Chem.* **1993**, 268, 7668–7677
- 137) E. J. M. V. Damme, A. K. Allen, W. J. Peumans, *FEBS Lett.* **1987**, 215, 1873–3468
- 138) K. H. Schlick, R. A. Udelhoven, G. C. Strohmeyer, M. Cloninger, *J. Mol. Pharm.* **2005**, 2, (4), 295–301.
- 139) A. Qin, J. W. Y. Lam, L. Tang, C. K. W. Jim, H. Zhao, J. Sun, B. Z. Tang, *Macromolecules*, **2009**, 42, 1421.
- 140) S. Umar, A. K. Jha, D. Purohit, A. Goel, *J. Org. Chem.* **2017**, 82, 4766–4773.
- 141) W. Guan, W. Zhou, C. Lu, B. Z. Tang, *Angew. Chem. Int. Ed.* **2015**, 54, 15160–15164.
- 142) J. X. Wang, Q. Chen, N. Bian, F. Yang, J. Sun, A. D. Qi, C. G. Yan, B. H. Han, *Org. Biomol. Chem.*, **2011**, 9, 2219–2226.
- 143) A. Grochmal, E. Ferrero, L. Milanesi, S. Tomas, *Am. Chem. Soc.* **2013**, 135, 10172–10177.
- 144) T. Yu, W. Zhuang, X. Su, B. Ma, J. Hu, H. He, G. Li, Y. Wang, *Bioconjugate Chem.* **2019**, 30, (7), 2075–2087.

8. Appendix

8.1 List of abbreviations

ACN	-	Acetonitrile
ACQ	-	Aggregation-caused quenching
ADS	-	Azido functionalized Diethylenetriamine Succinic acid amide
AFM	-	Atomic force microscopy
AIE	-	Aggregation induced emission
AIEE	-	Aggregation induced enhanced emission
ATE	-	Aromatic thioether luminophore
BADS	-	p-(azidomethyl)benzoyl diethylenetriamine succinic acid
BOC	-	butyloxycarbonyl
BOP	-	Benzotriazol-1-yl-oxy-tris- (dimethylamino)phosphoniumhexafluoro-phosphate
BSA	-	Bovine serum albumin
CATE	-	Carboxylated aromatic thioether luminophore
CMC	-	Critical micelle concentration
ConA	-	Concanavalin A
CRD	-	Carbohydrate recognition domain
CuAAC	-	Copper(I)-catalyzed azide-alkyne cycloaddition
DCC	-	Dicyclohexylcarbodiimide
DCM	-	Dichloromethane
DDS	-	Double bond functionalized Diethylenetriamine Succinic acid amide
DIPEA	-	<i>N,N</i> -Diisopropylethylamine
DMF	-	Dimethylformamide
DNA	-	Deoxyribonucleic acid
DVB	-	para-Divinylbenzene
EDS	-	Ethylene glycol-diamine-succinic acid building block
ESI-MS	-	Electron spray ionization - mass spectrometry
<i>et al.</i>	-	et alii
Fmoc	-	fluorenylmethoxycarbonyl
GCP	-	Guanidiniocarbonylpyrrole

gly	-	Glycine
GNA	-	Galanthus Nivalis Agglutinin
HEPES	-	(4-(2-Hydroxyethyl)-1-piperazineethanesulfonic acid)
HOBt	-	Hydroxybenzotriazole
HPLC	-	High pressure liquid chromatography
Hz	-	Hertz
LC	-	Liquid chromatography
LCA	-	Lens culinaris Agglutinin
m	-	multiplet
m	-	milli
M	-	Molar
MALDI-TOF	-	Matrix Assisted Laser Desorption Ionization-Time of Flight
MDS	-	Methyl succinyl Diethylenetriamine Succinic acid amide
MG 2%	-	Microgels with 2% methacrylic acid as anionic comonomer
MG 5%	-	Microgels with 5% methacrylic acid as anionic comonomer
MLL	-	mixed-lineage Leukemia protein
MS	-	Mass spectroscopy
NLS	-	Nuclear localization signal
nm	-	Nanometer
NMR	-	Nuclear magnetic resonance
ODS	-	4-((8-Aminooctyl)amino)-4-oxobutanoic acid
PAA	-	Poly (acrylic acid)
PBS	-	Phosphate-buffered saline
PEG	-	Polyethylene glycol
pK _a	-	Acid constant
ppm	-	parts per million
PSA	-	Pisum sativum Agglutinin
PyBOP	-	Benzotriazol-1-yloxy-tripyrrolidino-phosphonium Hexafluorophosphate
RNA	-	Ribonucleic acid
RP	-	reversed Phase
s	-	Singlet
SDS	-	Sodium dodecyl sulfate
SDS-Page	-	Sodium dodecyl sulfate polyacrylamide gel electrophoresis

SEM	-	Scanning electron microscope
SPPoS		Solid phase polymer synthesis
SPPS	-	Solid phase peptide synthesis
SPR	-	Surface plasmon resonance
SPS	-	Solid phase synthesis
t	-	Triplet
TDS	-	Triple bond functionalized Diethylenetriamine
		Succinic acid amide
TFA	-	Trifluoroacetic acid
TIPS	-	Triisopropyl silane
TPE	-	Tetraphenylethane
UHR-MS		Ultra High Resolution - Mass Spectrometry
UV	-	Ultraviolet light
δ	-	Chemical shift
α	-	alpha
β	-	beta
ζ	-	zeta

9. Acknowledgments

Die vorliegende Dissertation wurde in der Zeit von Dezember 2016 bis September 2020 unter der Leitung von Frau Prof. Dr. Laura Hartmann am Institut für Makromolekulare Chemie der Heinrich-Heine-Universität Düsseldorf angefertigt.

An dieser Stelle möchte ich mich bei allen bedanken, die mich auf vielfältige Weise bei meiner Arbeit unterstützt haben:

- Bei Frau Prof. Dr. Laura Hartmann für die Möglichkeit in Ihrem Arbeitskreis meine Promotionsarbeit anfertigen zu dürfen und für konstruktive Gespräche, welche sowohl zu meiner fachlichen als auch persönlichen Weiterentwicklung beigetragen haben.
- Bei Herrn Prof. Dr. Thomas J. J. Müller für die Übernahme des Korreferates und eine für mich wegweisende Empfehlung für den Studiengang Chemie.
- Bei Frau Dr. Monir Tabatabai für zahlreiche Anregungen zu meinen Projekten und eine Vielzahl von Korrekturen zu experimentellen Versuchsreihen.
- Bei Alexander Höing, Serap Ueclue, Matthias Killa, Alexander Banger und Hauke Lukas Junghans für eine tolle Zusammenarbeit innerhalb der unterschiedlichen Projekte und Ihren Einsatz bei der Fertigstellung der Veröffentlichungen.
- Bei Christoph Gerke und Alexander Banger für die tolle Zeit, die wir im und außerhalb des Labors hatten.

Mein Dank gilt darüber hinaus dem gesamten Team und allen Doktoranden des Lehrstuhls für eine gute Arbeitsatmosphäre, die stete Hilfsbereitschaft und den Teamgeist, gemeinsam etwas verwirklichen zu wollen. Auch unsere Weihnachtsfeiern und Reisen nach Malta oder Holland werden mir in Erinnerung bleiben.

Nicht zuletzt gilt mein Dank meinen Eltern, meiner Familie und meinen Freunden, die mich während meiner gesamten Studienzeit unterstützt und mir zu jeder Zeit mit Rat und Tat zur Seite gestanden haben, was mir die notwendige Ruhe und Sicherheit für die Erstellung dieser Arbeit gegeben hat.
